# Accepted Manuscript


ONS-donor ligand based Pt(II) complexes display extremely high anticancer potency through autophagic cell death pathway

Faiz-Ur Rahman, Amjad Ali, Hong-Quan Duong, Inam Ullah Khan, Muhammad Zeeshan Bhatti, Zhan-Ting Li, Hui Wang, Dan-Wei Zhang

PII: S0223-5234(18)31095-X

DOI: https://doi.org/10.1016/j.ejmech.2018.12.052

Reference: EJMECH 10986

To appear in: *European Journal of Medicinal Chemistry*

Received Date: 21 September 2018

Revised Date: 6 December 2018

Accepted Date: 21 December 2018

Please cite this article as: F.-U. Rahman, A. Ali, H.-Q. Duong, I.U. Khan, M.Z. Bhatti, Z.-T. Li, H. Wang, D.-W. Zhang, ONS-donor ligand based Pt(II) complexes display extremely high anticancer potency through autophagic cell death pathway, *European Journal of Medicinal Chemistry* (2019), doi: https://doi.org/10.1016/j.ejmech.2018.12.052.

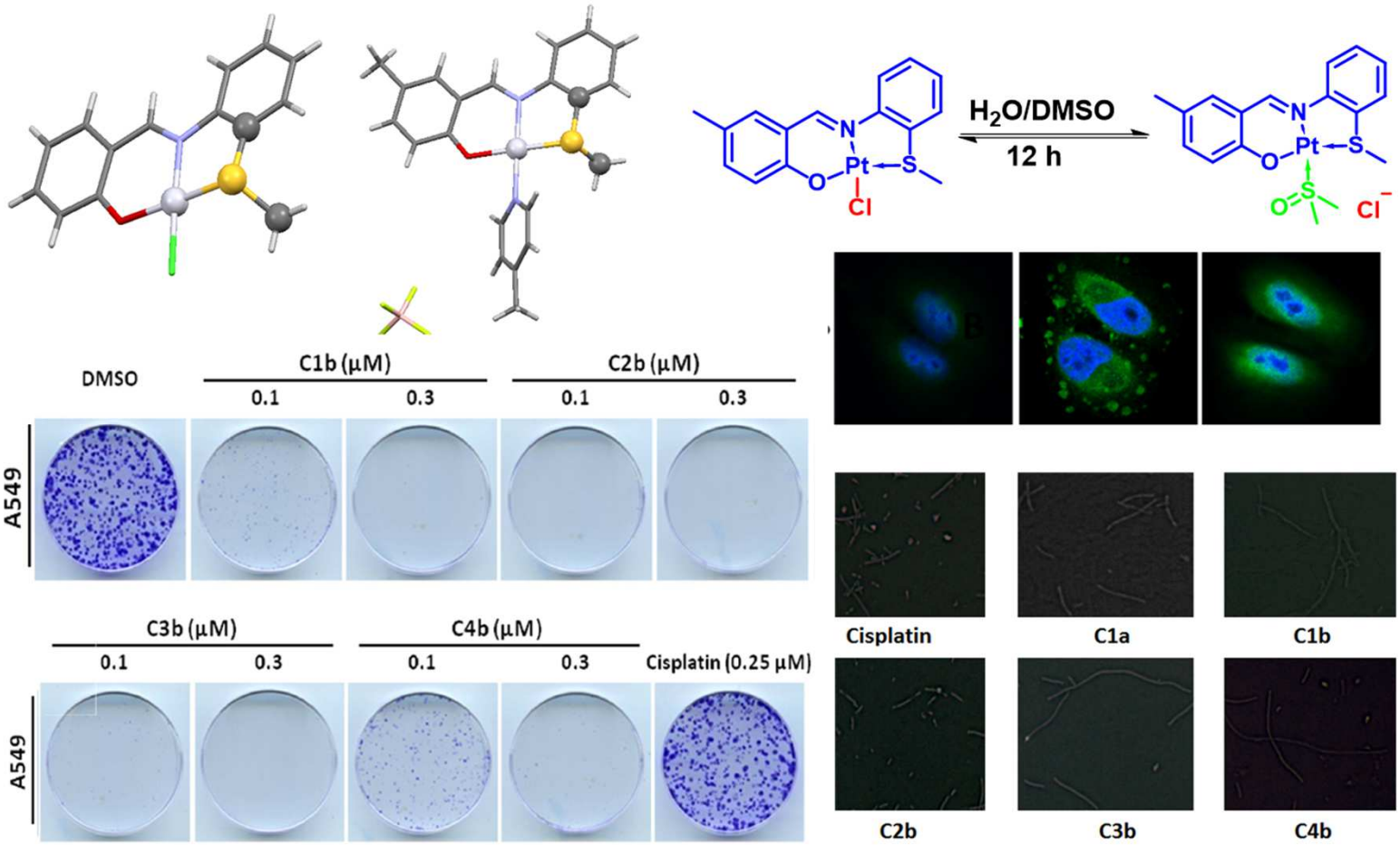


ONS-donor ligand based Pt(II) complexes with high anticancer activity were prepared. They induced autophagic cell death via LC3-I/LC3-II and recruitment of LC3B to autophagosomal membranes through activation of AKT/p21. These complexes showed strong cell growth retardation effect on *E. Coli* and resulted in filamentous morphology.

# ONS-donor ligand based Pt(II) complexes display extremely high anticancer potency through autophagic cell death pathway

Faiz-Ur Rahman[a,b,1], Amjad Ali[c,1], Hong-Quan Duong[d,1], Inam Ullah Khan[e], Muhammad Zeeshan Bhatti[c,f], Zhan-Ting Li[a], Hui Wang[a]* and Dan-Wei Zhang[a]*

[a]Center for Supramolecular Material and Catalysis, Department of Chemistry, Shanghai University, Shanghai 200444, China.

[b]Department of Chemistry, Fudan University, 2005 Songhu Road, Shanghai 200438, China

[c]Shanghai Key Laboratory of Regulatory Biology, Institute of Biomedical Sciences, School of Life Sciences, East China Normal University, 500 Dongchuan Road, Shanghai 200241, China

[d]Institute of Research and Development, Duy Tan University, K7/25 Quang Trung, Danang 57000, Vietnam.

[e]Laboratory of Molecular Immunology, State Key Laboratory of Genetic Engineering, School of Life Sciences, Fudan University, 220 Handan Road, Shanghai 200433, China.

[f]Department of Biological Sciences, National University of Medical Sciences, Rawalpindi, 46000, Pakistan.

*Corresponding Authors E-mail: zhangdw@fudan.edu.cn (D.-W. Zhang), wanghui@fudan.edu.cn (H. Wang)

Tel.: +86 21 65643576

## Abstract

The current study unveils ONS-donor ligand based Pt(II) complexes with unusual anticancer potency showing higher anticancer effect as compared to cisplatin. This series of Pt(II)(R-salicylaldimine)Cl (**C1a-C4a**) (R = 5-H, 5-$CH_3$, F, 3-$CH_3O$) complexes were prepared in single step in good isolated yields from commercially avialable materials. The chloride ancillary ligand of “a” series (**C1a-C4a**) was replaced with 4-picoline and “b” series of four complexes Pt(II)(R-

[1] F. -U. Rahman, A. Ali and H.-Q. Duong have equal contribution in this work

salicylaldimine)(4-picoline)$BF_4$ (**C1b-C4b**) (R = 5-H, 5-$CH_3$, F, 3-$CH_3O$) was obtained. All these complexes were characterized by different structure elucidation techniques. Among these, the structures of **C1a**, **C2a**, **C2b** and **C3b** were determined in solid state by single crystal X-ray analysis. We found quick aquation of "a" series of complexes in DMSO/water mixture that was well investigated by $^1$H NMNR, LCMS and ESI-MS, while "b" series of these complexes was quite stable over a month as described by the $^1$H NMNR in DMSO/$D_2O$ mixture. This ONS-donor ligand based class of Pt(II) complexes showed unusual anticancer potency in non-small cell lung cancer A549, colorectal cancer HT-29 and triple negative breast cancer MDA-MB-231 cells. These Pt(II) complexes induced PARP cleavage and significantly inhibited colony formation ability of cancer cells. Mechanistically, we found reduced aggressive growth of cancer cells by the induction of autophagic cell death via LC3-I/LC3-II expression and recruitment of LC3B to autophagosomal membrane. These complexes induced p21 expression, that suggested their potentials to suppress cell cycle progression. Significant activation of caspase3/7-dependent apoptotic signaling was observed in cancer cells treated with these Pt(II) complexes. Morphological changes of cancer cells suggested their potentials to modulate epithelial-mesenchymal-transition (EMT) like features of cancer cells. Gel electrophoresis study revealed their interaction with plasmid DNA. Similarly, strong growth retardation effect and filamentous morphology was observed in *Escherichia coli* (*E. coli*). These ONS-donor Pt(II) complexes possessed strong anticancer effect in multiple human cancer cells via activation of multiple pathways for apoptotic and autophagic cell death.

**Key words**

ONS-donor Pt(II) complexes, *In vitro* cytotoxicity, Caspase 3/7 activation, Autophagy, *E. Coli* growth.

## 1. Introduction

Platinum-based complexes have been approved as anticancer drugs (Fig. 1). According to an estimation, more than 50% of cancer treatments comprised of these platinum based drugs [1-3]. The major limitations associated with these drugs were their poor activity in certain types of cancers, inactivation by intracellular biomolecules, side effects and timely acquired or intrinsic resistance in cancer patients [4-8]. These limitations increase the need for developing new platinum-based anticancer agents with new assemblies which could increase the potency and minimize the other related limitations [9]. In designing of new platinum-based chemotherapeutic agents, emphasis was placed on the diversity of the coordinated ligands and new agents were prepared with different mode of action and favourable cytotoxicity in cancer cells as compared to the classical cisplatin [1, 10-15]. Though a number of, may be in thousands cytotoxic platinum complexes were reported but most of them were abandoned during initial clinical trials due to their inappropriate clinical effects [2, 16]. Struggles to develop novel platinum based chemotherapeutic drugs were continued for example Lippard and co-worker recently discovered a new class of monofunctional antineoplastic agents synthesized from cisplatin, finding a way to become platinum based anticancer drug candidates those showed better activities compared to the parent cisplatin [17-21].

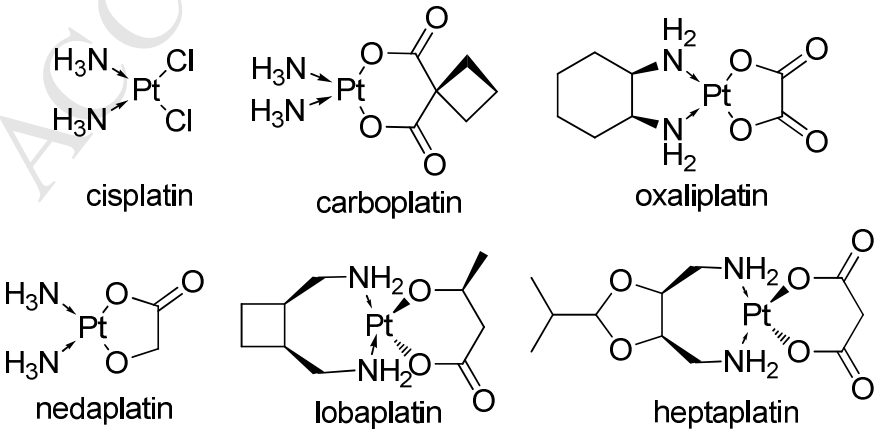

**Fig. 1** Clinically administered (approved) platinum based anticancer drugs; cisplatin, carboplatin and oxaliplatin are globally approved while nedaplatin, lobaplatin and heptaplatin are regionally approved in China, South Korea and Japan respectively.

Non-small cell lung carcinoma (NSCLC), colorectal carcinoma (CRC) and triple negative breast cancer (TNBC) are the most common and aggressive cancers develop in human body [22, 23]. Triple negative breast cancer has ability to metastasize to secondary parts of the body such as lungs, brain and colon. TNBC is a highly metastatic disease and cell from these patients often show very aggressive nature in culture. Mutations in these tumors make them highly aggressive, which is characterized by uncontrolled cell growth. Activation of growth factor receptor signaling, amplification of tumor promoting proteins and inhibition of tumor suppressor genes functions play a key role in cancer cell growth, survival and proliferation [24]. One of the hallmarks of cancer cells is to show resistance against chemotherapeutic agents due to activation of survival signaling, which in turn decreases the survival rate of cancer patients and contribute to poor prognosis[25]. Cancer cells often show less induction of apoptosis due to constant activation of multiple oncogenic signaling. Cancer cells often follow apoptotic signaling for cell death but in most cases, cell death also occurs through induction of autophagy[26, 27]. Autophagy is the alternative mechanism for cancer cell death, in which autophagosome play critical role in cell death. Activation of LC3-I and LC3-II proteins represents activation of autophagy mediated cell death[26].

Cancer patients showing resistance to conventional chemotherapeutic or other targeted therapies such as endocrine therapy and immunotherapy finally succumb to metastatic disease, which is one of the leading cause of cancer related mortality [28]. Currently, several anticancer agents are in clinical trials due to their cytotoxicity towards cancer cells. However, in most cases these agents display several side effects and therefore most of the clinical trials failed [2, 29, 30].

Therefore, identification and characterization of novel chemotherapeutic agents are considered important in clinical trials for more effective treatment and prolong survival of cancer patients. The final goal of these treatments is to reduce tumor burden and prevent recurrence and relapse.

An important property of S-donor ligand is the incorporation of chirality on sulfur center after coordination with metal [31-33]. The neighboring group attached to sulfur affect the R or S stereoisomer formation on sulfur center. If the attached alkyl group is achiral like phenyl and methyl (methyl phenyl thioether) there is always expected a racemic mixture of R and S stereoisomers [34]. The presence of a neighboring chiral center attached to sulfur increase the particular anti or syn stereoisomers formation after coordination with metal [33]. This property of chirality on sulfur on a S-donor ligand was reported in a number of important metal catalyzed chiral catalysis [35]. Similarly, the already chiral sulfoxide ligand were also reported in some studies that retained its particular chirality after coordination with metal and functioned as chiral catalyst [36, 37]. Salicylaldimine based related ligand bearing such chirality or incorporation of chirality on S-donor atom after coordination with metal was observed but up to our knowledge it was not discussed previously [25, 38-41].

Salicylaldimine chelating ligands are important assemblies for the synthesis of a number of metal complexes, some of them were studied for their biological properties [42-45]. Platinum complexes of salicylaldimine ligands were mostly reported for their photo physical properties [46-49]. There are limited examples of platinum complexes based on salicylaldimine ligands with anticancer effect [50]. Heteroliptic Pt(II) complexes of salicylaldimine and cyclooctene co-ligands were reported for better anticancer effect in brain cancer [51]. We recently dedicated our efforts to the synthesis and characterization of salicylaldimine based mixed ligands Pt(II) complexes with anticancer activities, genes activation and effective bacterial growth retardation

[52-57]. We established easy, productive and reproducible synthetic methodologies for these complexes from commercially available raw materials. In search of potent Pt(II) anticancer agents we continued our efforts to explore further structurally modified salicylaldimine based complexes and their anticancer properties.

In the current study we synthesized ONS-donor salicylaldimine ligand based Pt(II) complexes and structurally characterized them in details. Further, we have identified these Pt(II) complexes for their potent *in vitro* anticancer effect in multiple human cancer cells. Several mechanistic assays were conducted to investigate and compare their potency with market available anticancer drug cisplatin. They induced significant cancer cell death via activation of autophagy and caspase3/7-dependent signalling. Superior growth retardation effect and filamentous morphology was observed in *Escherichia coli* (*E. coli)* as compared to cisplatin.

## 2. Materials and methods

### 2.1. General experimental and materials (chemistry)

All analytical grade solvents and reagents were purchased from commercial sources and used without further purification unless otherwise mentioned. $K_2PtCl_4$ was purchased from Energy Chemical Company Shanghai. $^{1}H$, $^{19}F$ and $^{13}C$ NMR analyses were conducted on bruker AVANCE III HD 400 MHz spectrophotometer at room temperature (298 K) in $CDCl_3$, $D_2O$ or DMSO-$d_6$. LC-MS and HR-ESI MS analyses were performed on Agilent LC coupled with HR-MS machine Bruker micrOTOF II. X-ray data were collected on a Bruker APEX DUO diffractometer with graphite-monochromatized Mo Kα radiation (λ= 0.71073 Å). All the structures were solved by Direct Method of SHELXS-97 and refined by full-matrix least squares techniques using the SHELXL-97 program within WINGX.[58, 59] Non-hydrogen atoms of the

crystallized compounds were refined with anisotropic temperature parameters. The hydrogen atoms attached to carbons were generated geometrically. Crystallographic data for **C1a**, **C2a**, **C2b** and **C3b**, CCDC 1482361-1482364, can be obtained from Cambridge Crystallographic Data Center 12 Union Road, Cambridge CB2 1EZ, UK; tel: +44-1223336408; fax: +44-1223336003; e-mail: deposit@ccdc.cam.ac.uk.

*2.1.1. General procedure for the synthesis of ligands (**L1** - **L4**)*

1 mmol of particular salicylaldehyde and 1 mmol of 2-(methylthio)aniline were taken in 10 mL of $CH_2Cl_2$/MeOH (1:1) mixture. The reaction mixture was stirred at 50 °C for 10 h. After completion the mixture was dried with anhydrous sodium sulfate and vacuum evaporated. **L1–L4** were recrystallized from cold ethanol in freezer and characterized as below. Spectroscopic characterization data were given below and original spectra were given in the ESI.

**L1**[25], Yield and spectroscopic analysis results were similar as reported previously. $^1$H NMR (400 MHz, CDCl3) δ 8.6 (s, 1H), 7.47 – 7.37 (m, 2H), 7.32 – 7.27 (m, 2H), 7.24 – 7.16 (m, 2H), 7.1 (d, J = 8.2 Hz, 1H), 7.0 (t, J = 7.4 Hz, 1H), 2.5 (s, 3H).

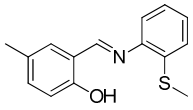


L2

**L2**, 63% isolated yield, yellow solid. $^1$H NMR (400 MHz, DMSO-$d_6$) δ 12.7 (s, 1H), 8.9 (s, 1H), 7.4 (s, 1H), 7.4 (d, *J* = 7.7 Hz, 1H), 7.34 – 7.26 (m, 2H), 7.26 – 7.18 (m, 2H), 6.9 (d, *J* = 8.4 Hz, 1H), 2.4 (s, 3H), 2.3 (s, 3H). $^{13}$C NMR (100 MHz, DMSO-$d_6$) δ 163.1, 158.5, 145.0, 134.9, 134.7, 133.0, 128.1, 128.0, 125.6, 125.0, 119.4, 118.0, 117.0, 20.4, 14.2. HRMS (ESI): Calcd for $C_{14}H_{13}NOSNa$ 280.0772: $[M+Na]^+$, Found: 280.0767.

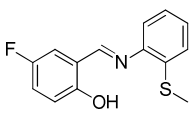


L3

**L3**, 78% isolated yield, yellowish orange solid. $^{1}$H NMR (400 MHz, DMSO-$d_6$) δ 12.7 (s, 1H), 8.9 (s, 1H), 7.5 (dd, *J* = 8.9, 3.2 Hz, 1H), 7.4 (d, *J* = 7.8 Hz, 1H), 7.35 – 7.20 (m, 4H), 7.0 (dd, *J* = 9.0, 4.5 Hz, 1H), 2.5 (s, 3H). $^{19}$F NMR (376 MHz, DMSO-$d_6$) δ -125.1 - -125.2 (m). $^{13}$C NMR (100 MHz, DMSO-$d_6$) δ 161.9, 161.9, 156.9, 155.3 (d, *J* = 234.5 Hz), 144.7, 135.1, 128.4, 125.4 (d, *J* = 54.5 Hz), 120.9 (d, *J* = 23.6 Hz), 119.9 (d, *J* = 7.7 Hz), 118.5 (d, *J* = 7.7 Hz), 118.0, 117.7 (d, *J* = 23.4 Hz), 14.2. HRMS (ESI): Calcd for $C_{14}H_{12}NFOSNa$ 284.0521: $[M+Na]^+$, Found: 284.0528

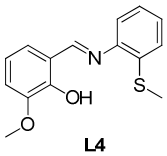


L4

**L4**, 87% isolated yield, red solid. $^{1}$H NMR (400 MHz, DMSO-$d_6$) δ 13.1 (s, 1H), 8.9 (s, 1H), 7.4 (d, *J* = 7.8 Hz, 1H), 7.34 – 7.29 (m, 2H), 7.26 – 7.20 (m, 2H), 7.1 (d, *J* = 7.9 Hz, 1H), 6.9 (t, *J* = 7.9 Hz, 1H), 3.8 (s, 3H), 2.4 (s, 3H). $^{13}$C NMR (100 MHz, DMSO-$d_6$) δ 163.4, 150.9, 148.4, 144.7, 134.9, 128.2, 125.6, 125.1, 124.6, 119.6, 119.1, 118.0, 116.2, 56.3, 14.2. HRMS (ESI): Calcd for $C_{15}H_{15}NO_2SNa$ 296.0721: $[M+Na]^+$, Found: 296.0704.

### *2.1.2. General procedure for the synthesis of* ***C1a–C4a***

$K_2PtCl_4$ (0.05 mmol) was taken in 1 mL of DMSO and 5 mL of methanol and stirred vigorously to dissolve the solid at room temperature. Particular ligand (**L1 - L4**), 0.05 mmol and NaOAc (0.05 mmol) were dissolved in 15 mL of MeOH in a 50 mL round bottom flask and heated to reflux. $K_2PtCl_4$ solution prepared previously was added to it in one portion and the mixture was stirred at reflux for 24 h. After completion, the mixture was cooled to rt and volatiles were evaporated to minimum volume (approx. 2 mL). 10 mL of water was added to the flask with constant stirring. The yellow to orange precipitate formed was filtered, washed with water and

dried in air. The solid complex (**C1a-C4a)** was further recrystallized form $CH_2Cl_2$-n-hexane and characterized as below. Spectroscopic characterization data were given below while the original spectra were given in the ESI.

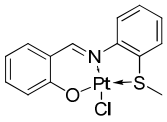


**C1a**

**C1a**, 78% yield, yellow solid. $^1$H NMR (400 MHz, DMSO-$d_6$) δ 9.6 (s, $J_{Pt-H}$ = 64 Hz 1H), 8.4 (d, $J$ = 8.6 Hz, 1H), 8.1 (d, $J$ = 7.7 Hz, 1H), 7.9 (d, $J$ = 6.9 Hz, 1H), 7.6 (t, $J$ = 7.6 Hz, 2H), 7.48 (t, $J$ = 7.5 Hz, 1H), 7.0 (d, $J$ = 8.6 Hz, 1H), 6.8 (t, $J$ = 7.4 Hz, 1H), 2.9 (s, 3H). $^{13}$C NMR (100 MHz, DMSO-$d_6$) δ 163.0, 153.5, 153.1, 137.2, 136.4, 132.0, 131.9, 129.8, 129.2, 121.1, 121.0, 119.0, 117.3, 28.4. HRMS (ESI): Calcd for $C_{14}H_{12}ClNOPtSNa$ 494.9874: $[M+Na]^+$, Found: 494.9869.

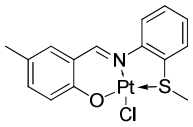


**C2a**

**C2a**, 81% isolated yield, yellow solid. $^1$H NMR (400 MHz, DMSO-$d_6$) δ 9.6 (s, $J_{Pt-H}$ = 64 Hz, 1H), 8.4 (d, $J$ = 8.5 Hz, 1H), 8.1 (d, $J$ = 7.8 Hz, 1H), 7.6 (s, 1H), 7.6 (t, $J$ = 7.3 Hz, 1H), 7.51 – 7.38 (m, 2H), 6.9 (d, $J$ = 8.7 Hz, 1H), 2.9 (s, 3H), 2.3 (s, 3H). $^{13}$C NMR (100 MHz, DMSO-$d_6$) δ 161.5, 153.1, 153.0, 139.0, 134.8, 132.0, 131.9, 129.6, 129.1, 125.5, 120.9, 120.6, 118.8, 28.3, 20.1. HRMS (ESI): Calcd for $C_{15}H_{14}ClNOPtSNa$ 509.0030: $[M+Na]^+$, Found: 509.0020.

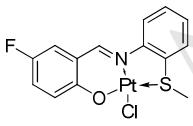


**C3a**

**C3a**, 83% yield, orange solid. $^1$H NMR (400 MHz, DMSO-$d_6$) δ 9.66 (s, $J_{Pt-H}$ = 68 Hz, 1H), 8.40 (d, $J$ = 8.5 Hz, 1H), 8.10 (d, $J$ = 7.7 Hz, 1H), 7.68 (d, $J$ = 9.6 Hz, 1H), 7.62 (t, $J$ = 7.8 Hz, 1H),

7.56 – 7.46 (m, 2H), 7.00 (dd, *J* = 9.3, 4.6 Hz, 1H), 2.90 (s, 3H). $^{19}$F NMR (376 MHz, DMSO-$d_6$) δ -129.0 - 129.2 (m). $^{13}$C NMR (100 MHz, DMSO-$d_6$) δ 159.8, 153.6 (d, *J* = 231 Hz), 152.8, 152.8, 152.8, 132.1, 132.0, 129.7 (d, *J* = 58.3 Hz), 125.7 (d, *J* = 25.0 Hz), 122.6 (d, *J* = 7.9 Hz), 119.8 (d, *J* = 3.0 Hz), 118.9, 118.3 (d, *J* = 22.6 Hz), 28.3. HRMS (ESI): (ESI): Calcd for $C_{14}H_{11}ClFNOPtSNa$ 512.9779: $[M+Na]^+$, Found: 512.9769.

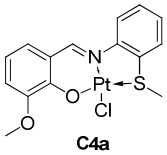


**C4a**

**C4a**, 87% isolated yield, reddish orange solid. $^1$H NMR (400 MHz, DMSO-$d_6$) δ 9.6 (s, $J_{Pt-H}$ = 60 Hz, 1H), 8.4 (d, *J* = 8.6 Hz, 1H), 8.1 (d, *J* = 7.8 Hz, 1H), 7.6 (t, *J* = 7.7 Hz, 1H), 7.5 – 7.4 (m, 2H), 7.2 (d, *J* = 7.3 Hz, 1H), 6.7 (t, *J* = 7.9 Hz, 1H), 3.8 (s, 3H), 2.9 (s, 3H). $^{13}$C NMR (100 MHz, DMSO-$d_6$) δ 154.7, 153.2, 153.1, 151.0, 132.0, 131.9, 129.6, 129.2, 127.3, 121.0, 118.9, 116.5, 116.4, 56.2, 28.4. HRMS (ESI): (ESI): Calcd for $C_{15}H_{14}ClNO_2PtSNa$ 524.9979: $[M+Na]^+$, Found: 524.9953.

### *2.1.3. General procedure for the synthesis of **C1b–C4b***

A mixture of 0.05 mmol of particular complex (**C1a** to **C4a)** and 0.05 mmol of $AgBF_4$ was stirred in 10 mL $CH_3CN$ at 60 °C for 2 h. Solid AgCl precipitated was filtered from the mixture through celite. The yellowish filtrate collected was evaporated to dryness and a yellow solid was obtained. It was added with 10 mL of $CH_2Cl_2$ and excess (2 drops) of 4-picoline. This mixture was stirred at rt for 24 h and evaporated. The yellow to orange solid recovered was dissolved in $CH_2Cl_2$ and passed through a 2 × 5 cm silica column eluted with 1 % $CH_3OH$-$CH_2Cl_2$. After evaporation of the volatile a yellow to orange solid for each complex (**C1b-C4b)** was recovered.

The solid was further recrystallized form $CH_2Cl_2$-n-hexane and characterized. Spectroscopic characterization data were given below while the original spectra were given in the ESI.

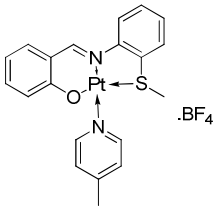


C1b

**C1b**, 73% isolated yield, orange solid. $^1$H NMR (400 MHz, DMSO-$d_6$) δ 9.5 (s, 1H), 8.8 (d, $J$ = 6.6 Hz, 2H), 8.5 (d, $J$ = 8.5 Hz, 1H), 8.1 (d, $J$ = 7.9 Hz, 1H), 8.0 (d, $J$ = 8.1 Hz, 1H), 7.7 – 7.65 (m, 1H), 7.64 – 7.6 (m, 3H), 7.5 (t, $J$ = 7.5 Hz, 1H), 7.0 (d, $J$ = 8.5 Hz, 1H), 6.9 (t, $J$ = 7.0 Hz, 1H), 2.8 (s, 3H), 2.5 (s, 3H). $^{19}$F NMR (376 MHz, DMSO-$d_6$) δ -148.2, -148.3. $^{13}$C NMR (100 MHz, DMSO-$d_6$) δ 162.7, 156.3, 153.4, 152.8, 152.0, 138.1, 136.9, 132.6, 132.3, 130.3, 128.3, 127.3, 121.3, 120.6, 119.4, 118.3, 28.7, 21.2. HRMS (ESI): Calcd for $C_{20}H_{19}N_2OPtS$ 530.0866: $[M\text{-}BF_4]^+$, Found: 530.0870.

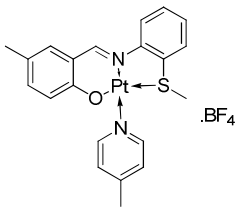


C2b

**C2b**, 79% isolated yield, yellowish organge solid. $^1$H NMR (400 MHz, DMSO-$d_6$) δ 9.4 (s, 1H), 8.8 (d, $J$ = 6.5 Hz, 2H), 8.5 (d, $J$ = 8.6 Hz, 1H), 8.1 (d, $J$ = 7.8 Hz, 1H), 7.7 (s, 1H), 7.7 (t, $J$ = 7.4 Hz, 1H), 7.6 (d, $J$ = 6.3 Hz, 2H), 7.5 (t, $J$ = 7.5 Hz, 1H), 7.5 (d, $J$ = 8.8 Hz, 1H), 6.9 (d, $J$ = 8.7 Hz, 1H), 2.8 (s, 3H), 2.5 (s, 3H), 2.3 (s, 3H). $^{19}$F NMR (376 MHz, DMSO-$d_6$) δ -148.2, -148.3. $^{13}$C NMR (100 MHz, DMSO-$d_6$) δ 161.2, 155.8, 153.4, 152.9, 152.0, 139.8, 135.4, 132.6, 132.3, 130.1, 128.3, 127.2, 126.6, 120.8, 120.4, 119.2, 28.6, 21.2, 20.1. HRMS (ESI): Calcd for $C_{21}H_{21}N_2OPtS$ 544.1022: $[M\text{-}BF_4]^+$, Found: 544.1034.

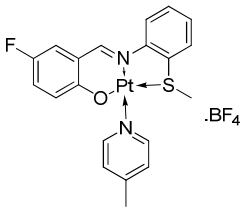


C3b

**C3b**, 68% yield, yellow solid. $^{1}$H NMR (400 MHz, DMSO-$d_6$) δ 9.5 (s, 1H), 8.8 (d, $J$ = 6.5 Hz, 2H), 8.4 (d, $J$ = 8.6 Hz, 1H), 8.2 (d, $J$ = 7.9 Hz, 1H), 7.8 (dd, $J$ = 9.5, 3.2 Hz, 1H), 7.7 (t, $J$ = 7.9 Hz, 1H), 7.64 – 7.50 (m, 4H), 7.0 (dd, $J$ = 9.4, 4.7 Hz, 1H), 2.8 (s, 3H), 2.5 (s, 3H). $^{19}$F NMR (376 MHz, DMSO-$d_6$) δ -127.6 – -127.8 (m), -148.2, -148.3. $^{13}$C NMR (100 MHz, DMSO-$d_6$) δ 159.6, 155.7, 154 (d, $J$ = 232.0 Hz), 153.5, 152.8, 152.0, 132.6, 132.4, 130.5, 128.3, 127.5, 126.5 (d, $J$ = 25.0 Hz), 122.3 (d, $J$ = 7.9 Hz), 120.2 (d, $J$ = 8.8 Hz), 119.3, 118.9 (d, $J$ = 22.8 Hz), 28.7, 21.2. HRMS (ESI): Calcd for $C_{20}H_{18}FN_2OPtS$ 548.0772: $[M\text{-}BF_4]^+$, Found: 548.0772.

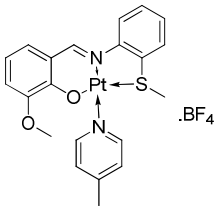


C4b

**C4b**, 82% isolated yield, orange solid. $^{1}$H NMR (400 MHz, DMSO-$d_6$) δ 9.4 (s, 1H), 8.8 (d, $J$ = 6.1 Hz, 2H), 8.4 (d, $J$ = 8.6 Hz, 1H), 8.1 (d, $J$ = 7.8 Hz, 1H), 7.6 (t, $J$ = 7.7 Hz, 1H), 7.6 (d, $J$ = 5.9 Hz, 2H), 7.5 (t, $J$ = 7.5 Hz, 1H), 7.4 (d, $J$ = 8.2 Hz, 1H), 7.2 (d, $J$ = 7.3 Hz, 1H), 6.8 (t, $J$ = 7.9 Hz, 1H), 3.8 (s, 3H), 2.8 (s, 3H), 2.5 (s, 3H). $^{19}$F NMR (376 MHz, DMSO-$d_6$) δ -148.2, -148.3. $^{13}$C NMR (100 MHz, DMSO-$d_6$) δ 155.8, 154.0, 153.4, 152.8, 151.9, 150.3, 132.6, 132.4, 130.2, 128.2, 127.6, 127.1, 121.2, 119.2, 117.5, 117.5, 56.6, 28.8, 21.2. HRMS (ESI): Calcd for $C_{21}H_{21}N_2O_2PtS$ 560.0971: $[M\text{-}BF_4]^+$, Found: 560.0975.

## 2.2. General experimental (Biology)

### *2.2.1. Cell culture and reagents*

Non-small cell lung cancer (A549), colorectal cancer (HT-29) and triple negative breast cancer (MDA-MB-231) cells were purchased from American Type Culture Collection (ATCC, Manassas, VA). HT-29 cells were cultured in McCoy's 5A supplemented with 10% heat-inactivated fetal bovine serum (HI-FBS; Gibco, Life Technologies, Naerum, Denmark) and 100 units/mL penicillin/streptomycin. MDA-MB-231 and A549 cells were cultured in DMEM supplemented with 10% HI-FBS, 1% glutamine and 100 units/mL penicillin/streptomycin.

### *2.2.2. MTS assay*

HT-29, MDA-MB-231 or A549 Cells counted by the TC20$^{TM}$ Automated Cell Counter (Bio-Rad, Pleasanton, CA, USA) were plated in 96-well flat bottom plates at a density of 2000 cells per well in triplicate and then treated with various concentrations (0, 1, 3, 5 and/or 10 µM) of each complexes (**C1a**, **C1b**, **C2a**, **C2b**, **C3a**, **C3b**, **C4a** and/or **C4b**) or cisplatin (10 µM) for 72 h. Cell viability was determined using the MTS assay reagent (CellTiter 96 AQueous one Solution Cell proliferation Assay; Promega, Madison, WI, USA) according to the manufacturer's protocol. The absorbance was measured at 490 nm using a Wallac Victor$^2$ 1420 Multilabel counter (Perkin Elmer, Wellesley, MA). Measurements were performed and the concentration required for a 50% inhibition of viability ($IC_{50}$) was determined graphically. Standard Graph was plotted by taking concentration of the complexes and relative cell viability. Percentage of cell survival in the untreated condition was designated as 100%. Relative cell viability = (experimental absorbance-background absorbance)/(absorbance of untreated control-background absorbance) x 100%.

*2.2.3. Clonogenic assay*

HT-29 and A549 cells were seeded in 60 cm dishes at a density of 3000 cells per dish in duplicate. 24 h after plating, various concentrations (0, 0.1, and/or 0.3 µM) of each complex (**C1b**, **C2b**, **C3b** and/or **C4b**) or cisplatin (0.25 µM) were added to each dish. After treatment for 24 h, cells were washed by PBS and further incubated for 15 days. Cells were subsequently stained with 0.5% crystal violet in 25% methanol-containing PBS. Colonies were examined under a light microscope and counted after capturing images, as described [60]

*2.2.4. Western blot analysis*

HT-29 or A549 cells were grown to ~70% confluency and reagents were added as indicated concentrations. Cells were lysed in a buffer containing 20 mM Tris-HCl, 0.5 M NaCl, Triton X-100, 1 mM EDTA, 1 mM EGTA, 10 mM β-glycophosphate, 10 mM NaF, 300 µM $Na_3VO_4$, 1 mM Benzamidine, 2 µM PMSF, and 1 mM DTT. The protein concentration was determined using the BCA protein assay (Thermo Scientific, Rockford, IL, USA). Proteins were separated on SDS-PAGE, transferred on to PVDF membrane, blocked in 5% nonfat milk and probed with the following antibodies: phospho-ERK1/2 (Y202/T204), phospho-AKT (S473), PARP, GAPDH and AKT (Cell Signaling Technology, Boston, MA, USA), ERK1/2 and p21 (Santa Cruz Biotechnology, Santa Cruz, CA, USA) and LC3B (Thermo Scientific). Then, the membranes were incubated with horseradish peroxidase (HRP)-conjugated secondary antibodies (Amersham Biosciences, GE Healthcare, Piscataway, NJ, USA) for 1.5 h. Signals were revealed by chemiluminescence (Thermo Scientific) according to the manufacturer's recommendation and exposed with X-ray film (Thermo Scientific).

*2.2.5. Caspase-3/7 activity assay*

Caspase-3/7 activities were quantified using the Caspase-3/7 Glo Assay (Promega) according to the manufacturer's protocol. HT-29 or A549 Cells were treated with various concentrations (0, 1 and/or 3 µM) of each complex (**C1b**, **C2b**, **C3b** and/or **C4b**) or cisplatin (10 µM) for 24 h and Caspase-3/7 activities were quantified from cell lysates. Luminescence was measured at 490 nm using Wallac Victor$^2$ 1420 Multilabel counter (Perkin Elmer). Luminescence values in vehicle-treated control samples were set to 1 and values obtained in other experimental conditions were relative to that.

*2.2.6. Immunofluorescences*

A549 cells ($1.5 \times 10^5$ per well of six-well plates) were seeded onto cover slip. Cells were untreated or treated with **C2b** (3 µM) or cisplatin (10 µM) for 18 h. After then, cells were rinsed with ice-cold PBS and fixed with 4% paraformaldehyde for 15 minutes at room temperature followed by permeabilization with 0.25% Triton X-100 for 10 minutes at room temperature. Cells were then incubated with 1% BSA for 45 minutes and subsequently incubated with primary antibodies for overnight at 4 °C followed by 1 h of incubation at room temperature with FITC-conjugated secondary antibodies. Images were acquired with the confocal system of Leica SP5 inverted microscope (Leica Microsystems, Wetzlar, Germany).

*2.2.7. Immunofluorescences*

Statistical comparisons were made using the two-tailed student's *t*-test where appropriate. Results were considered significant in all experiments at * means $P < 0.05$, ** means $P < 0.01$ and *** means $P < 0.001$. Data were expressed as the mean ± SD of the mean.

## 3. Results

### 3.1. Chemistry

#### *3.1.1. Synthesis and structure elucidation*

The new series of Pt(II) complexes of ONS-donor substituted salicylaldimine ligands viz Pt(II)(salicylaldimine)Cl (**C1a**), Pt(II)(5-methylsalicylaldimine)Cl (**C2a**), Pt(II)(5-fluorosalicylaldimine)Cl (**C3a**) and Pt(II)(3-methoxysalicylaldimine)Cl (**C4a**) were prepared in excellent isolated yields (Scheme 1). Chloride ancillary ligand in **C1a**-**C4a** was further exchanged with 4-picoline. **C1a**-**C4a** was treated with an equivalent amount of $AgBF_4$ and excess 4-picoline subsequently and a new series of four complexes i.e. Pt(II)(salicylaldimine)(picoline)$BF_4$ (**C1b**), Pt(II)(5-methylsalicylaldimine)(picoline)$BF_4$ (**C2b**), Pt(II)(5-fluorosalicylaldimine)(picoline)$BF_4$ (**C3b**) and Pt(II)(3-methoxysalicylaldimine)(picoline)$BF_4$ (**C4b**) were obtained in excellent isolated yields (Scheme 1). The structures of all ligands and complexes were characterized by $^{1}H$, $^{19}F$ and $^{13}C$ NMR spectroscopy and high-resolution electrospray ionization (HR-ESI) mass spectrometry (ESI Fig. S9-48). Structures of **C1a**, **C2a**, **C2b** and **C3b** were determined by single crystal X-ray analysis.

In case of each ligand (L1-L4), we can observe the phenolic OH proton chemical shift in the most downfield region 12.7-13.12 ppm for **L1**-**L4**. The imine proton chemical shifts for these ligands were also observed in nearly similar region (8.6-8.9 ppm). The other prominent peak of methyl attached to sulfur atom was similar in all ligand and observed around 2.45 ppm. When each ligand was reacted with $K_2PtCl_4$ and **C1a**-**C4a** were prepared we observed the disappearance of phenolic "OH" proton for each ligand, showing the covalent bond formation between Pt(II) and O atoms. similarly clear changes were observed in the imine proton chemical shift which was shifted about 1 ppm up-field in each complex as compared to the respective

ligand. The $CH_3$ protons chemical shift of the methyl group attached to S atom was also shifted about 0.4 ppm downfield as compared to the chemical shift observed in case of each free ligand (**L1**-**L4**), showing the coordination of Pt(II) with S atom. The other aromatic protons were also shifted little up or down field. In case of "b" series of complexes we found three new chemical shifts two doublet peaks in the aromatic regions around 8.82 and 7.62 ppm each for two protons of the pyridine part of 4-picoline and one singlet peak around 2.48 ppm for three proton of the methyl group of 4-picoline. This showed the coordination of one 4-picoline as co-ligand to Pt(II) center. $^{13}C$ NMR peaks of each ligand and complex showed similar trend. The imine carbon peak was observed the most downfield for each ligand and Pt(II) complex. Each carbon chemical shift was shifted little up or down field in "a" series of complexes as compared to the respective ligand and all these peaks were found similar in "b" series of complexes. In "b" series three new signals in the aromatic region were observed, assigned to pyridine part and one in the up field region assigned to methyl carbon of the co-ligand 4-picoline.

Each symmetrical salicylaldimine ligand (**L1**-**L4**) coordinate with Pt metal and gave a racemic mixture of asymmetric complex (**C1a**-**C4a**) bearing S-donor atom as stereo-center. Both these stereo-isomers can be observed in the single crystal packing of **C1a**, **C2a**, **C2b** and **C3b** (Fig. 3). The selectivity for a particular stereoisomer is difficult to optimize and similarly isolation of these isomers may also be difficult.

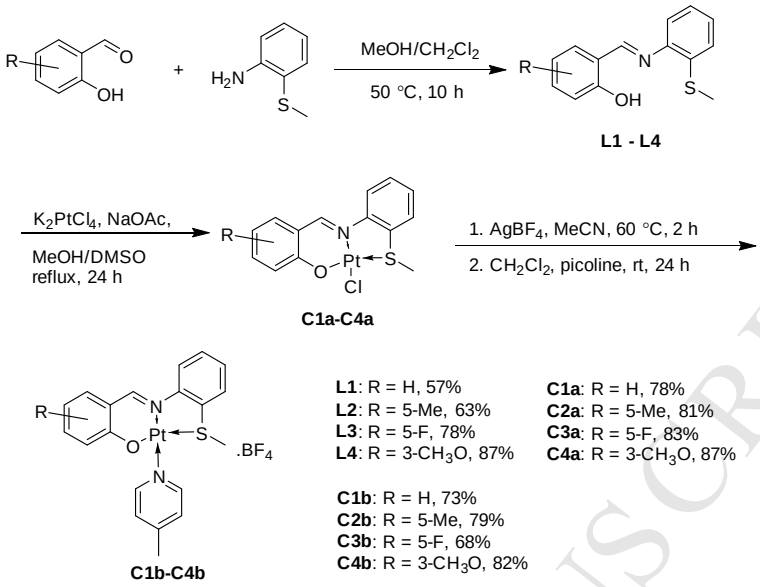


**Scheme 1.** Synthetic route for **L1-L4**, **C1a-C4a** and **C1b-C4b**

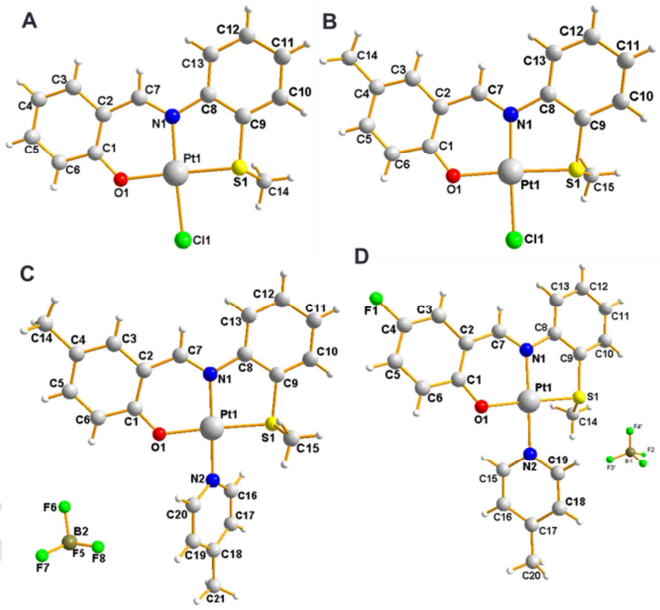


**Fig. 2.** Single crystal plot of (A) **C1a**, (B) **C2a**, (C) **C2b** and (D) **C3b**.

### *3.1.2. Single crystal description of **C1a**, **C2a**, **C2b** and **C3b***

X-ray quality crystals of **C1a**, **C2a**, **C2b** and **C3b** were grown from $CH_2Cl_2$–n-hexane solution of these complexes. The ORTEP plot of these crystals was displayed in Fig. 2. The crystal

structure refinement parameters for these complexes are summarized in ESI table S1 and structure plots of these complexes were displayed in ESI Fig S5-8. All these complexes crystalized in monoclinic crystal systems where Pt adopts square planner symmetry. The single crystal packing of each complex was consisted of racemic mixture of R and S stereoisomers with S donor atom of salicylaldimine as stereo center (Fig. 3). Three peripheries of Pt in **C1a** and **C2a** were occupied by ONS-donor atoms of salicylaldimine ligand and the fourth position was occupied by ancillary chloride that occupied *trans* position to salicylaldimine N-donor atom. **C2b** and **C3b** symmetry was similar to the fore-mentioned except the ancillary $Cl^-$ was replaced by 4-picoline. Selected bond lengths, angles and torsion angles of **C1a**, **C2a**, **C2b** and **C3b** were summarized in Table 1. The sum of bond angles around Pt in all these complexes was *ca.* 360º (Table 1). The bond lengths of the donor atoms of the salicylaldimine ligand and Pt center were comparable in all these complexes (Table 1 entry 1-3). The bond length between Pt(1) and ancillary Cl(1) in **C1a** and **C2a** were quiet matching (Table 1 entry 4) while in **C2b** and **C3b** the bond length between Pt(1) and N(2) were equal (Table 1 entry 4). The bond angles among donor atoms in **C1a** and **C2a** showed similarity. Similarly, **C2b** and **C3b** were similar while the bond angles of complexes in both these group were quite different from each other. ONS-salicylaldimine donor ligand in all these complexes occupied almost planner symmetry around Pt(II) center.

**Table 1.** Selected bond length (Å), angles (°) of **C1a, C2a, C2b** and **C3a**

| Entry | Bond/Angle | C1a | C2a | C2b | C3b |
|---|---|---|---|---|---|
| *Bond length* (Å) | | | | | |
| 1 | Pt(1)-O(1) | 1.991(4) | 1.989(5) | 1.956(6) | 1.977(3) |
| 2 | Pt(1)-N(1) | 1.995(5) | 1.975(5) | 1.988(7) | 1.983(4) |
| 3 | Pt(1)-S(1) | 2.2136(17) | 2.212(2) | 2.226(3) | 2.2227(15) |
| 4 | Pt(1)-Cl(1)/N(2) | 2.322(2) | 2.319(2) | 2.039(7) | 2.039(4) |
| *Bond angle* (°) | | | | | |
| 5 | ∠O(1)-Pt(1)-N(1) | 94.17(19) | 94.9(2) | 93.8(3) | 94.99(14) |
| 6 | ∠O(1)-Pt(1)-S(1) | 176.06(15) | 177.02(14) | 176.44(18) | 177.75(10) |
| 7 | ∠N(1)-Pt(1)-S(1) | 87.25(15) | 87.48(16) | 88.0(2) | 86.92(11) |

| | | | | | |
|---|---|---|---|---|---|
| 8 | ∠O(1)-Pt(1)-Cl(1)/N(2) | 88.56(14) | 88.13(14) | 85.3(3) | 85.54(14) |
| 9 | ∠N(1)-Pt(1)-Cl(1)/N(2) | 177.27(14) | 176.86(16) | 178.3(3) | 175.98(15) |
| 10 | ∠S(1)-Pt(1)-Cl(1)/N(2) | 90.03(7) | 89.47(7) | 92.9(2) | 92.64(11) |

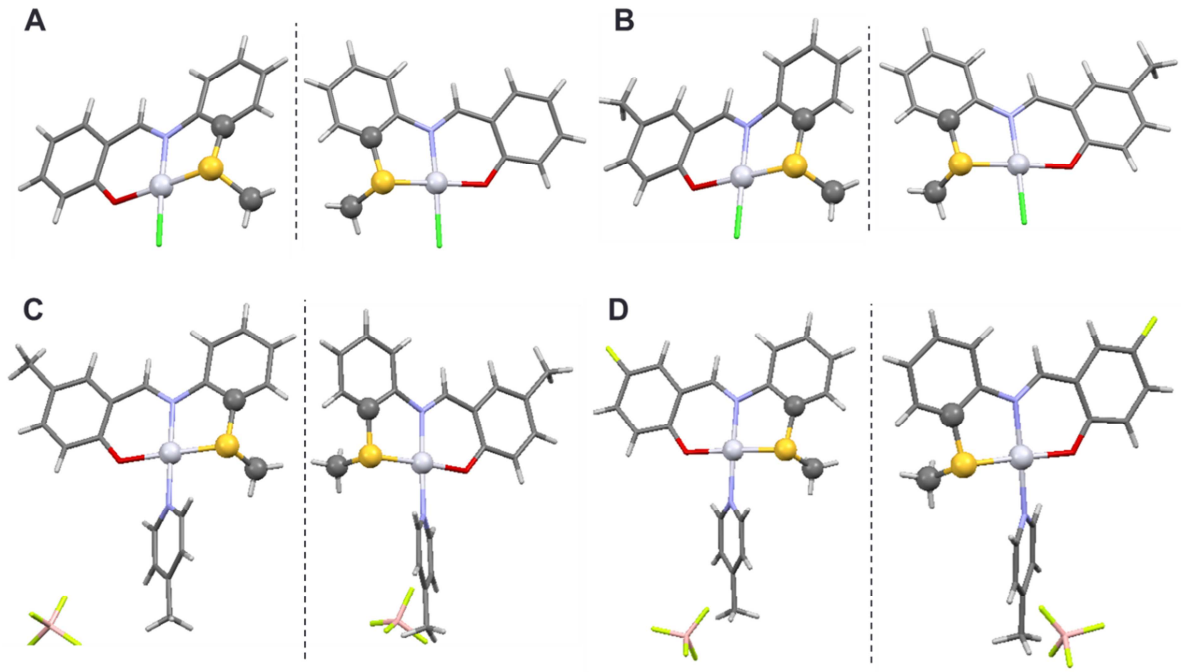


**Fig. 3** Single crystal plot of *R* and *S* stereo isomers observed in single crystal packing (A) **C1a**, (B) **C2a**, (C) **C2b** and (D) **C3b**, S donor atom having a lone pair and three different atoms (Pt(1), C(9) and C(14/15)) attached showed stereo- isomerism.

### *3.1.3. Stability/aquation of reference complexes **C2a** and **C2b***

Platinum complexes and approved platinum-based drugs have low or no solubility in water or cell culture media therefore their stock solutions are prepared in dimethyl sulfoxide (DMSO) or other organic solvent for their *in vitro* or *in vivo* biological screening [61]. Similarly platinum anticancer complexes were exposed to aquation in solution state and in most cases the ancillary chloride is exchanged by water or any donor co-solvent like DMSO so the solution based investigation of their stability or aquation is important and it also affect the biological properties of a platinum complexes [62, 63]. The ultimate target of platinum complexes is DNA or other

biomolecules that function as a carrier for platinum complexes. The aquation of chloride ancillary ligand prior to binding with DNA is considered an important step in interaction of a metal complex with DNA [64, 65]. In the presence of DMSO this aquation may be replaced by the coordination of DMSO to Pt which may alter the structure of the platinum complex and in turn affect the anticancer activity [61].

To check this aquation and stability of the current complexes, we took **C1a** and **C1b** as reference compounds and checked their stability in 17% $D_2O$/DMSO-$d_6$ mixture using $^1$H NMR spectroscopy. We observed different behavior in case of **C1a** in which we observed aquation over the passage of time and in the aquated complex water was exchanged by DMSO (Scheme 2). In shorter time (12 h) the equilibrium was reached and that remained constant for at least one month (Fig. 4).


**Scheme 2** Dissociation of **C1a** in DMSO/water mixture showing replacement of $Cl^-$ by DMSO

By the replacement of $Cl^-$ ligand of Pt by DMSO we observed a new set of same number of peaks in slight up field or downfield for a new closely related compound. In the $^1$H NMR spectra taken in pure DMSO-$d_6$ (Fig. 4), we did not observe such replacement of $Cl^-$ even after long time that showed water is crucial for such dissociation and showed involvement of water in this process. To confirm this phenomenon we performed LC-HRMS analysis for similar mixture in prepared in non-deuterated water/DMSO mixture (ESI Fig. S2-3). We found a new single charge specie which m/z was equal to **C1a-DMSO**. This confirmed the aquation by water and then replacement of water by DMSO donor ligand. Similarly we conducted HR-MS analysis for **C2a**

in pure DMSO and we found only $[M+H]^+$ peak (ESI Fig. S4). This proved in the absence of water such replacement of $Cl^-$ by DMSO was not possible.

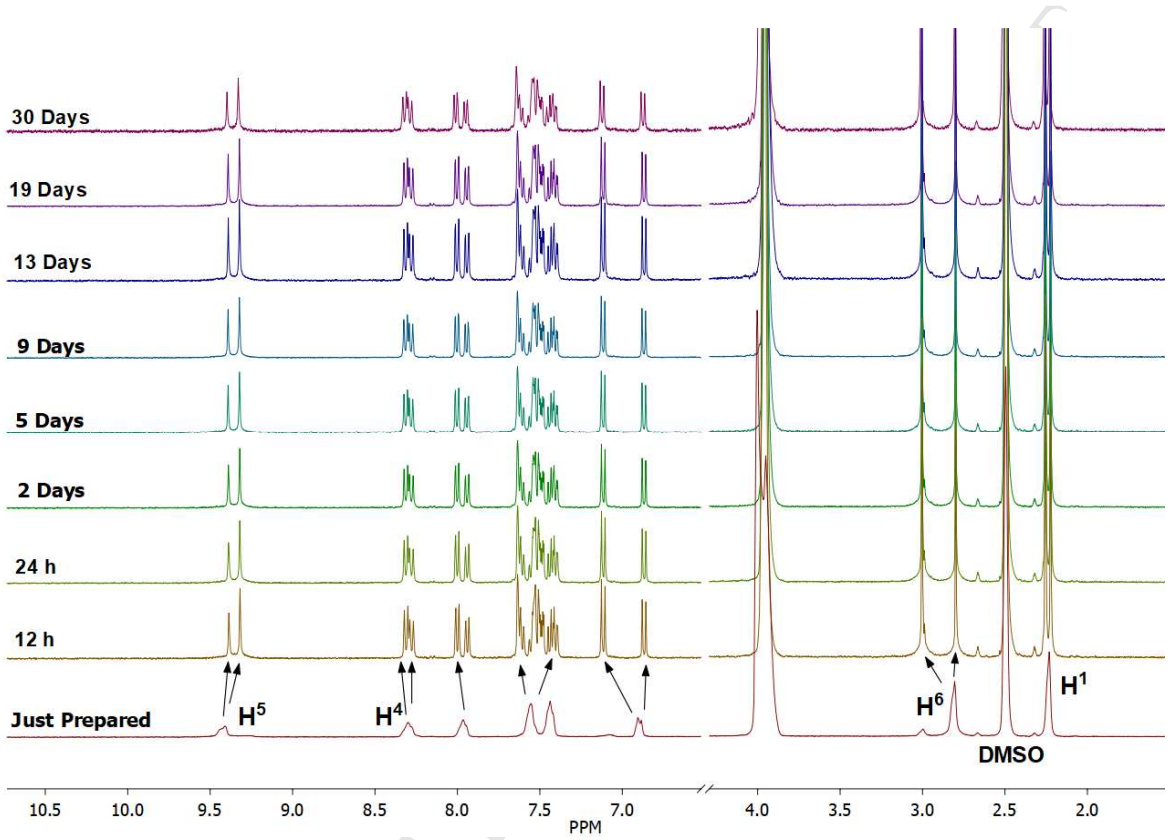


**Fig. 4** Stability analysis of **C1a** in 17 % $D_2O$/DMSO at mentioned time points. The new peak appearance showed the displacement of the ancillary $Cl^-$ ligand by DMSO or $D_2O$ and the equilibrium was established at 12 h time point that remained unchanged up to 30 days.

**C2b** was taken as a reference compound for "b" series of these complexes. Repeated $^1H$ NMR spectra were recorded over 30 days (ESI Fig. S1). No changes were observed in the respective proton chemical shifts, it showed **C2b** was quite stable under these conditions and also denoted that "b" series of these complexes is a highly stable group of complexes with higher anticancer effect.

The ultimate target of Pt complexes was confirmed to be DNA and the formation of Pt-DNA adduct, that further inhibited DNA replication and resulted in apoptosis. In some studies, it was

shown that cisplatin is aquated inside cell or it interacted with other biomolecules like S-donor amino acid to reach the ultimate target DNA inside nucleus and there by stop cells growth [9, 62, 65-67]. So considering these facts hydrolysis may be a positive property of platinum complexes and it facilitates the interaction of these complexes (**C1a-C4a**) with other biomolecule and DNA. Considering "b" series (**C1b-C4b**) of complexes the S-donor atom of the ligand may work as labile group to interact with DNA. This idea may need further experimentation, which could be a matter of further mechanistic studies.

### 3.2. Results (Biology)

#### *3.2.1. In vitro cytotoxicity analysis of **C1a-C4a** or **C1b-C4b***

To investigate the effect of **C1a-C4a** or **C1b-C4b** on cancer cell growth and proliferation, we performed MTS assay (Fig. 5). We tested the effect of **C1a-C4a** or **C1b-C4b** in colorectal cancer HT-29, triple negative breast cancer MDA-MB-231 and non-small cell lung cancer A549 cells. We observed that all these complexes possessed significant cytotoxic effect towards these cancer cells in dose-dependent manner (0, 1, 3, 5 and 10 µM). The $IC_{50}$ value for each complex calculated in three types of cancer cells (Table 2) was far lower from that calculated for cisplatin, showing the stronger cytotoxic property of this class of complexes as compared to cisplatin.

Fig. 5 and table 2 described cytotoxic profile of each of these complexes showing the effect of different substituent on phenolic part of the ligand in each complex. The $IC_{50}$ value of "a" series of complexes (**C1a-C4a**) was observed in the range 2.11-2.65 µM that was about 5 times more as compared to that of cisplatin. The anticancer effect of "b" series of complexes (**C1b-C4b**) was better as compared to "a" series and cisplatin (Table 2). Among these complexes, **C2b** showed the highest cytotoxicity in all kind of cancer cells. The lowest $IC_{50}$ value (0.08 µM) for **C2b** was observed in MDA-MB-231 cells.

Furthermore, the effect of **C1b**, **C2b** and **C3b** was stronger in comparison to other complexes in these cancer cells. Remarkably, cancer cells treated with **C1b** and **C2b** lead to huge cell death as compared with other complexes or cisplatin. Low concentrations of these complexes (1 and/or 3 µM) were enough to initiate significant cell death and thereby suppress cancer cell growth. Taking together, these results suggested that all these complexes have huge potential to suppress cancer cell growth. Among these, the anticancer effect of **C1b**, **C2b** and **C3b** was higher than the other counterparts in cancer cells.

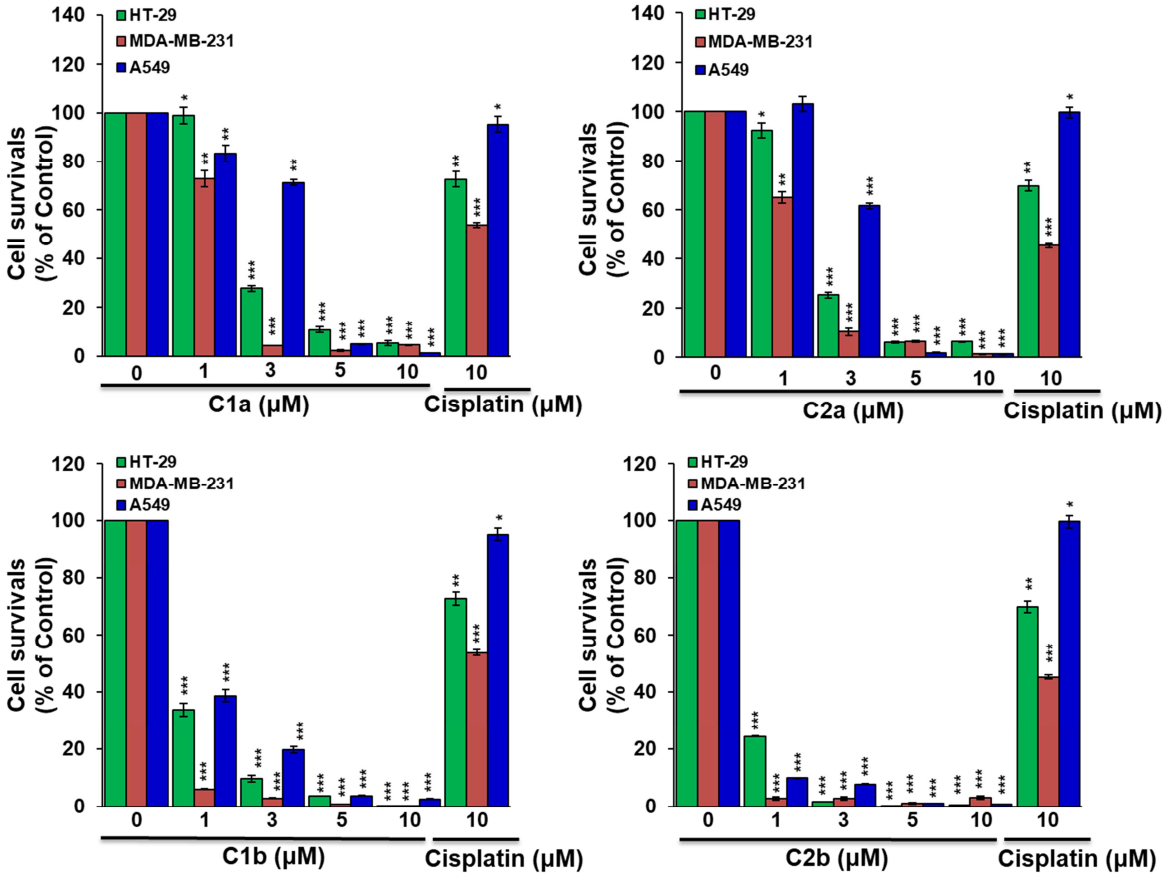

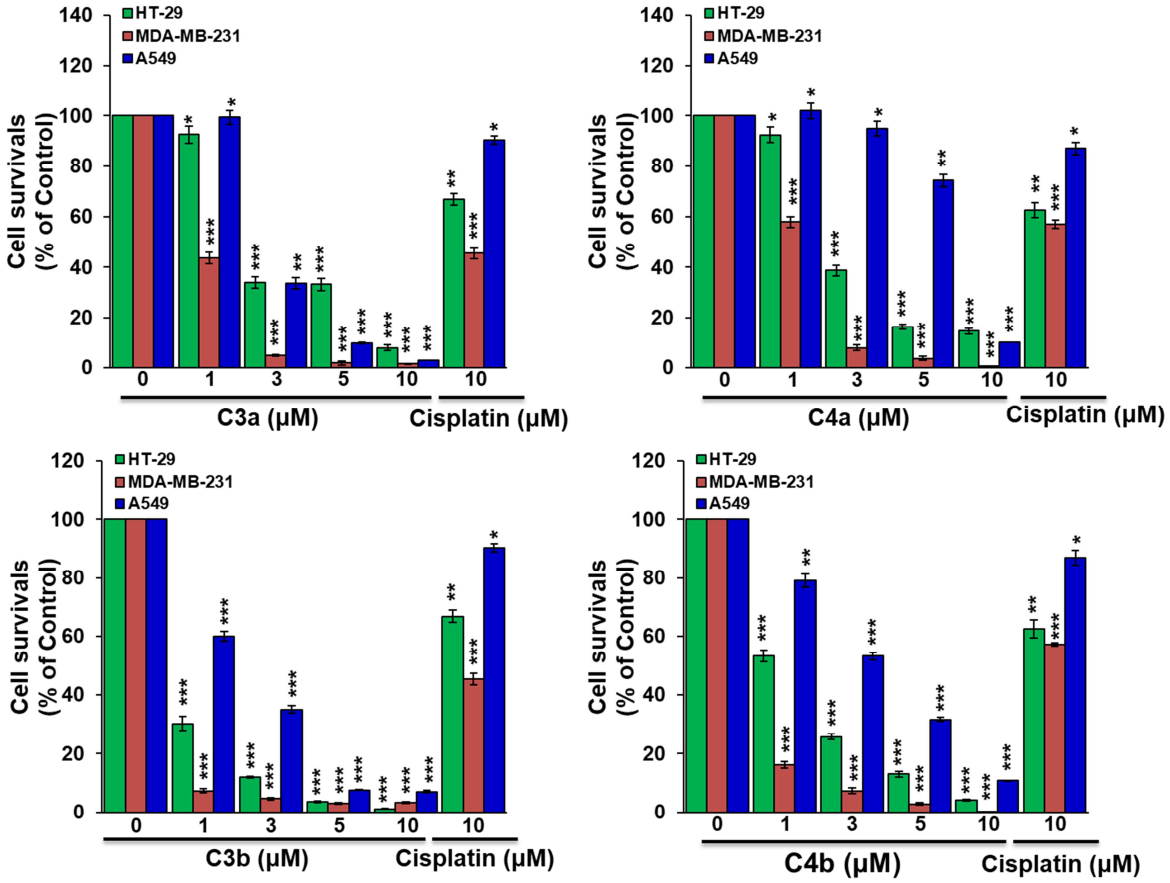


**Fig. 5 C1a-C4a** or **C1b-C4b** reduced cell growth ability of multiple cancer cells; MTS assay of HT-29, MDA-MB-231 and A549 cells treated with various concentrations (0, 1, 3, 5 and 10 μM) of each of **C1a-C4a**, **C1b-C4b** or cisplatin (10 μM) for 72 h and used to determine cell viability. Data from two independent experiments performed in triplicate are shown as mean ± SD. (*P < 0.05; **P < 0.01; ***P< 0.005).

**Table 2.** *In vitro* antitumor effect(s) of **C1a-C4a** and **C1b-C4b** in various human cancer cells; $IC_{50}$ (μM

| Complex | C1a | C1b | C2a | C2b | C3a | C3b | C4a | C4b | cisplatin |
|---|---|---|---|---|---|---|---|---|---|
| HT-29 | 2.11 | 0.61 | 2.31 | 0.22 | 2.87 | 0.66 | 2.65 | 1.02 | >10 |
| MDA-MB-231 | 1.07 | 0.17 | 1.27 | 0.08 | 0.72 | 0.13 | 1.11 | 0.53 | ≥10 |

$IC_{50}$ is defined as the concentration of a cytotoxic agent that is required for 50% inhibition of cells growth.

### *3.2.2. **C1b-C3b** induced apoptotic cell death (PARP cleavage)*

Our results showed that **C1b-C3b** exhibited significant cytotoxic effect, therefore we decided to carry out further experiments with these complexes. To this end, we tested the effect of these

complexes in induction of apoptotic cell death by detection of PARP cleavage and Caspase-3/7 activation, which are significant markers of apoptosis. We treated HT-29 and A549 cells with 1 µM and 3 µM of **C1b-C3b** or with cisplatin (10 µM). We observed strong induction of PARP cleavage induced by **C2b** and **C3b** in HT-29 cells (Fig. 6). In contrast, we observed activation of PARP cleavage only by **C2b** in A549 cells. In both cell lines, **C2b** was involved in strong activation of PARP cleavage (Fig. 6), suggesting its important role in the induction of apoptotic cell death by PARP cleavage.

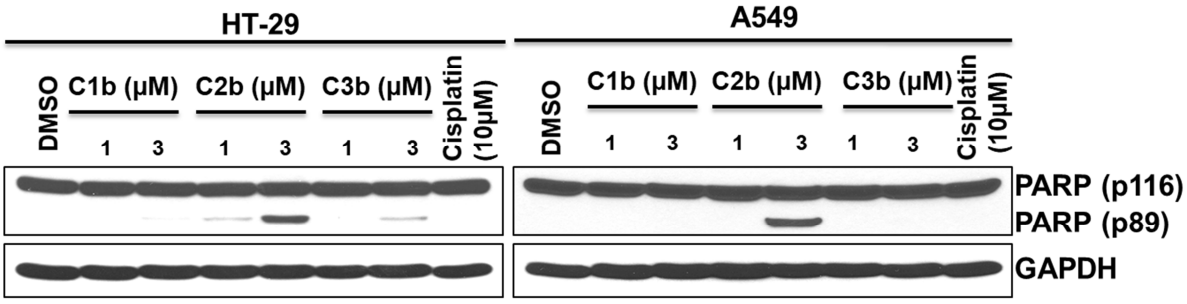


**Fig. 6** Western blot analysis of HT-29 and A549 cells treated with various concentrations of **C1b-C3b** or cisplatin (10 µM) for 24 h and used to detect PARP cleavage to measure apoptotic cell death. Anti-GAPDH antibody was used as loading and transfer control.

Next, Caspase-3/7 dependent signaling is considered important for the activation of apoptosis. In most cases, activation of apoptotic signaling is coupled with activation of Caspase-3/7 dependent pathway. Thus, induction of Caspase-3/7 suggested initiation of apoptosis. Therefore, we decided to check the effect of these complexes on the induction of Caspase-3/7 dependent signaling in cancer cells. Importantly, we observed strong activation of Caspase-3/7 in response to **C1b-C4b** in both HT-29 and A549 cells (Fig. 7). These results points towards the role of these complexes in the initiation of apoptosis by Caspase-3/7 dependent pathways, suggesting that **C1b-C4b** have the ability to activate apoptotic signaling pathways through Caspase-3/7 activation. Taking together, these results from Fig. 6 and Fig. 7 showed that these complexes induce apoptotic cell death by activation of PARP cleavage and Caspase-3/7.

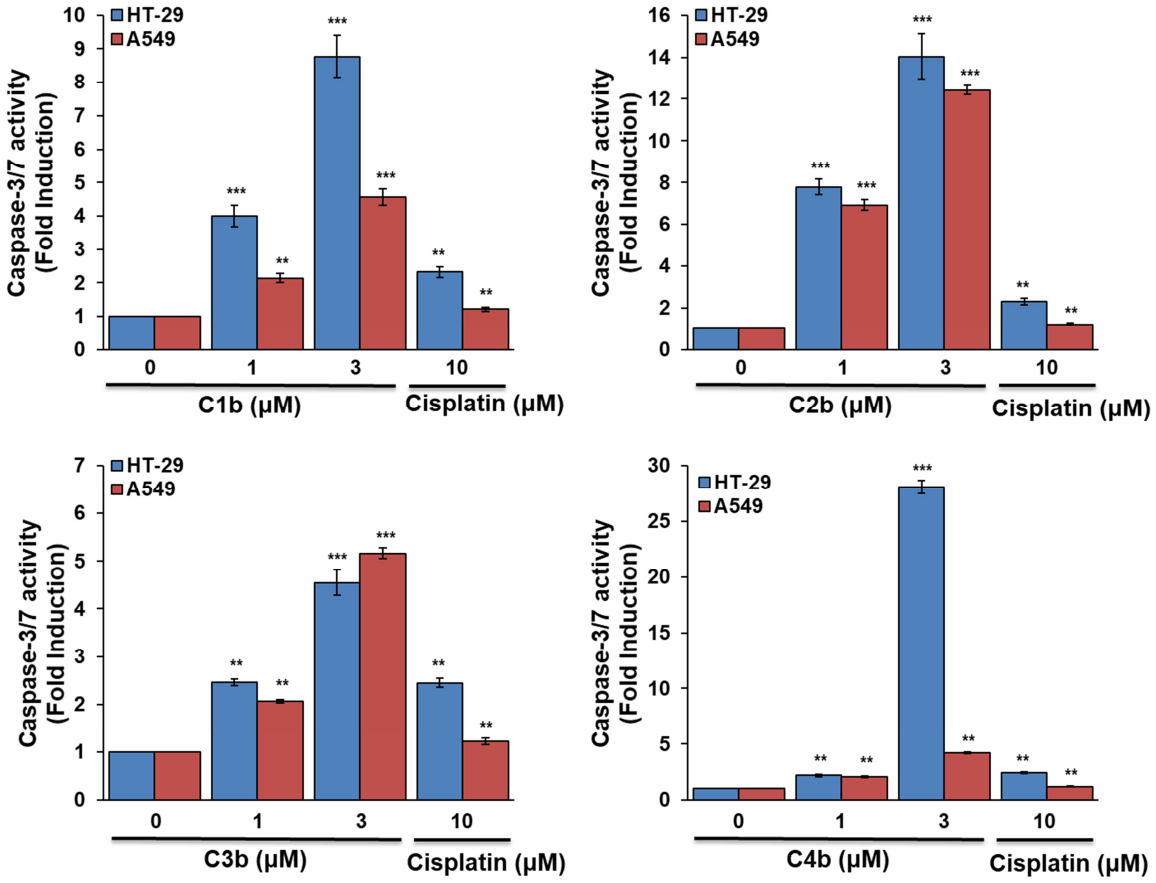


**Fig. 7** Caspase-3/7 activity assay; HT-29 and A549 cells were treated with various concentrations of **C1b-C4b** or cisplatin (10 μM) for 24 h and used to determine the apoptotic cell death. Experiments were repeated three times in duplicate and similar results were obtained. Data are shown as mean ± SD (*P < 0.05; **P < 0.01; ***P< 0.005).

### *3.2.3. **C1b-C4b** suppressed colony formation ability of cancer cell*

Cancer cells have the ability to form colonies due to uncontrolled cell growth coupled with abnormal DNA synthesis. Colony formation ability of cancer cells often leads to tumor burden *in vivo* and in most cases these colonies show resistance to cancer drugs. Activation of survival signaling plays key role in the clonogenic formation ability of cancer cells. Therefore, we tested the effect of **C1b-C4b** on the clonogenic formation ability of HT-29 and A549 cells. Interestingly, we observed that different doses of **C1b-C4b** were able to inhibit the colony formation ability of both HT-29 and A549 cells in comparison to cisplatin (Fig. 8). These complexes seemed to exert strong cytotoxic effect and thereby suppress their clonogenic

formation ability in these cells, suggesting their potentials to block the colony formation ability of cancer cell and play important role in the induction of apoptotic.

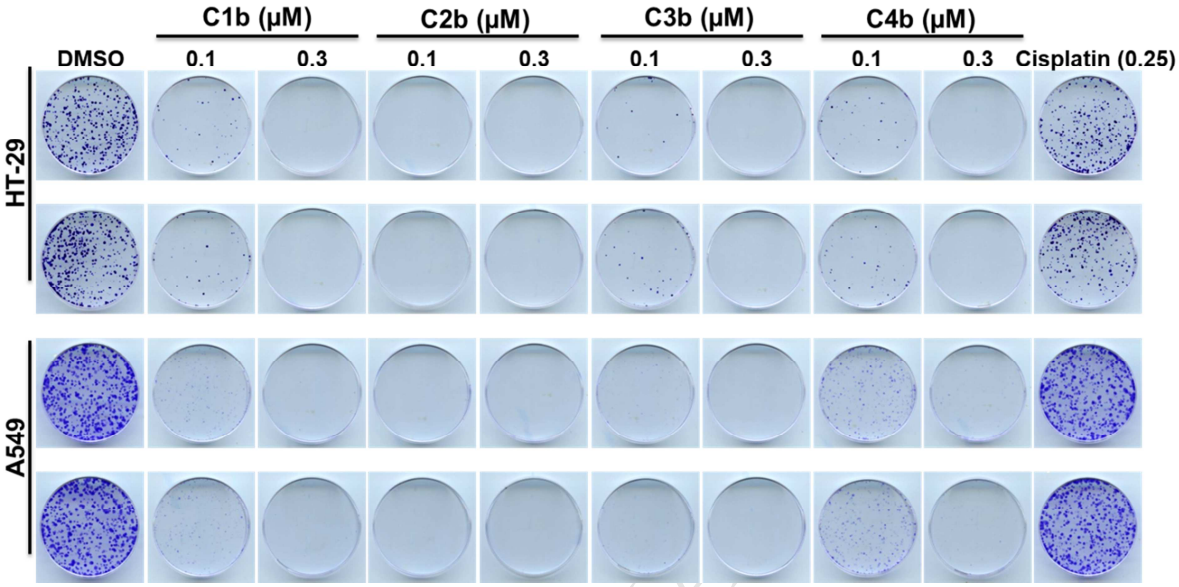


**Fig. 8** Colony formation assay; A549 and HT-29 cells were treated with various concentrations of **C1b-C4b** or cisplatin (0.25 μM) for 24 h and used to determine the long-term response. Representative photograph of clonogenic assay results are shown. Experiments were repeated three times and similar results were obtained.

### *3.2.4. **C1b-C3b** regulate MAPK signaling and p21 expression*

Next, we determined the effect of **C1b-C3b** on the regualtion of mitogen activated protein kinases (MAPK) and p21 expression. To this end, we selected ERK1/2 and AKT which are parts of MAPK signaling. Intersetingly, we found that the effect of these complexes on the regulation of both ERK1/2 and AKT signaling was not obviuos (Fig. 9A), representing that these complexes may not target these signaling pathhways and may exert effect in context-dependent manner (Fig. 9A). Furthermore, we tested the effect on p21 expression in cancer cells treated with **C1b-C3b**. p21 is a tumor suppressor protein, which plays critical role in the inhibition of cell cycle progression by blocking DNA synthesis. We observed strong induction of p21 protein levels in both HT-29 and A549 cells, when traeted with these complexes (Fig. 9B). p21 activation suggested that **C1b-C3b** have potential to suppress cell cycle progression by inhibiting

DNA synthesis. In sum, our results suggested that these **C1b-C3b** exert their cytotoxic effect in a context-dependent manner which is obviuos from p21 regulation in these cancer cells.

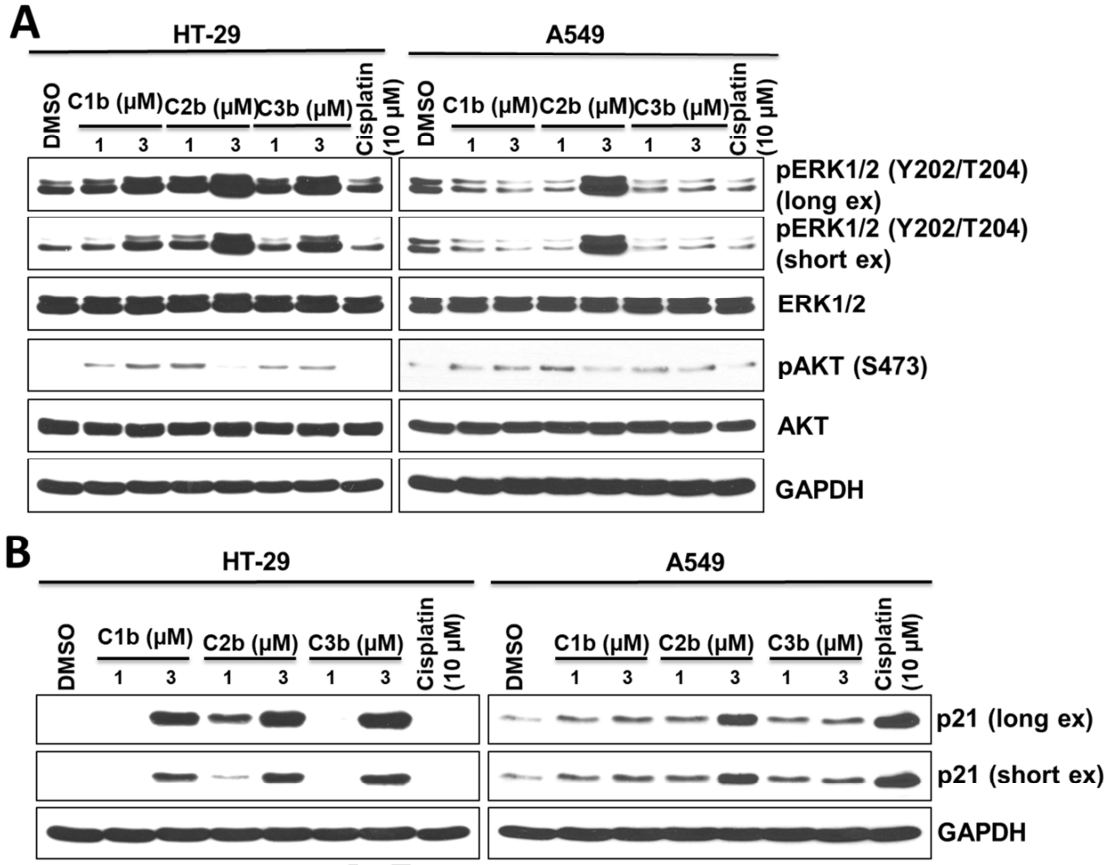


**Fig. 9** Effect(s) of **C1b-C3b** on the activation of ERK1/2, AKT and p21 signaling pathways; (A) Western blot of HT-29 and A549 cells treated with various concentrations of **C1b-C3b** or cisplatin (10 µM) for 24 h was used to determine with indicated antibodies. Anti-GAPDH antibody was used as loading and transfer control (B) The enhanced expression of p21 induced by **C1b-C3b**; Western blot of HT-29 and A549 cells treated with various concentrations of **C1b-C3b** or cisplatin (10 µM) for 24 h and used to determine the expression with indicated antibodies.

### *3.2.5. Induction of autophagic cell death*

Autophagy play important roles in cancer cell death via autophagosome. In most cases cancer cells follow autophagy mediated cell death in contrast to canonical apoptotic signaling, thus activation of autophagy and autophagy mediated cellular signaling is considered important in cancer cell death. Therefore, we also determined the effect of these complexes on autophagic

cancer cell death mechanism. To this end, we carried out immunoflorescence experiment to detect the activation of LC3B, which is a significant marker of autophagy. Importantly, we observed activation of LC3B in A549 cancer cells treated with 3 µM of **C2b** (Fig. 10A). To further confirm these results, we performed western blot to detect LC3-I and LC3-II protein expressions in cancer cells in response to the treatment with these complexes. We observed activation of LC3-I/LC3-II protein levels in response to the treatment with **C1b**-**C3b** in both HT-29 and A549 cells, which further supported the activation of autophagy mediated cell death signaling by these complexes (Fig. 10B). Taken together, these results suggested potentials of these complexes in activation of autophagic cell death and thereby suppress the growth of cancer cells.

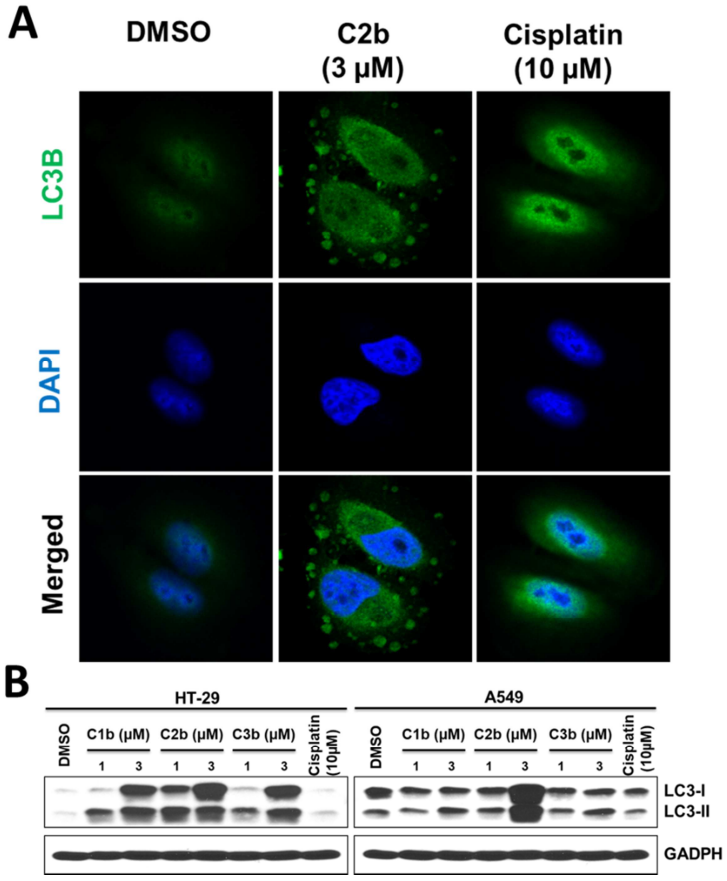

**Fig. 10** Induction of autophagic cell death; (A) The Immunofluorescence analysis of A549 cells treated with **C2b** (3 µM) or cisplatin (10 µM) for 18 h and immunostained with an anti-LC3B antibody (B) **C1b-C3b** significantly induced autophagic cell death; Western blot analysis of HT-29 and A549 cells treated with various concentrations of **C1b-C3b** or cisplatin (10 µM) for 24 h and used to detect LC3-I and LC3-II expression to measure autophagic cell death. Anti-GAPDH antibody was used for a loading and transfer control.

### *3.2.6. **C1b-C4b** modulate the EMT-like feature of cancer cells*

Epithelial-mesenchymal-transition (EMT) plays important role in the invasion and metastasis of cancer. Most of the cancer cells exhibit EMT-like features, which help them to invade into blood stream and thereby promote cancer metastasis. Blocking of EMT-like features of cancer cells plays an important role in the inhibition of cancer metastasis. Therefore, we checked the effect of **C1b-C4b** on morphology of both HT-29 and A549 cells, which exhibits EMT-like features. We observed changes in the morphology of these cancer cells upon treatment with **C1b-C4b** (Fig. 11). We found that these cancer cells shrinked upon treatment with **C1b-C4b** that was coupled with the loss of EMT-like features (Fig. 11). In summary, these results suggested that **C1b-C4b** can inhibit EMT-like features of these cancer cells and thereby play a role in the suppression of cancer metastasis.

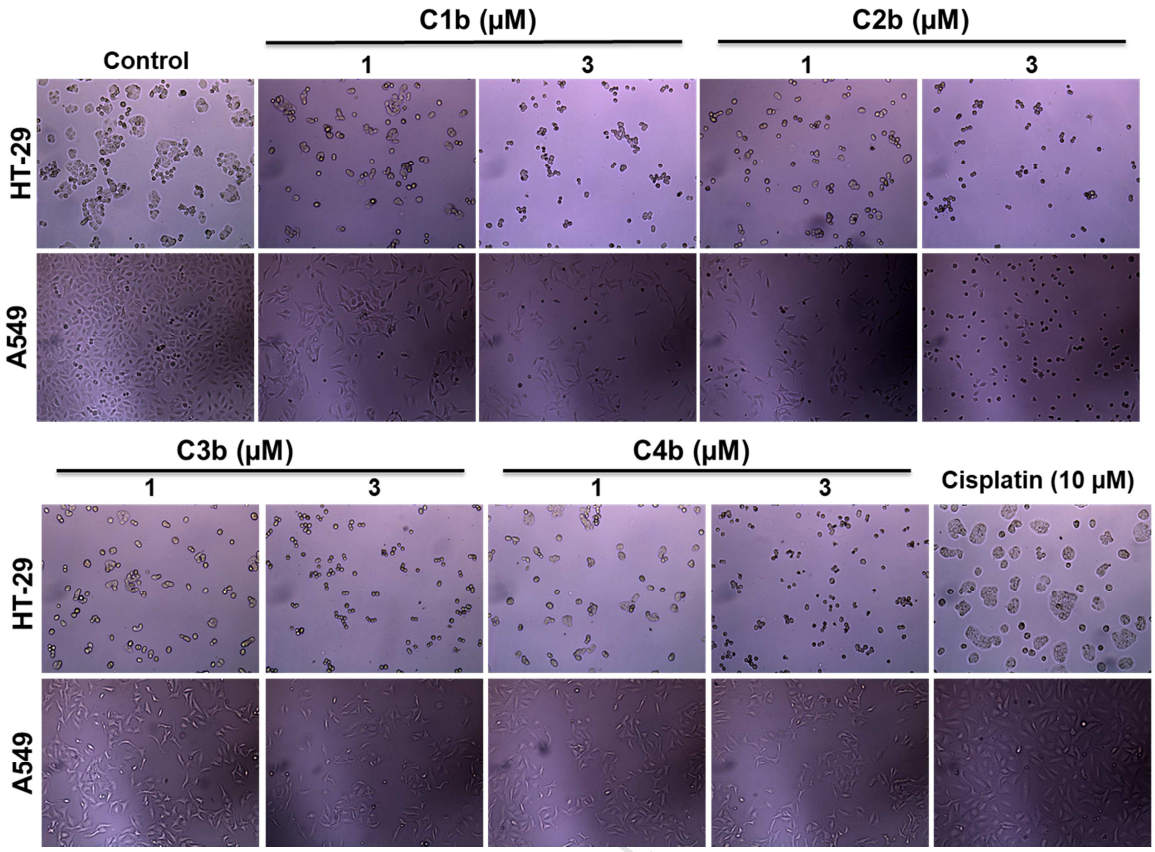


**Fig. 11** Representative images showing cells morphological changes; A549 and HT-29 cells were treated with various concentrations of **C1b**-**C4b** or cisplatin (10 μM) for 24 h and images were taken.

### *3.2.7. Effect on growth of bacterial (E. coli) cells*

In addition to the *in vitro* anticancer effect study on cancer cells, we checked the effect of these complexes on bacterial cell growth. Several studies showed the effect of anticancer agents on bacterial cell growth and morphological features. Moreover, effect of anticancer Pt(II) complexes on bacterial cell growth and morphology became an important analysis [19]. It can be related to the serendipity and discovery of cisplatin as anticancer drug [68-71]. Therefore, we decided to check the effect of our complexes on growth rate and morphological features of *E. coli* cells. Interestingly we observed high growth retardation effect on bacterial cell upon treatment with **C1a**, **C1b**, **C2b**, **C3b** and **C4b** (Fig. 12A-B). Similarly, we observed filamentous morphology in *E. coli* cells when treated with these complexes (Fig. 12C). Consistently,

combination with our previous results these complexes have potential to retard bacterial cell growth coupled with morphological changes. These results suggest the importance of these complexes as potential agents for the inhibition of cell growth.

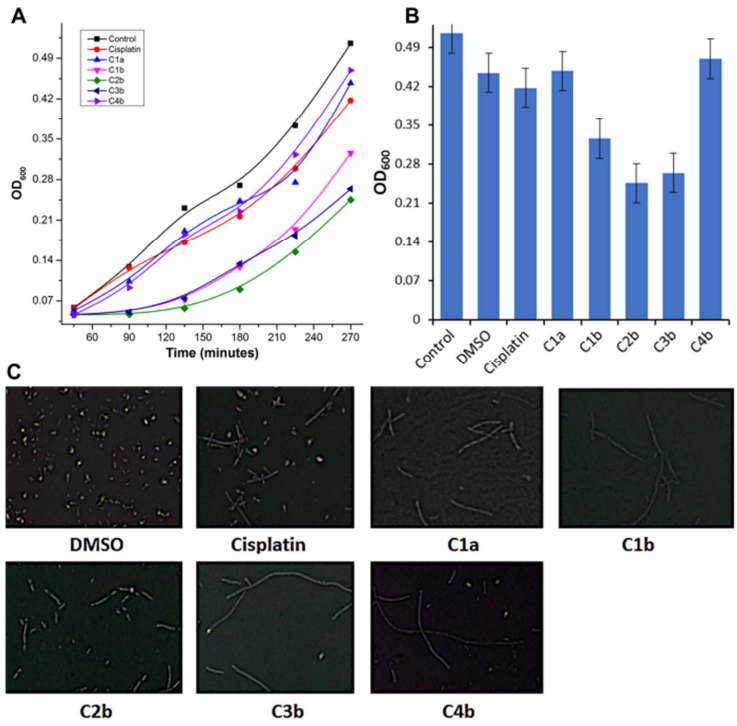


**Fig. 12** Effect on the growth of *E. coli* in comparison with cisplatin; (A) Plot of growth (OD) versus time, data points represent the average of three independent experiments (B) Comparison of growth inhibition at the final time point 4.5 h. Error bars represent the average of three independent experiments (mean ±S.D.) (C) Effect of Pt(II) complexes and cisplatin on morphology of *E. coli*; *E. coli* was incubated with 20 µM of each of these compounds for 4.5 h and imaged.

### *3.2.8. DNA binding analyzed by gel electrophoresis*

One of the most important and common features of Pt(II) complexes is the binding with DNA and thereby change the conformation, which is considered critical for anticancer activity. Binding of metallic complexes with DNA prevent proper synthesis of DNA molecule and thereby play a role in the inhibition of cancer cell growth. Therefore, we studied to binding ability of these Pt(II) complexes with DNA by gel electrophoresis. To this end, we tested the interaction of these complexes with pUC19 plasmid DNA as a target. It has been shown that

binding of metal complexes with DNA exhibit slow migration across the gel during gel electrophoresis. We observed pUC19 plasmid DNA incubated with **C1a**, **C1b**, **C2b**, **C3b** and **C4b** displayed slower migration as compared to the control (Fig. 13). Taken together, these results indicated the interaction of these complexes with DNA and suggested their diverse mode of action.

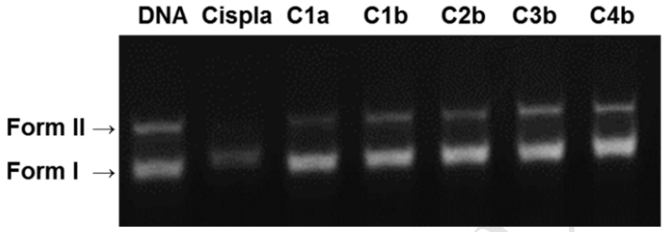


**Fig. 13** Gel electrophoresis picture showing relative retardation of DNA; pUC19 DNA was incubated with 20 µM of the indicated Pt(II) complexes at 37 °C for 24 h and gel electrophoresed.

## 4. Discussions

We reported ONS-donor salicylaldimine ligand based Pt (II) complexes consisting of two series **C1a-C4a** and **C1b-C4b**. The "a" series of complexes was converted to heteroliptic "b" series by replacement of the chloride ancillary ligand with 4-picoline which was easily achieved using silver salt mediated abstraction of the chloride from complexes in "a" series. Simple and reproducible methodologies were devised for their synthesis from commercially available reagents. These complexes were obtained in high isolated yields and characterized successfully by different spectroscopic or spectrophotometric analyses. Four complexes were characterized in solid state by single crystal X-ray analysis. A series of related structure of these complexes studied here demonstrated their feasible synthesis and structure confirmation and similarly these modifications affected their biological activities to certain extent. We successfully investigated these complexes to be potent anticancer agents, which was demonstrated by several mechanistic

anticancer investigations of these complexes on different types of human cancer cells and bacteria (*E. coli*).

One of the major hallmark of the cancer cells is to show resistance against anticancer agents. Activation of growth factor related signaling plays the most important role in the survival of cancer cells therefore, the effect of most anticancer drugs remains less active. In clinical trials, most of the anticancer agents fails to show promising results due to continuous resistance against cancer cells. Tumors are heterogeneous in nature, which consist of several types of mutations, activation of multiple growth factor receptors and amplification of oncogenic proteins. Cancer cells derived from these tumors also exhibit heterogeneous nature. Therefore, most of the drugs show less cytotoxic effect towards cancer cells or their effect is lowered with long drug exposure time. Thus, design of novel and potential anticancer agents remains challenging in the field of cancer therapeutics. Current study focused on the design and synthesis of potent Pt(II) complexes and their effect on the growth of cancer cells.

We showed that **C1a-C4a** and **C1b-C4b** possessed strong anticancer activity in multiple human cancer cells including non-small cell lung cancer, colorectal cancer and triple negative breast cancer. We found that these complexes could inhibit the growth of multiple cancer cells. Moreover, these complexes have the potential to suppress the colony formation ability of cancer cells and thus play important role in growth retardation. Mechanistically, we observed strong induction in PARP cleavage and Caspase-3/7 activation, which suggested the induction of apoptotic cell death in cancer cells. Our results suggested that A549, HT-29 and MDA-MB-231 cells show less resistance to these complexes and their cytotoxic effect was much stronger than cisplatin against these cancer cell lines.

These complexes induced the expression of p21 tumor suppressor protein, which play a key role in the inhibition of cell cycle progression and DNA synthesis. p21 activation suggested that these complexes can inhibit both DNA synthesis and cell cycle progression. In contrast, their effect on ERK1/2 and AKT signaling was not obvious, which suggested the context-dependent role of these complexes in term of mechanistic study.

Moreover, we observed induction of autophagic cell death and activation of LC3B in cancer cells treated with these complexes. These results showed that they exerted their cytotoxic effect both through the activation of autophagic and apoptotic cell death. Activation of both these signaling in response seems to be interesting observation and may explain the better cytotoxic nature of these complexes.

We also observed morphological features of cancer cells upon treatment with these complexes. Generally, cancer cells possess EMT-like features, which help them in invasion and migration. EMT-like features of cancer cells play important role in cancer metastasis. Interestingly, we observed that EMT-like features of both HT-29 and A549 cells were lost upon treatment with these complexes and showed rounded morphology instead of EMT-like, which suggested the inhibition of EMT-like features of cancer cells by changing their morphology. These complexes may play important role in the inhibition of invasion and migration coupled with suppression of cancer metastasis.

Gel electrophoresis showed stronger interaction of these complexes with DNA that also makes them ideal anticancer agents to be used in the field of cancer therapy. These results indicated that this interaction in cancer cells might inhibit DNA synthesis and replication. This could explain the growth retardation of cancer cells in response to these complexes. Importantly, these complexes also inhibited the growth of bacteria and changed the morphology of bacterial cells.

In conclusion, this study explored a potent class of Pt(II) complexes as interesting therapeutic agents. Diverse mode of action of these complexes makes them ideal for testing in multiple human cancer cells. The most striking feature of these complexes was the induction of autophagic and apoptotic cell death mechanisms in multiple cancer cells. Importantly, these complexes could be a potential class of chemotherapeutic agents in clinical trials and might be helpful in treatment of resistant cancer cells in near future. These complexes could serve as the inducer of autophagy and apoptosis in multiple aggressive cancer cells, which also points towards their importance in the field of cancer therapy. Our results suggested the importance and potential of this class of complexes which could be further investigated in details as a new class of anticancer agents in the field of cancer therapy. The current study may provide a base for further *in vivo* study and exploration of their potent cytotoxic nature.

## Acknowledgements

The authors acknowledge the Ministry of Science and Technology of China (2013CB834501), The Science and Technology Commission of Shanghai Municipality (13NM1400200), the National Natural Science Foundation of China (No. 21102017) and China postdoctoral association for providing postdoctoral fellowship.

## Appendix A. Supplementary data

Supplementary data, NMR, ESI-MS spectra related to this article can be found at http://dx.doi.org/10.

## References

[1] S.J. Berners-Price, Activating platinum anticancer complexes with visible light, Angew. Chem. Int. Ed., 50(2011) 804-5.

[2] N.J. Wheate, S. Walker, G.E. Craig, R. Oun, The status of platinum anticancer drugs in the clinic and in clinical trials, Dalton Trans, 39(2010) 8113-27.

[3] N. Cutillas, G.S. Yellol, C. de Haro, C. Vicente, V. Rodríguez, J. Ruiz, Anticancer cyclometalated complexes of platinum group metals and gold, Coord. Chem. Rev., 257(2013) 2784-97.

[4] B. Köberle, M.T. Tomicic, S. Usanova, B. Kaina, Cisplatin resistance: Preclinical findings and clinical implications, Biochim. Biophys. Acta, 1806(2010) 172-82.

[5] N. Milosavljevic, C. Duranton, N. Djerbi, P.H. Puech, P. Gounon, D. Lagadic-Gossmann, M.T. Dimanche-Boitrel, C. Rauch, M. Tauc, L. Counillon, M. Poet, Nongenomic effects of cisplatin: acute inhibition of mechanosensitive transporters and channels without actin remodeling, Cancer Res., 70(2010) 7514-22.

[6] R.S.A. J A Levi, D N Dalley, Haemolytic anemia after cisplatin, Br. Med. J., 282(1981) 2003–4.

[7] J.R. García-Berrocal, J. Nevado, R. Ramírez-Camacho, R. Sanz, J.A. González-García, C. Sánchez-Rodríguez, B. Cantos, P. España, J.M. Verdaguer, A. Trinidad Cabezas, The anticancer drug cisplatin induces an intrinsic apoptotic pathway inside the inner ear, Br. J. Pharmacol., 152(2007) 1012-20.

[8] D.J. Stewart, Mechanisms of resistance to cisplatin and carboplatin, Crit Rev Oncol Hematol, 63(2007) 12-31.

[9] J.J. Wilson, S.J. Lippard, Synthetic methods for the preparation of platinum anticancer complexes, Chem. Rev., 114(2013) 4470-95.

[10] W.J. Guo, Y.M. Zhang, L. Zhang, B. Huang, F.F. Tao, W. Chen, Z.J. Guo, Q. Xu, Y. Sun, Novel monofunctional platinum(II) complex Mono-Pt induces apoptosis-independent autophagic cell death in human ovarian carcinoma cells, distinct from cisplatin, Autophagy, 9(2013) 996-1008.

[11] Z. Guo, W.L. Tong, M.C. Chan, Luminescent oligo(ethylene glycol)-functionalized cyclometalated platinum(II) complexes: cellular characterization and mitochondria-specific localization, Chem Commun (Camb), 50(2014) 1711-4.

[12] B.W. Harper, A.M. Krause-Heuer, M.P. Grant, M. Manohar, K.B. Garbutcheon-Singh, J.R. Aldrich-Wright, Advances in platinum chemotherapeutics, Chem. Eur. J., 16(2010) 7064-77.

[13] G. Ma, Y. Min, F. Huang, T. Jiang, Y. Liu, Thioether binding mediates monofunctional platinum antitumor reagents to trans configuration in DNA interactions, Chem. Commun., 46(2010) 6938-40.

[14] T. Marzo, D. Cirri, L. Ciofi, C. Gabbiani, A. Feis, N. Di Pasquale, M. Stefanini, T. Biver, L. Messori, Synthesis, characterization and DNA interactions of [$Pt_3$(TPymT)$Cl_3$], the trinuclear platinum(II) complex of the TPymT ligand, J. Inorg. Biochem., 183(2018) 101-6.

[15] J. Molas Saborit, A. Caubet, R.F. Brissos, L. Korrodi-Gregorio, R. Perez-Tomas, M. Martinez, P. Gamez, pH-Driven preparation of two related platinum(ii) complexes exhibiting distinct cytotoxic properties, Dalton Trans, 46(2017) 11214-22.

[16] E. Wong, C.M. Giandomenico, Current Status of platinum-based antitumor drugs, Chem. Rev., 99(1999) 2451-66.

[17] G.Y. Park, J.J. Wilson, Y. Song, S.J. Lippard, Phenanthriplatin, a monofunctional DNA-binding platinum anticancer drug candidate with unusual potency and cellular activity profile, PNAS, 109(2012) 11987-92.

[18] D. Wang, G. Zhu, X. Huang, S.J. Lippard, X-ray structure and mechanism of RNA polymerase II stalled at an antineoplastic monofunctional platinum-DNA adduct, PNAS, 107(2010) 9584-9.

[19] T.C. Johnstone, S.M. Alexander, W. Lin, S.J. Lippard, Effects of monofunctional platinum agents on bacterial growth: a retrospective study, J. Am. Chem. Soc., 136(2014) 116-8.

[20] T.C. Johnstone, S.J. Lippard, The chiral potential of phenanthriplatin and its influence on guanine binding, J. Am. Chem. Soc., 136(2014) 2126-34.

[21] W. Zhou, M. Almeqdadi, M.E. Xifaras, I.A. Riddell, O.H. Yilmaz, S.J. Lippard, The effect of geometric isomerism on the anticancer activity of the monofunctional platinum complex trans-[$Pt(NH_3)_2$(phenanthridine)Cl]$NO_3$, Chem Commun (Camb), 54(2018) 2788-91.

[22] J.H. Schiller, D.R. Gandara, G.D. Goss, E.E. Vokes, Non-small-cell lung cancer: then and now, J Clin Oncol, 31(2013) 981-3.

[23] F.A. Haggar, R.P. Boushey, Colorectal cancer epidemiology: incidence, mortality, survival, and risk factors, Clin Colon Rectal Surg, 22(2009) 191-7.

[24] A. Mantovani, P. Allavena, A. Sica, F. Balkwill, Cancer-related inflammation, Nature, 454(2008) 436-44.

[25] X. Song, Z. Wang, J. Zhao, T.S. Hor, Sodium cubane and double-cubane aggregates of hybridised salicylaldimines and their transmetallation to nickel for catalytic ethylene oligomerisation, Chem Commun (Camb), 49(2013) 4992-4.

[26] N. Mizushima, T. Yoshimori, B. Levine, Methods in mammalian autophagy research, Cell, 140(2010) 313-26.

[27] Z. Jin, W.S. El-Deiry, Overview of cell death signaling pathways, Cancer Biology & Therapy, 4(2014) 147-71.

[28] C. Holohan, S. Van Schaeybroeck, D.B. Longley, P.G. Johnston, Cancer drug resistance: an evolving paradigm, Nat. Rev. Cancer, 13(2013) 714-26.

[29] N. Muhammad, Z. Guo, Metal-based anticancer chemotherapeutic agents, Curr. Opin. Chem. Biol., 19(2014) 144-53.

[30] A.M. Burger, H.-H. Fiebig, Preclinical Screening for New Anticancer Agents, in: W.D. Figg, H.L. McLeod (Eds.), Handbook of anticancer pharmacokinetics and pharmacodynamics, Humana Press, Totowa, NJ, 2004, pp. 29-44.

[31] M. Mellah, A. Voituriez, E. Schulz, Chiral sulfur ligands for asymmetric catalysis, Chem. Rev., 107(2007) 5133-209.

[32] R. Malacea, E. Manoury, J.-C. Daran, R. Poli, Synthesis, characterization and crystal structures of two new platinum complexes with planar chiral 1,2-disubstituted ferrocenes containing phosphine and thioether donor groups, J. Mol. Struct., 890(2008) 249-54.

[33] E. Schulz, A. Voituriez, New sulfur-coordinating chiral ligands for the Tsuji-Trost reaction, Russ. Chem. Bull., 52(2003) 2588-94.

[34] U. Hernández-Balderas, N. Andrade-López, J.G. Alvarado-Rodríguez, R. Moreno-Esparza, M. Paneque, Hydrogen bond networks in five- and eight-membered palladium and platinum complexes derived from bis(2-aminophenyl)ether and bis(2-aminophenyl)thioether ligands, Polyhedron, 90(2015) 165-74.

[35] D.A. Evans, K.R. Campos, J.S. Tedrow, F.E. Michael, M.R. Gagné, Application of chiral mixed phosphorus/sulfur ligands to palladium-catalyzed allylic substitutions, J. Am. Chem. Soc., 122(2000) 7905-20.

[36] K.K. Andersen, W. Gaffield, N.E. Papanikolaou, J.W. Foley, R.I. Perkins, Optically active sulfoxides. The synthesis and rotatory dispersion of some diaryl sulfoxides, J. Am. Chem. Soc., 86(1964) 5637-46.

[37] K. Hiroi, Y. Suzuki, I. Abe, R. Kawagishi, New chiral sulfoxide ligands possessing a phosphano or phosphanoamino functionality in palladium-catalyzed asymmetric allylic nucleophilic substitution reactions, Tetrahedron, 56(2000) 4701-10.

[38] M. Kalita, K.J. Tamuli, P. Barman, B. Sarma, R. Baruah, H.P. Deka Boruah, Synthesis, crystal structure, bioactivities of Ni(II), Cu(II), Co(II) and Pd(II) complexes with unsymmetrical thioether donor Schiff base: Phosphine free Pd(II) complex catalyzed Suzuki reaction, Polyhedron, 97(2015) 140-7.

[39] S.B. Kumar, A. Solanki, S. Kundu, Copper(II) and palladium(II) complexes with tridentate NSO donor Schiff base ligand: Synthesis, characterization and structures, J. Mol. Struct., 1143(2017) 163-7.

[40] S. Kathiresan, S. Mugesh, M. Murugan, F. Ahamed, J. Annaraj, Mixed-ligand copper(ii)-phenolate complexes: structure and studies on DNA/protein binding profiles, DNA cleavage, molecular docking and cytotoxicity, RSC Adv, 6(2016) 1810-25.

[41] J.W. Roebuck, J.R. Turkington, D.M. Rogers, P.J. Bailey, V. Griffin, A.J. Fischmann, G.S. Nichol, M. Pelser, S. Parsons, P.A. Tasker, Preorganized tridentate analogues of mixed hydroxyoxime/carboxylate nickel extractants, Dalton Trans, 45(2016) 3734-42.

[42] P. Govender, A.K. Renfrew, C.M. Clavel, P.J. Dyson, B. Therrien, G.S. Smith, Antiproliferative activity of chelating N,O- and N,N-ruthenium(II) arene functionalised poly(propyleneimine) dendrimer scaffolds, Dalton Trans, 40(2011) 1158-67.

[43] M. Haghdoost, G. Golbaghi, M. Létourneau, S.A. Patten, A. Castonguay, Lipophilicity-antiproliferative activity relationship study leads to the preparation of a ruthenium(II) arene complex with considerable in vitro cytotoxicity against cancer cells and a lower in vivo toxicity in zebrafish embryos than clinically approved cis -platin, Eur. J. Med. Chem., 132(2017) 282-93.

[44] B.C.E. Makhubela, M. Meyer, G.S. Smith, Evaluation of trimetallic Ru(II)- and Os(II)-Arene complexes as potential anticancer agents, J. Organomet. Chem., 772-773(2014) 229-41.

[45] F.-U. Rahman, M.Z. Bhatti, A. Ali, H.-Q. Duong, Y. Zhang, X. Ji, Y. Lin, H. Wang, Z.-T. Li, D.-W. Zhang, Dimetallic Ru(II) arene complexes appended on bis-salicylaldimine induce cancer cell death and suppress invasion via p53-dependent signaling, Eur. J. Med. Chem., 157(2018) 1480-90.

[46] F. Zheng, A.T. Hutton, C.G. van Sittert, J.R. Moss, S.F. Mapolie, Synthesis, structural characterization and cis-trans isomerization of novel (salicylaldiminato)platinum(II) complexes, Dalton Trans, 42(2013) 11163-79.

[47] N. Komiya, M. Okada, K. Fukumoto, D. Jomori, T. Naota, Highly phosphorescent crystals of vaulted trans-bis(salicylaldiminato)platinum(II) complexes, J. Am. Chem. Soc., 133(2011) 6493-6.

[48] C.M. Che, C.C. Kwok, S.W. Lai, A.F. Rausch, W.J. Finkenzeller, N. Zhu, H. Yersin, Photophysical properties and OLED applications of phosphorescent platinum(II) Schiff base complexes, Chem. Eur. J., 16(2010) 233-47.

[49] F.-U. Rahman, H. Wang, D.-W. Zhang, Z.-T. Li, 42 members new hydroquinone bridged supramolecular macrocycle and its tetra-nuclear mixed ligands Pt(II) complex: A synthetic, structural and spectroscopic investigation, Inorg. Chem. Commun., 97(2018) 157-65.

[50] M. Proetto, W. Liu, A. Hagenbach, U. Abram, R. Gust, Synthesis, characterization and in vitro antitumour activity of a series of novel platinum(II) complexes bearing Schiff base ligands, Eur. J. Med. Chem., 53(2012) 168-75.

[51] A.E. Patterson, J.J. Miller, B.A. Miles, E.L. Stewart, J.-M.E.J. Melanson, C.M. Vogels, A.M. Cockshutt, A. Decken, P. Morin Jr, S.A. Westcott, Synthesis, characterization and anticancer properties of (salicylaldiminato)platinum(II) complexes, Inorg. Chim. Acta, 415(2014) 88-94.

[52] F.U. Rahman, A. Ali, R. Guo, W.K. Wang, H. Wang, Z.T. Li, Y. Lin, D.W. Zhang, Efficient one-pot synthesis of trans-Pt(II)(salicylaldimine)(4-picoline)Cl complexes: effective agents for enhanced expression of p53 tumor suppressor genes, Dalton Trans, 44(2015) 9872-80.

[53] F.-U. Rahman, A. Ali, R. Guo, Y.-C. Zhang, H. Wang, Z.-T. Li, D.-W. Zhang, Synthesis and anticancer activities of a novel class of mono- and di-metallic Pt(II)(salicylaldiminato)(DMSO or picolino)Cl complexes, Dalton Trans, 44(2015) 2166-75.

[54] F.-U. Rahman, A. Ali, I. Khan, R. Guo, L. Chen, H. Wang, Z.-T. Li, Y. Lin, D.-W. Zhang, Synthesis and characterization of *trans*-Pt(II)(salicylaldimine)(pyridine/pyridine-4-carbinol)Cl complexes: *In vivo* inhibition of *E. coli* growth and *in vitro* anticancer activities, Polyhedron, 100(2015) 264-70.

[55] F.-U. Rahman, A. Ali, I.U. Khan, H.-Q. Duong, R. Guo, H. Wang, Z.-T. Li, D.-W. Zhang, Novel phenylenediamine bridged mixed ligands dimetallic square planner Pt(II) complex inhibits

MMPs expression via p53 and caspase-dependent signaling and suppress cancer metastasis and invasion, Eur. J. Med. Chem., 125(2017) 1064-75.

[56] F.U. Rahman, A. Ali, I.U. Khan, H.Q. Duong, S.B. Yu, Y.J. Lin, H. Wang, Z.T. Li, D.W. Zhang, Morpholine or methylpiperazine and salicylaldimine based heteroleptic square planner platinum (II) complexes: *In vitro* anticancer study and growth retardation effect on *E. coli*, Eur. J. Med. Chem., 131(2017) 263-74.

[57] F.U. Rahman, M.Z. Bhatti, A. Ali, H.Q. Duong, Y. Zhang, B. Yang, S. Koppireddi, Y. Lin, H. Wang, Z.T. Li, D.W. Zhang, Homo- and heteroleptic Pt(II) complexes of ONN donor hydrazone and 4-picoline: A synthetic, structural and detailed mechanistic anticancer investigation, Eur. J. Med. Chem., 143(2017) 1039-52.

[58] G. M. Sheldrick, *SHELXS-97, Programs for X-ray Crystal Structure Solution;* University of Göttingen: Göttingen, Germany, 1997; L. J. Farrugia, WINGX, *A Windows Program for Crystal Structure Analysis*; University of Glasgow, Glasgow, UK, 88.

[59] G. Sheldrick, A short history of SHELX, Acta Crystallogr. Sec. A, 64(2008) 112-22.

[60] H. Q. Duong, H. J. Kim, H. J. Kang, Y.-S. Seong, I. Bae, ZSTK474, a PI3K inhibitor, suppresses proliferation and sensitizes human pancreatic adenocarcinoma cells to gemcitabine, Oncol. Rep., 27(2011) 182-8.

[61] M.D. Hall, K.A. Telma, K.E. Chang, T.D. Lee, J.P. Madigan, J.R. Lloyd, I.S. Goldlust, J.D. Hoeschele, M.M. Gottesman, Say no to DMSO: dimethylsulfoxide inactivates cisplatin, carboplatin, and other platinum complexes, Cancer Res., 74(2014) 3913-22.

[62] J. Reedijk, Platinum anticancer coordination compounds: study of DNA binding inspires new drug design, Eur. J. Inorg. Chem., 2009(2009) 1303-12.

[63] S. Ahmad, Kinetic aspects of platinum anticancer agents, Polyhedron, 138(2017) 109-24.

[64] C.M. Clavel, E. Păunescu, P. Nowak-Sliwinska, A.W. Griffioen, R. Scopelliti, P.J. Dyson, Modulating the anticancer activity of ruthenium(II)–arene complexes, J. Med. Chem., 58(2015) 3356-65.

[65] L. Cubo, D.S. Thomas, J. Zhang, A.G. Quiroga, C. Navarro-Ranninger, S.J. Berners-Price, [$^{1}$H,$^{15}$N] NMR studies of the aquation of cis-diamine platinum(II) complexes, Inorg. Chim. Acta, 362(2009) 1022-6.

[66] S.E. Sherman, S.J. Lippard, Structural aspects of platinum anticancer drug interactions with DNA, Chem. Rev., 87(1987) 1153-81.

[67] Ž.D. Bugarčić, J. Bogojeski, B. Petrović, S. Hochreuther, R. van Eldik, Mechanistic studies on the reactions of platinum(ii) complexes with nitrogen- and sulfur-donor biomolecules, Dalton Trans, 41(2012) 12329-45.

[68] B. Rosenberg, E. Renshaw, L. Vancamp, J. Hartwick, J. Drobnik, Platinum induced filamentous growth in *Escherichia Coli*, J. Bacteriol., 93(1967) 716-21.

[69] B. Rosenberg, L. Vancamp, E.B. Grimley, A.J. Thomson, Inhibition of growth or cell division in *Escherichia Coli* by different ionic species of platinu(IV) complexes, J. Biol. Chem., 242(1967) 1347-52.

[70] B. Rosenberg, L. Vancamp, T. Krigas, Inhibition of cell division in *Escherichia Coli* by electrolysis products from a platinum electrode, Nature, 205(1965) 698-9.

[71] B. Rosenberg, L. Vancamp, J.E. Trosko, V.H. Mansour, Platinum compounds - a new class of potent antitumour agents, Nature, 222(1969) 385-6.

- ONS-donor Pt(II) complexes synthesis and structure study
- Aquation and stability of Pt(II) complexes
- Potent anticancer Pt(II) complexes
- Apoptosis via multiple genes activation pathways
- Autophagy induction
- *E. coli* growth retardation and filamentous morphology

# Supporting Information

*for*

# ONS-donor ligand based Pt(II) complexes display extremely high anticancer potency through autophagic cell death pathway

Faiz-Ur Rahman[a,b,1], Amjad Ali[c,1], Hong-Quan Duong[d,1], Inam Ullah Khan[e], Muhammad Zeeshan Bhatti[c,f], Zhan-Ting Li[a], Hui Wang[a]* and Dan-Wei Zhang[a]*

[a]Center for Supramolecular Material and Catalysis, Department of Chemistry, Shanghai University, Shanghai 200444, China.

[b]Department of Chemistry, Fudan University, 2005 Songhu Road, Shanghai 200438, China

[c]Shanghai Key Laboratory of Regulatory Biology, Institute of Biomedical Sciences, School of Life Sciences, East China Normal University, 500 Dongchuan Road, Shanghai 200241, China

[d]Institute of Research and Development, Duy Tan University, K7/25 Quang Trung, Danang 57000, Vietnam.

[e]Laboratory of Molecular Immunology, State Key Laboratory of Genetic Engineering, School of Life Sciences, Fudan University, 220 Handan Road, Shanghai 200433, China.

[f]Department of Biological Sciences, National University of Medical Sciences, Rawalpindi, 46000, Pakistan.

*Corresponding Authors E-mail: zhangdw@fudan.edu.cn (D.-W. Zhang), wanghui@fudan.edu.cn (H. Wang)

Tel.: +86 21 65643576

[1] F. -U. Rahman, A. Ali and H.-Q. Duong have equal contribution in this work

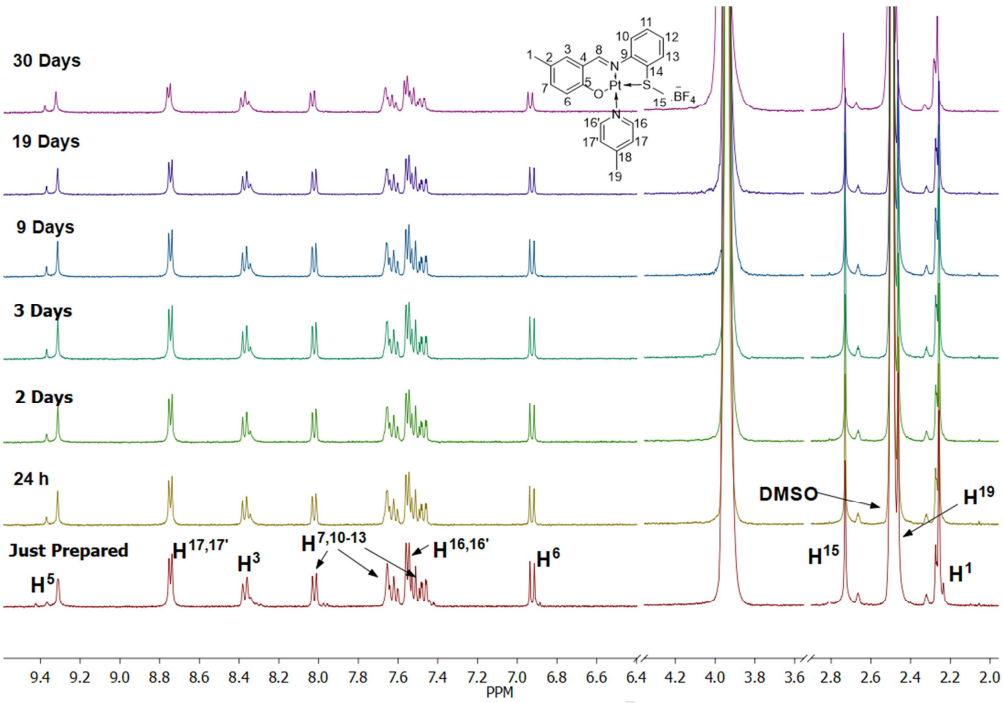


**Fig. S1** Stability analysis of **C2b** in 17 % $D_2O$/DMSO, at mentioned time points; the spectra plot over one month showed no change in the respective proton signals therefore we can say **C2b** is stable in the current medium.

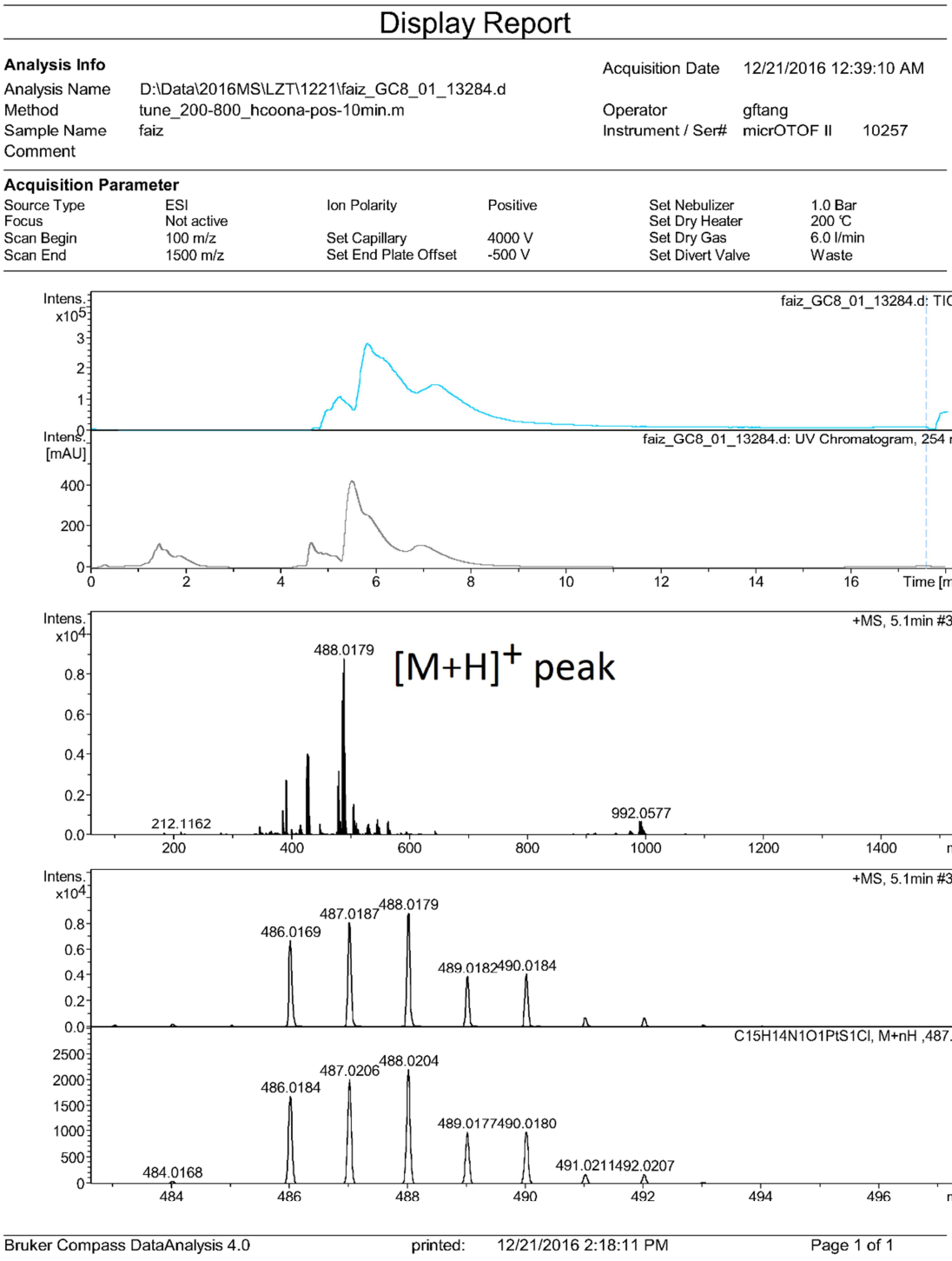


**Fig. S2** Stability analysis of **C2a** in 17 % $D_2O$/DMSO by LC-HRMS; **C2a** was dissolved in mixture of water/DMSO 24 h before the analysis. Expanded peak for [**C2a**+nH]$^+$

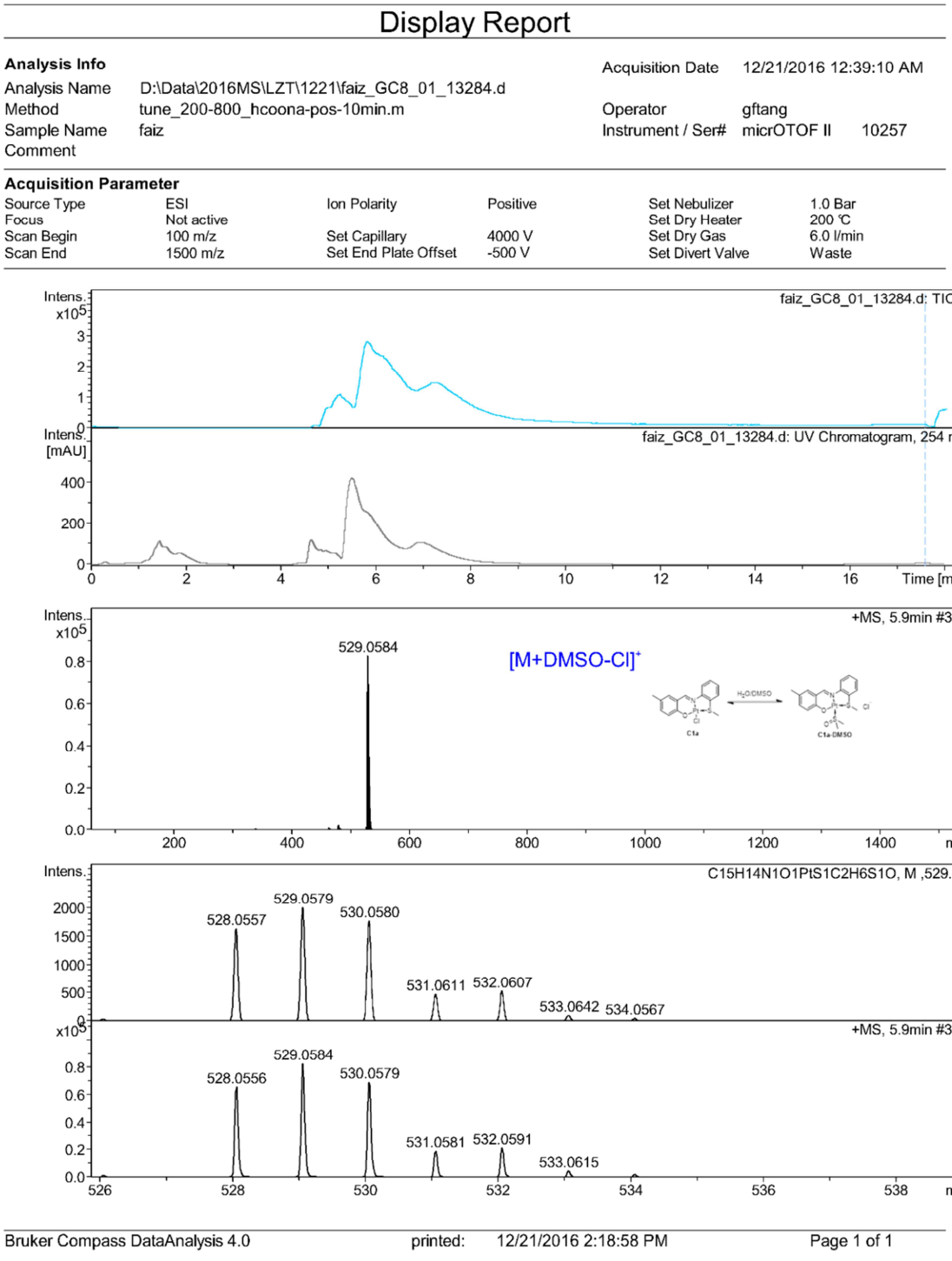


**Fig. S3** Stability analysis of **C2a** in 17 % $D_2O$/DMSO by LC-HRMS; **C2a** was dissolved in mixture of water/DMSO 24 h before the analysis. Expanded peak for [**C2a**+DMSO-Cl]$^+$

Display Report

**Analysis Info**

| | | | |
|---|---|---|---|
| Analysis Name | D:\Data\2016MS\LZT\1223\C2A_GA3_01_13441.d | Acquisition Date | 12/22/2016 2:51:59 PM |
| Method | tune_200-800_hcoona-pos-8min.m | Operator | gftang |
| Sample Name | C2A | Instrument / Ser# | micrOTOF II 10257 |
| Comment | | | |

**Acquisition Parameter**

| | | | | | |
|---|---|---|---|---|---|
| Source Type | ESI | Ion Polarity | Positive | Set Nebulizer | 1.0 Bar |
| Focus | Not active | | | Set Dry Heater | 200 ℃ |
| Scan Begin | 100 m/z | Set Capillary | 4000 V | Set Dry Gas | 6.0 l/min |
| Scan End | 1500 m/z | Set End Plate Offset | -500 V | Set Divert Valve | Waste |

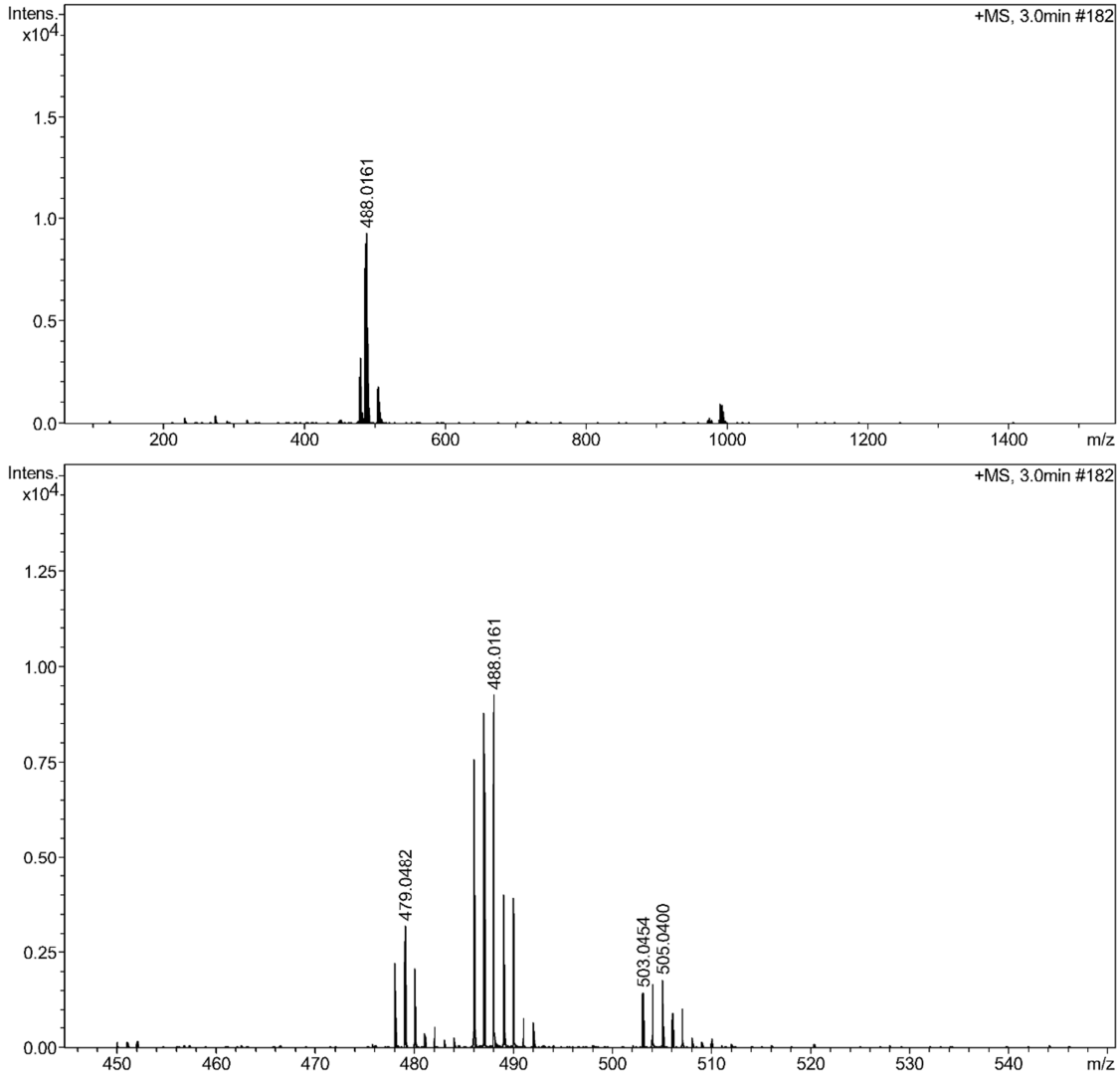


Bruker Compass DataAnalysis 4.0 printed: 12/23/2016 10:30:54 AM Page 1 of 1

**Fig. S4** HR-ESI-MS spectrum of **C2a**, the solution of **C2a** was prepared in DMSO 24 h before the analysis and checked by MS machine.

**Table S1 data and structure refinement of the complexes C1a, C2a, C2b and C3b**

| | C1a | C2a | C2b | C3b |
|---|---|---|---|---|
| Empirical formula | $C_{14.50}H_{13}Cl_2NOPtS$ | $C_{30.5}H_{29}C_{l3}N_2O_2Pt_2S_2$ | $C_{21}H_{21}BF_4N_2OPtS$ | $C_{20}H_{18}BF_5N_2OPtS$ |
| Formula weight | 515.31 | 1016.21 | 631.36 | 635.32 |
| Temperature (K) | 293(2) | 293(2) | 293(2) | 293(2) |
| Crystal system | Monoclinic | Monoclinic | Monoclinic | Monoclinic |
| Space group | P 21/n | C 2/c | P 21/n | P 21/n |
| Unit cell dimensions | | | | |
| a (Å) | 12.997(7) | 30.525(11) | 8.482(4) | 8.203(3) |
| b (Å) | 7.776(4) | 12.953(5) | 24.453(12) | 18.107(7) |
| c (Å) | 15.518(8) | 18.866(7) | 21.804(11) | 14.307(6) |
| α (°) | 90 | 90 | 90 | 90 |
| β (°) | 104.189(7) | 115.432(5) | 94.408(6) | 101.977(5) |
| γ (°) | 90 | 90 | 90 | 90 |
| Volume ($Å^3$) | 1520.4(14) | 6737(4) | 4509(4) | 2078.8(14) |
| Z | 4 | 8 | 8 | 4 |
| Density (calculated) ($mg/m^3$) | 2.251 | 2.004 | 1.860 | 2.030 |
| Absorption coefficient ($mm^{-1}$) | 9.712 | 8.689 | 6.364 | 6.910 |
| F(000) | 972 | 3848 | 2432 | 1216 |
| Crystal size ($mm^3$) | 0.320 x 0.300 x 0.120 | 0.300 x 0.120 x 0.100 | 0.400 x 0.320 x 0.050 | 0.400 x 0.220 x 0.200 |
| Theta range for data collection (°) | 1.836 to 25.991 | 1.477 to 26.997 | 1.253 to 25.998 | 1.839 to 25.999 |
| Index ranges | -16<=h<=15, -9<=k<=9, -19<=l<=11 | -38<=h<=36, -16<=k<=16, -24<=l<=23 | -10<=h<=10, -30<=k<=27, -26<=l<=20 | -10<=h<=10, -21<=k<=22, -17<=l<=13 |
| Reflections collected | 6684 | 16256 | 20458 | 9378 |
| Independent reflections | 2976 [R(int) = 0.0560] | 7220 [R(int) = 0.0707] | 8773 [R(int) = 0.0812] | 4063 [R(int) = 0.0534] |

| | | | | |
|---|---|---|---|---|
| Completeness to theta = 25.242° (%) | 99.8 | 99.7 | 99.3 | 99.7 |
| Absorption correction | Semi-empirical from equivalents | Semi-empirical from equivalents | Semi-empirical from equivalents | Semi-empirical from equivalents |
| Max. and min. transmission | 1.000 and 0.172 | 1.000 and 0.365 | 1.000 and 0.334 | 1.000 and 0.270 |
| Refinement method | Full-matrix least-squares on $F^2$ | Full-matrix least-squares on $F^2$ | Full-matrix least-squares on $F^2$ | Full-matrix least-squares on $F^2$ |
| Data / restraints / parameters | 2976/14 /201 | 7220/0 /379 | 8773/23/555 | 4063/48/310 |
| Goodness-of-fit on $F^2$ | 1.011 | 0.724 | 0.861 | 0.919 |
| Final R indices [I>2sigma(I)] | $R1^{[a]}$ = 0.0363, $wR2^{[b]}$ = 0.0882 | $R1^{[a]}$ = 0.0369, $wR2^{[b]}$ = 0.0598 | $R1^{[a]}$ = 0.0537, $wR2^{[b]}$ = 0.1136 | $R1^{[a]}$ = 0.0287, $wR2^{[b]}$ = 0.0646 |
| R indices (all data) | $R1^{[a]}$ = 0.0407, $wR2^{[b]}$ = 0.0900 | $R1^{[a]}$ = 0.0797, $wR2^{[b]}$ = 0.0630 | $R1^{[a]}$ = 0.1027, $wR2^{[b]}$ = 0.1262 | $R1^{[a]}$ = 0.0383, $wR2^{[b]}$ = 0.0662 |
| Extinction coefficient | 0.0055(3) | n/a | n/a | n/a |
| Largest diff. peak and hole (e.$Å^{-3}$) | 1.632 and -2.078 | 1.252 and -1.048 | 1.309 and -1.367 | 1.402 and -0.797 |

[a] $R1 = \Sigma_{\text{all reflections}} |F_0 - F_c| / \Sigma_{\text{all reflections}} |F_0|$, [b] $wR2 = [\Sigma w(F_0^2 - F_c^2)^2 / \Sigma(w(F_0^2)^2)]^{1/2}$.

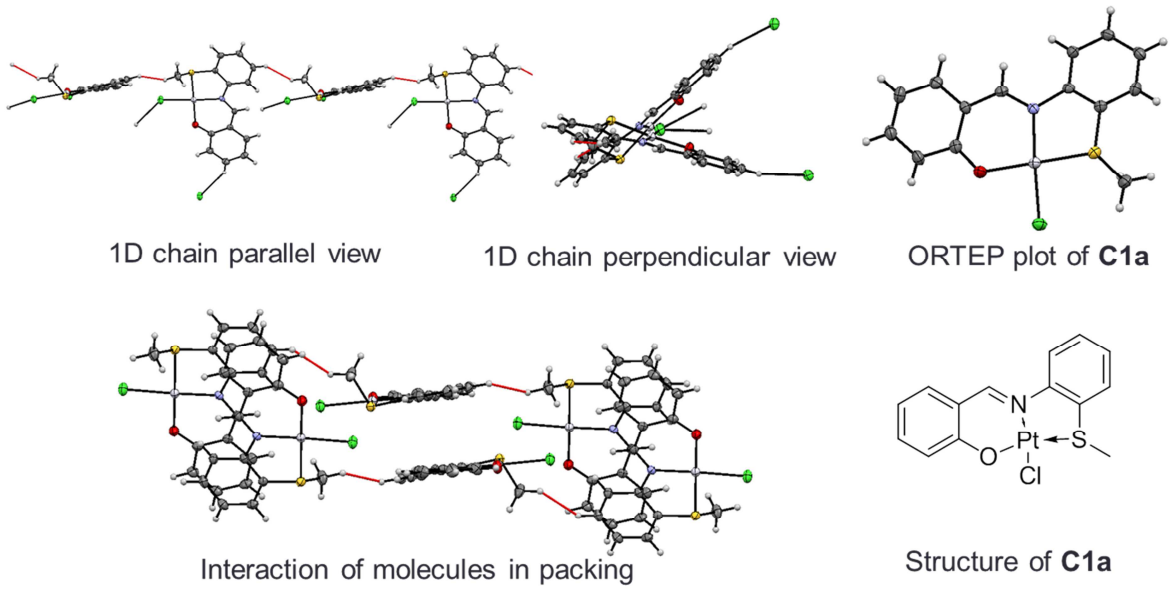


**Fig. S5** Structure, ORTEP plot, orientation in crystal packing and different intermolecular interactions in **C1a**

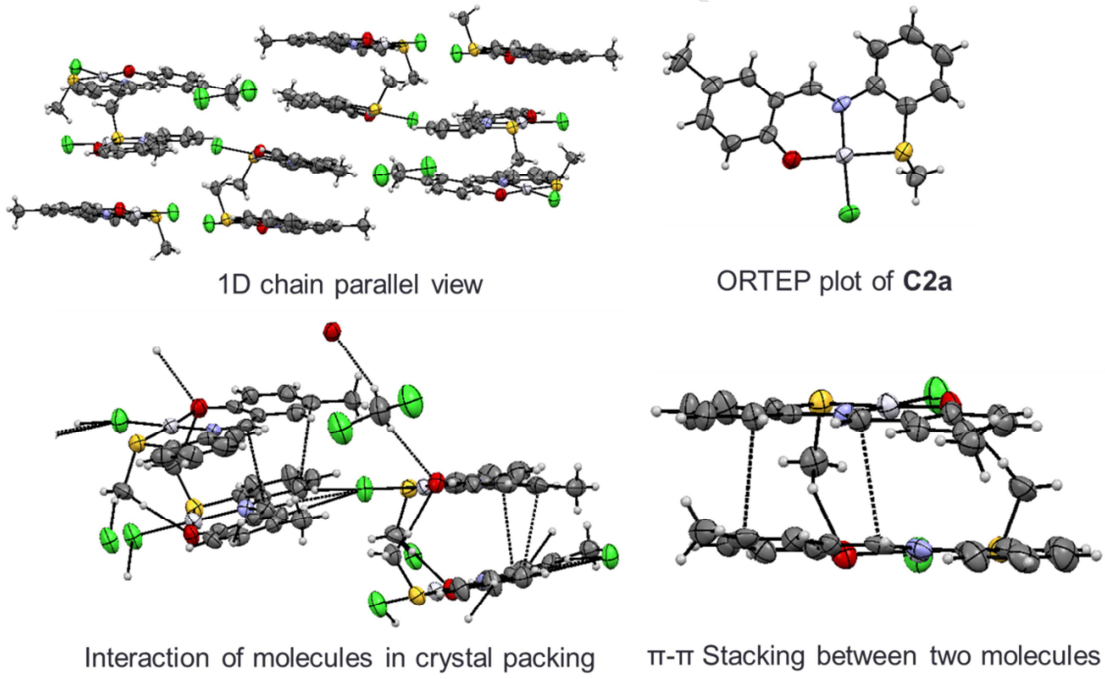


**Fig. S6** ORTEP plot, orientation in crystal packing and different intermolecular interactions in **C2a**

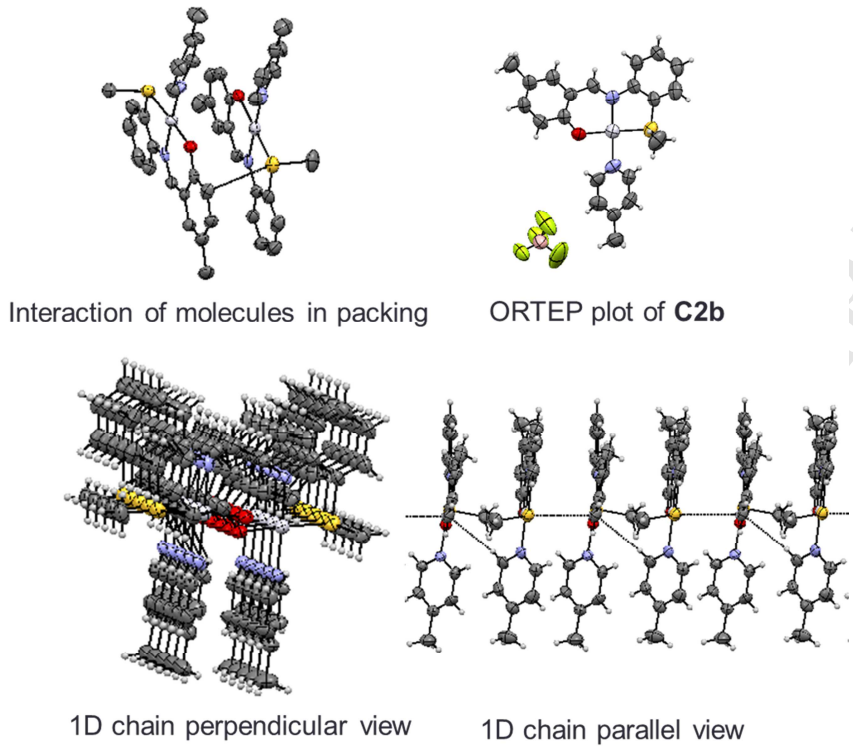


**Fig. S7** ORTEP plot, orientation in crystal packing and different intermolecular interactions in **C2b**

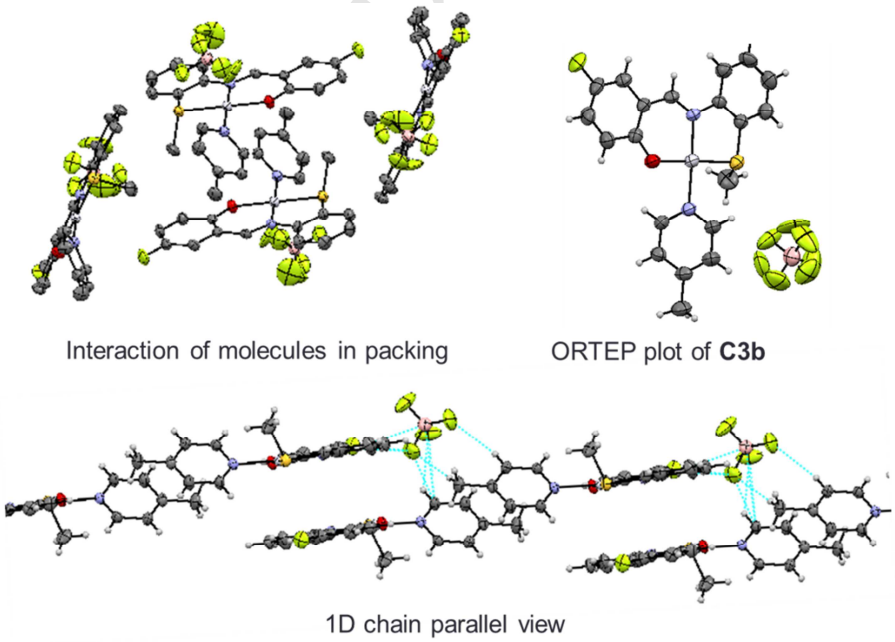


**Fig. S8** ORTEP plot, orientation in crystal packing and different intermolecular interactions in **C3b**

## $^{1}$H, $^{13}$C and $^{19}$F NMR spectra of all ligands

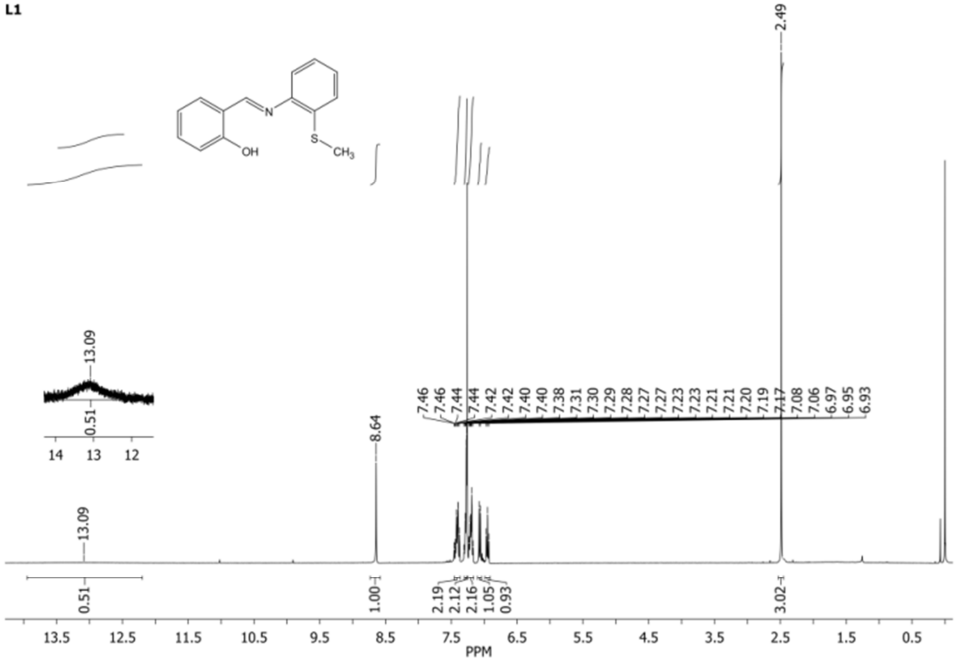


**Fig. S1** $^{1}$H NMR of **L1** in $CDCl_3$ at 25°C

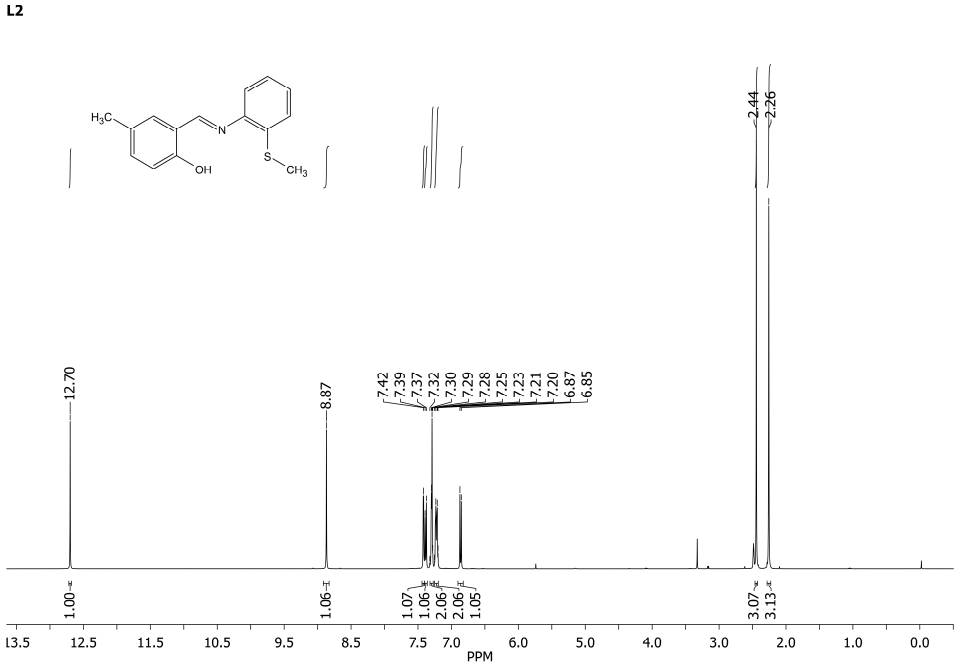


**Fig. S2** $^{1}$H NMR of **L2** in DMSO-$d_6$ at 25°C

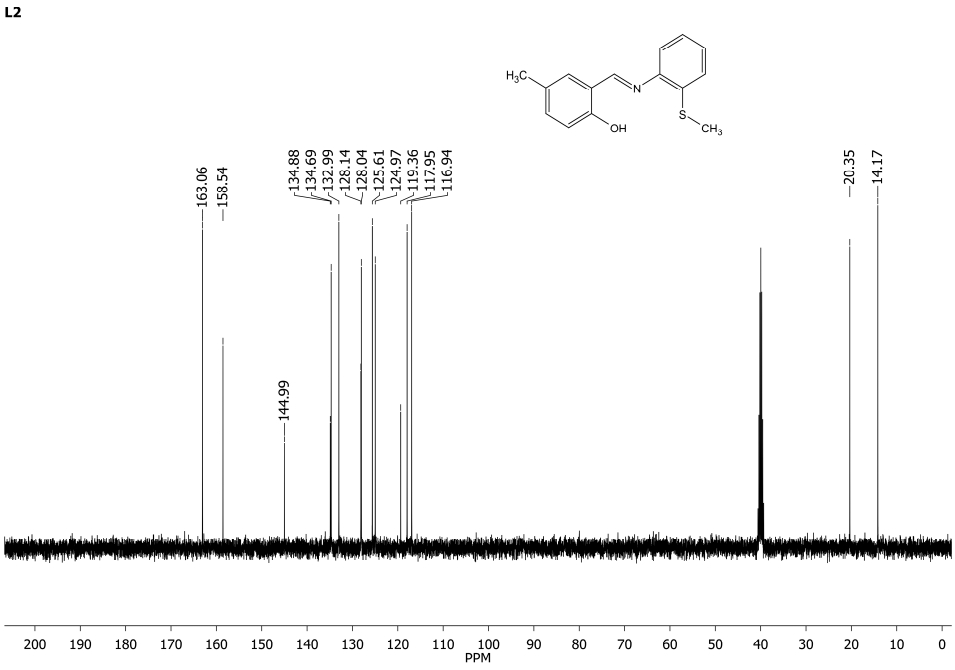


**Fig. S3** $^{13}$C NMR of **L2** in DMSO-$d_6$ at 25°C

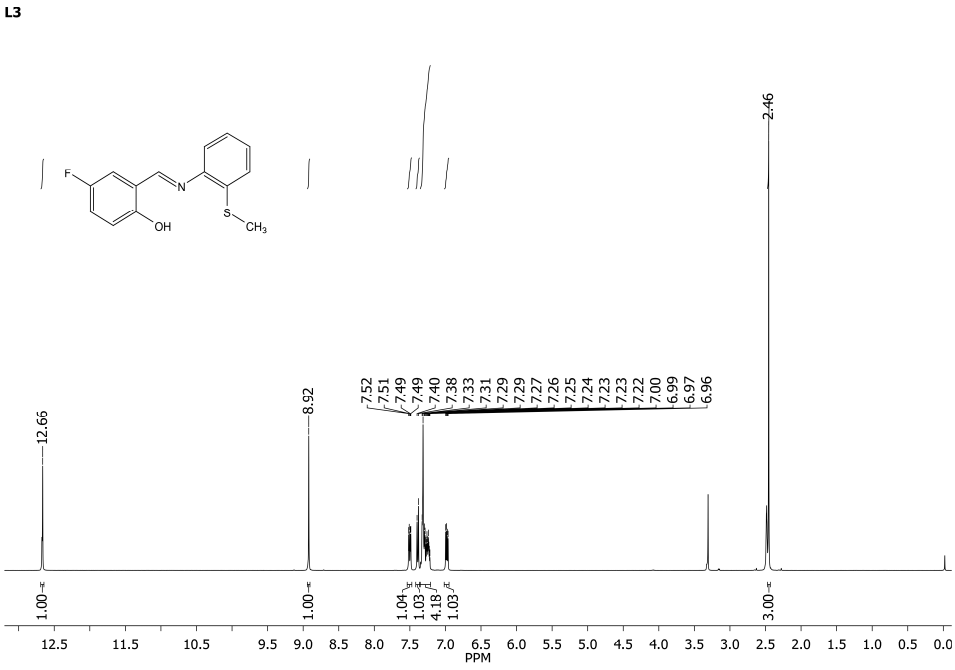


**Fig. S4** $^{1}$H NMR of **L3** in DMSO-$d_6$ at 25°C

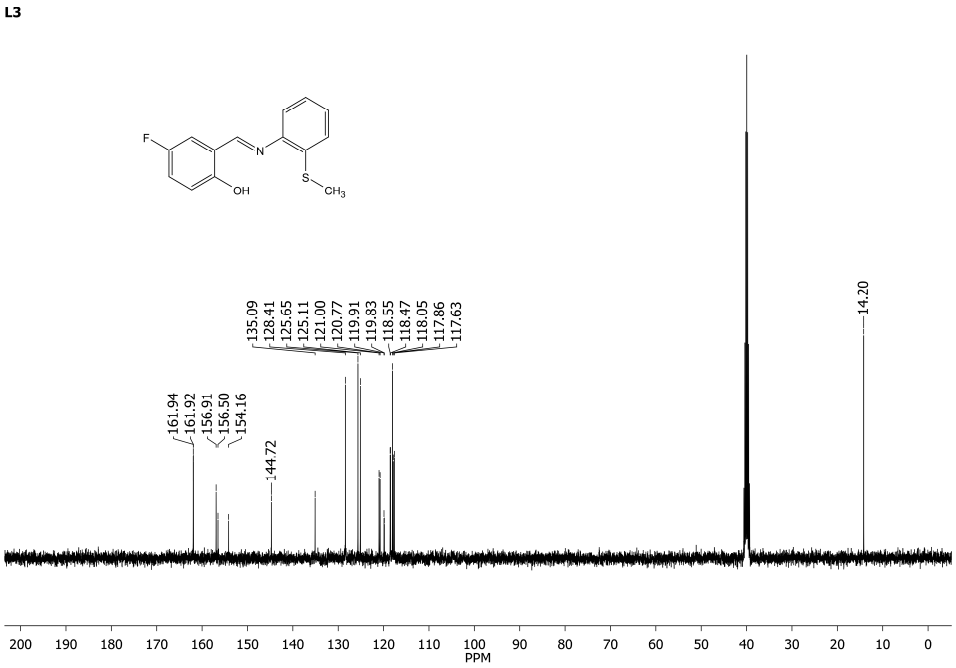


**Fig. S5** $^{13}$C NMR of **L3** in DMSO-$d_6$ at 25°C

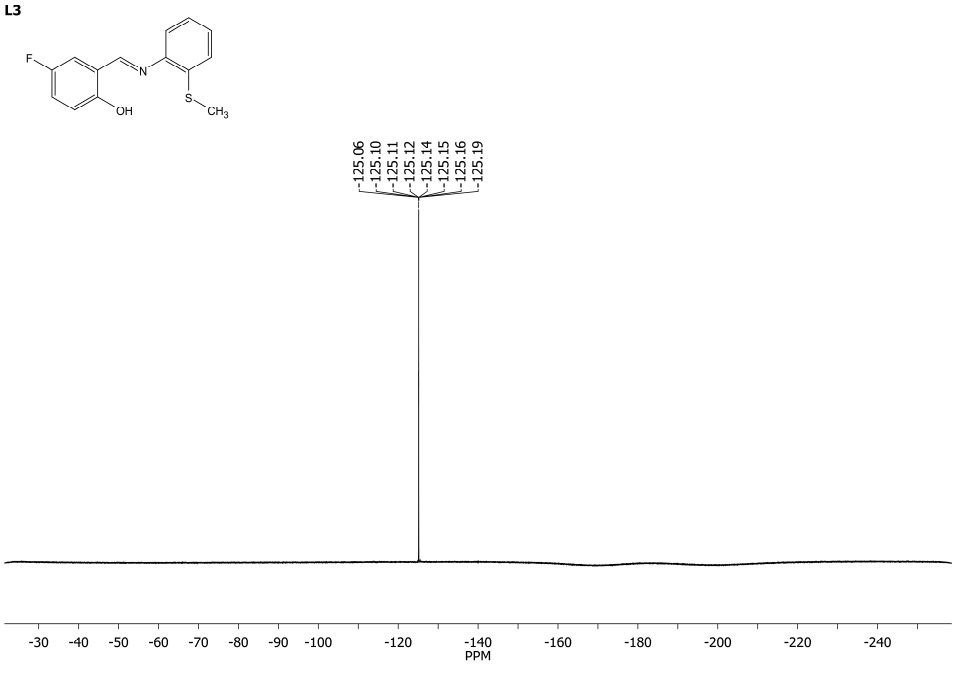


**Fig. S6** $^{19}$F NMR of **L3** in DMSO-$d_6$ at 25°C

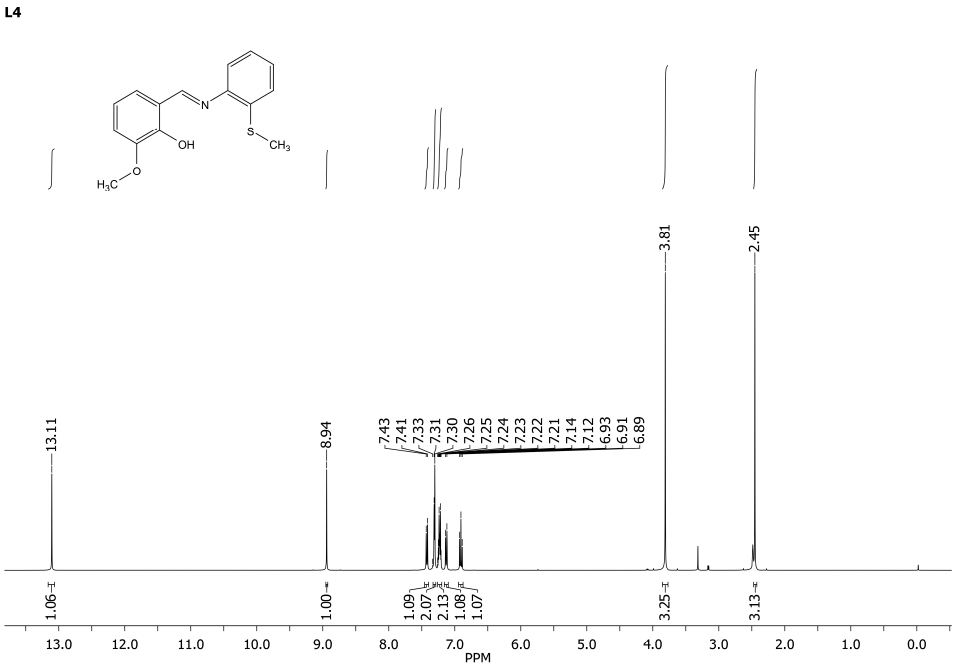


**Fig. S7** $^{1}$H NMR of **L4** in DMSO-$d_6$ at 25°C

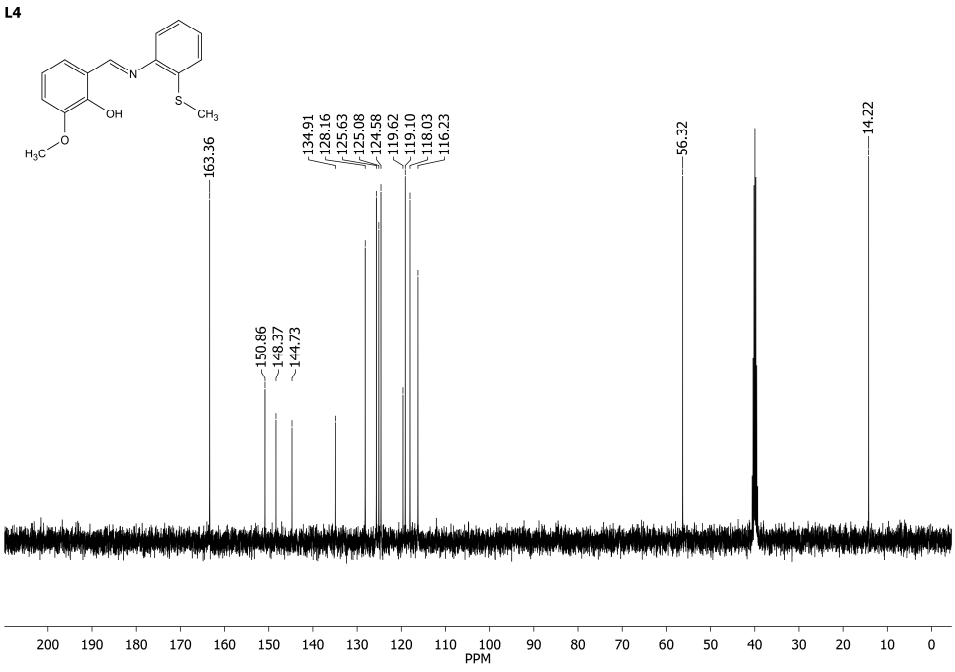


**Fig. S8** $^{1}$H NMR of **L4** in DMSO-$d_6$ at 25°C

## $^{1}$H, $^{13}$C and $^{19}$F NMR spectra of all platinum complexes

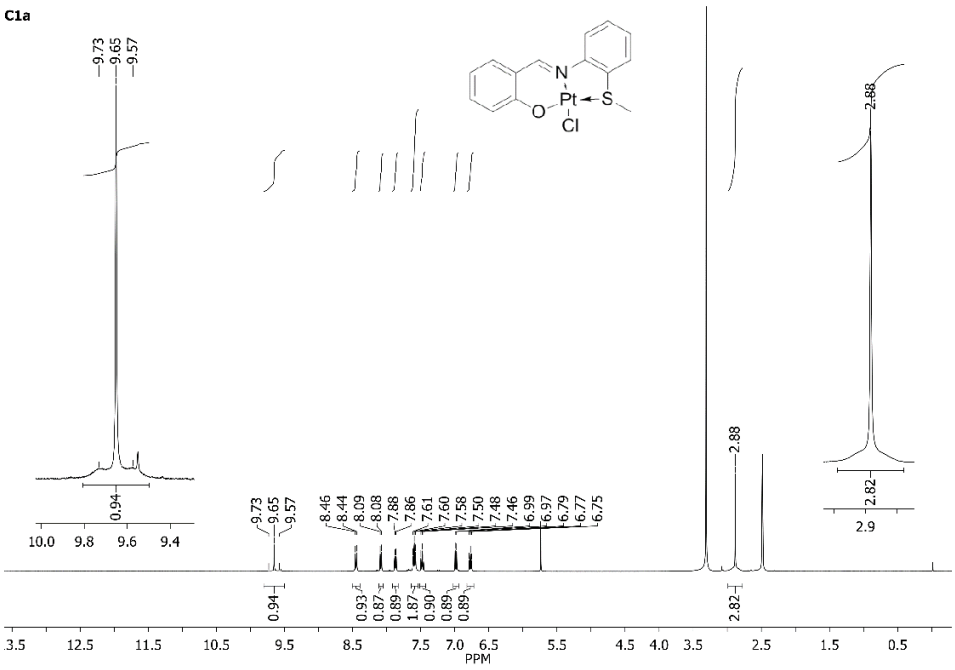


**Fig. S9** $^{1}$H NMR of **C1a** in DMSO-$d_6$ at 25°C

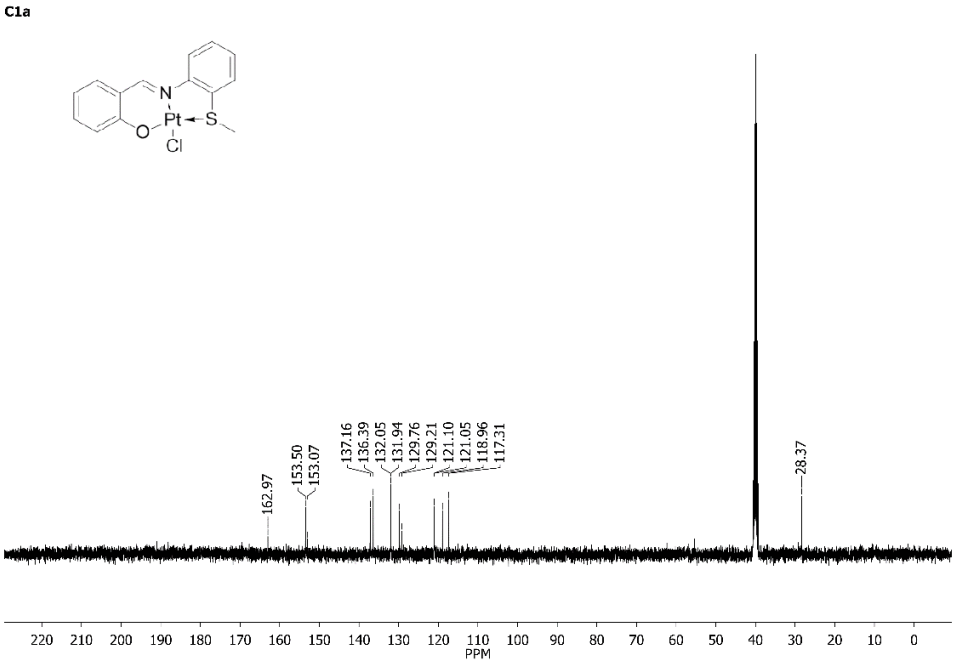


**Fig. S10** $^{13}$C NMR of **C1a** in DMSO-$d_6$ at 25°C

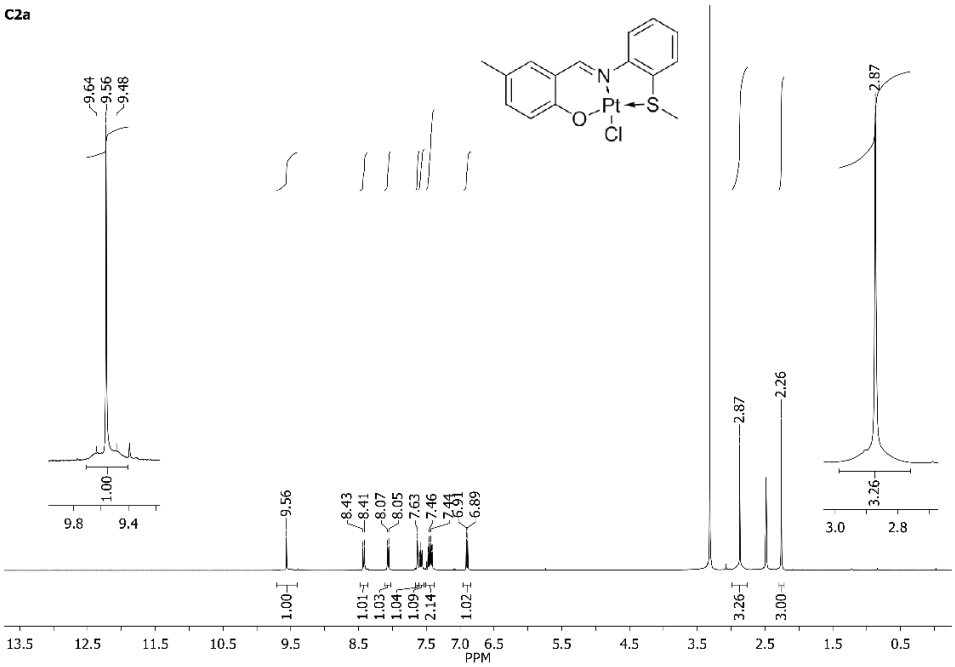


**Fig. S11** $^{13}$H NMR of **C2a** in DMSO-$d_6$ at 25°C

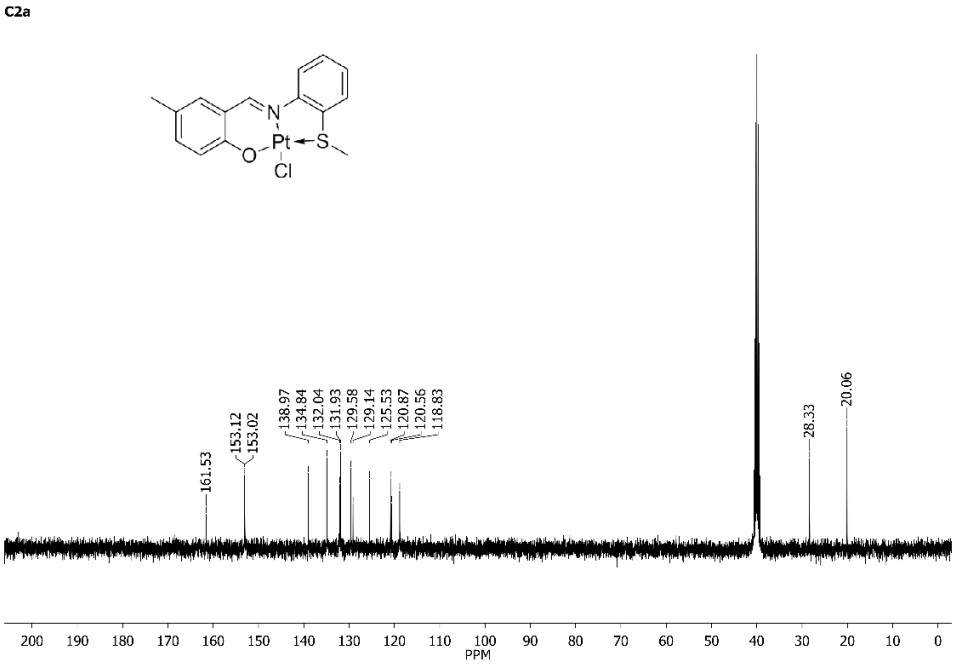


**Fig. S12** $^{13}$C NMR of **C2a** in DMSO-$d_6$ at 25°C

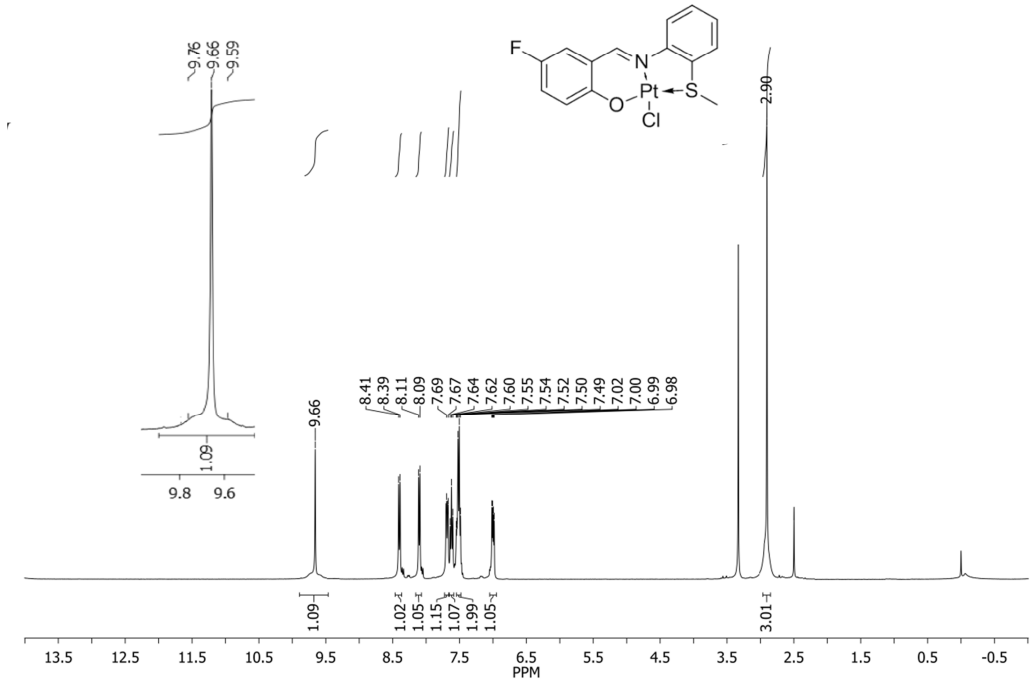


**Fig. S13** $^{1}$H NMR of **C3a** in DMSO-$d_6$ at 25°C

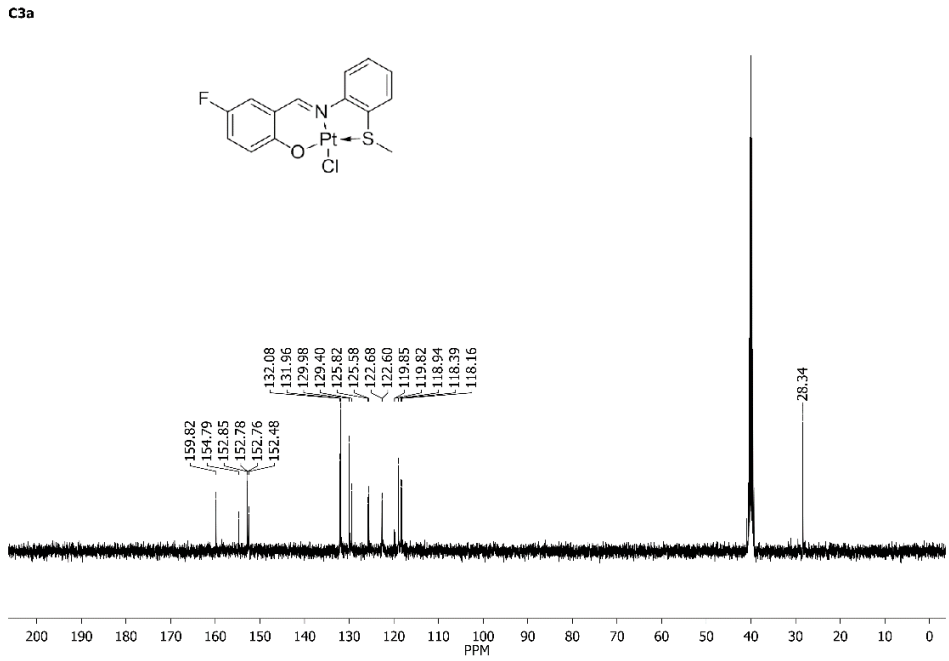


**Fig. S14** $^{13}$C NMR of **C3a** in DMSO-$d_6$ at 25°C

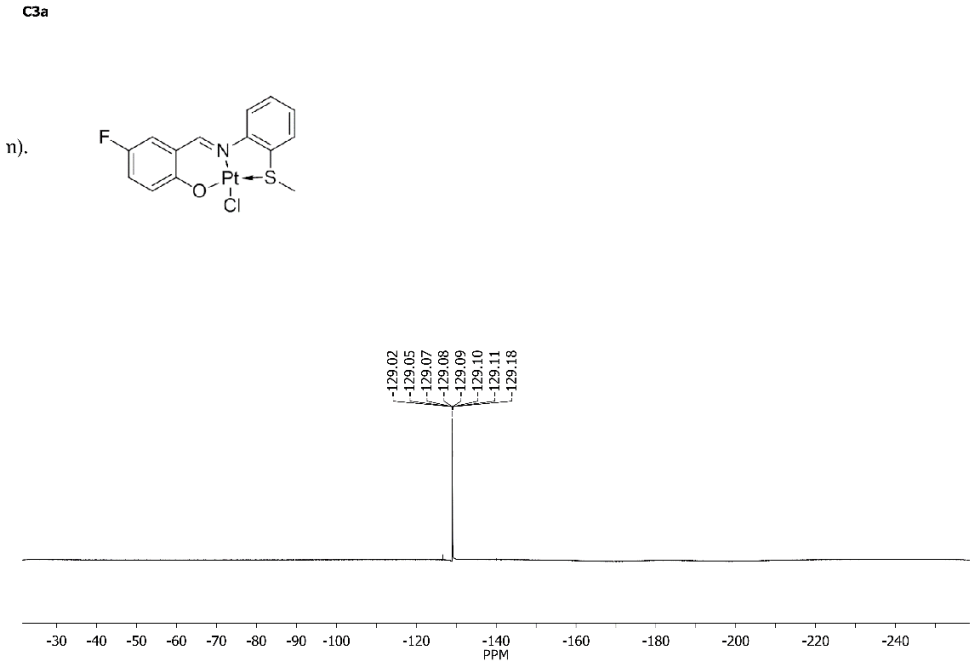


**Fig. S15** $^{19}$F NMR of **C3a** in DMSO-$d_6$ at 25°C

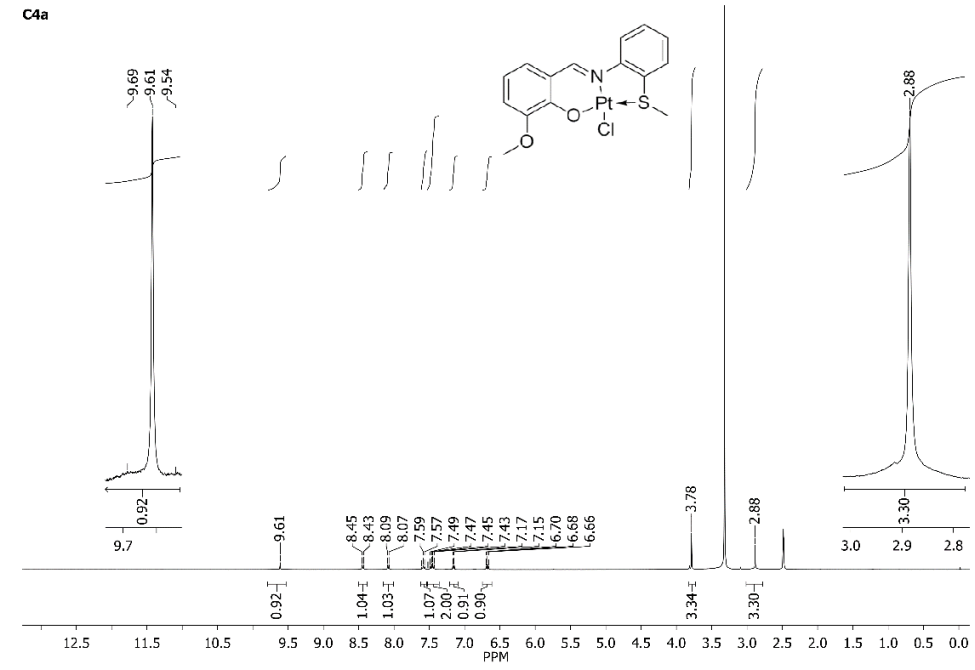


**Fig. S16** $^{1}$H NMR of **C4a** in DMSO-$d_6$ at 25°C

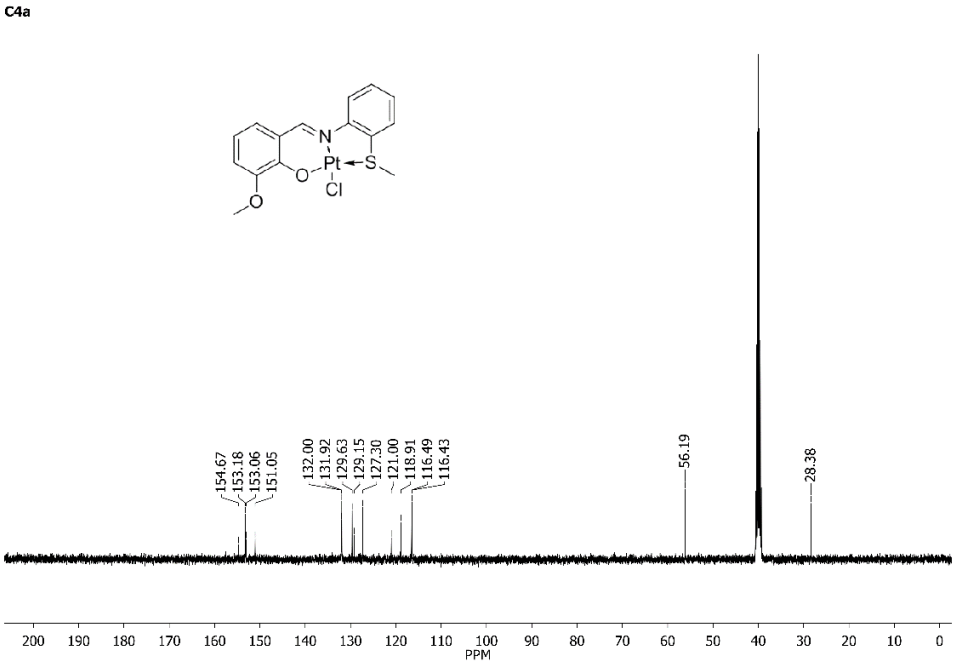


**Fig. S17** $^{13}$C NMR of **C4a** in DMSO-$d_6$ at 25°C

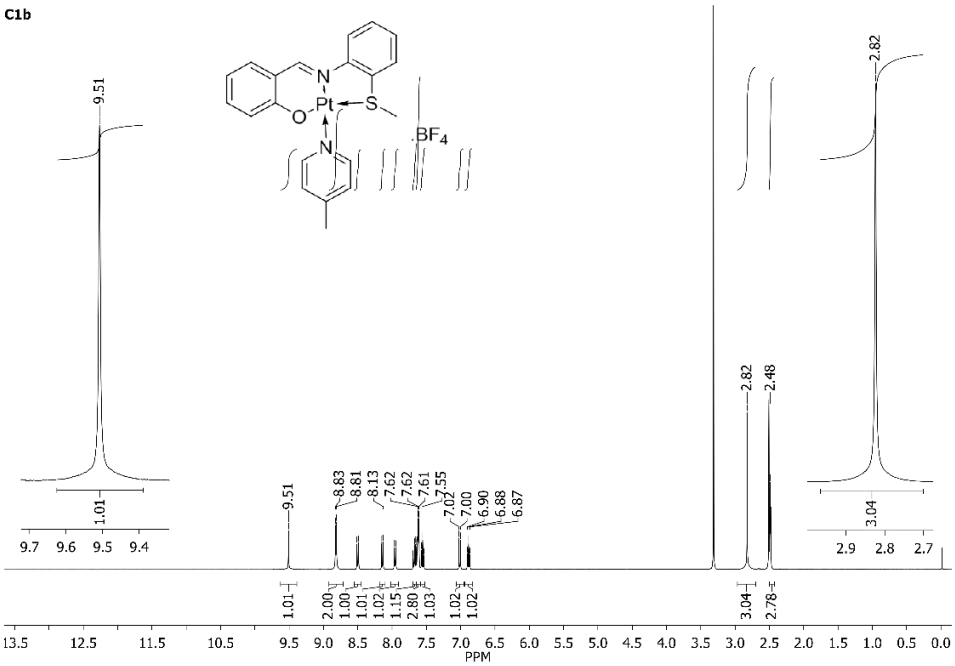


**Fig. S18** $^{1}$H NMR of **C1b** in DMSO-$d_6$ at 25°C

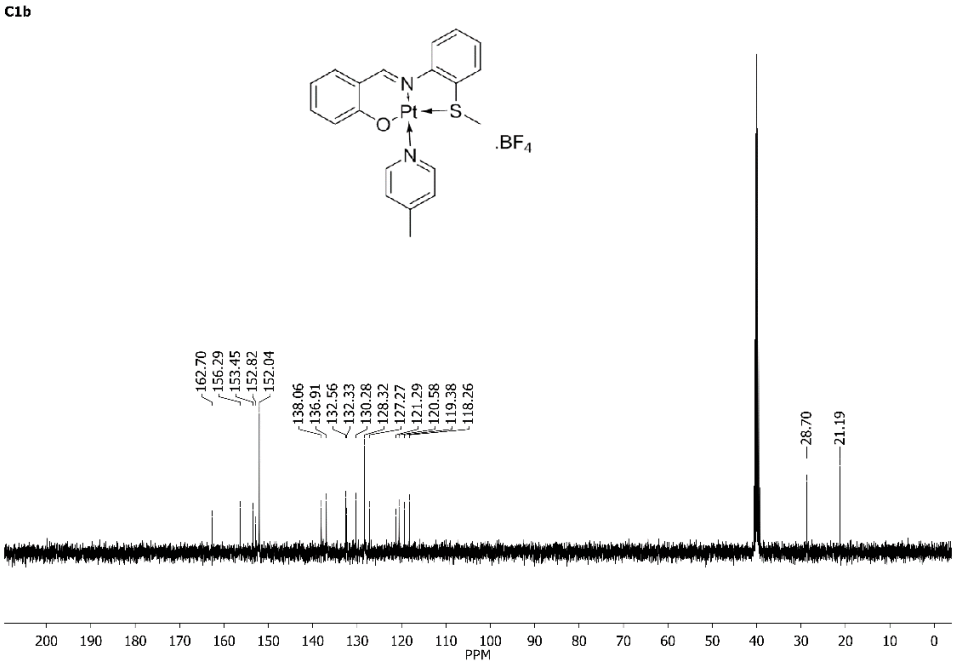


**Fig. S19** $^{13}$C NMR of **C1b** in DMSO-$d_6$ at 25°C

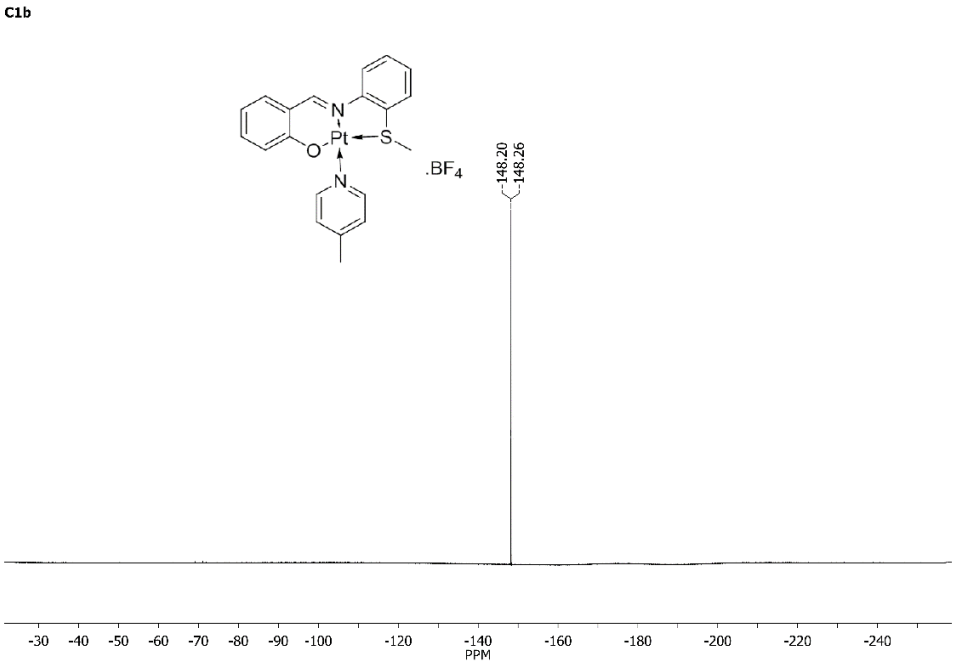


**Fig. S20** $^{19}$F NMR of **C1b** in DMSO-$d_6$ at 25°C

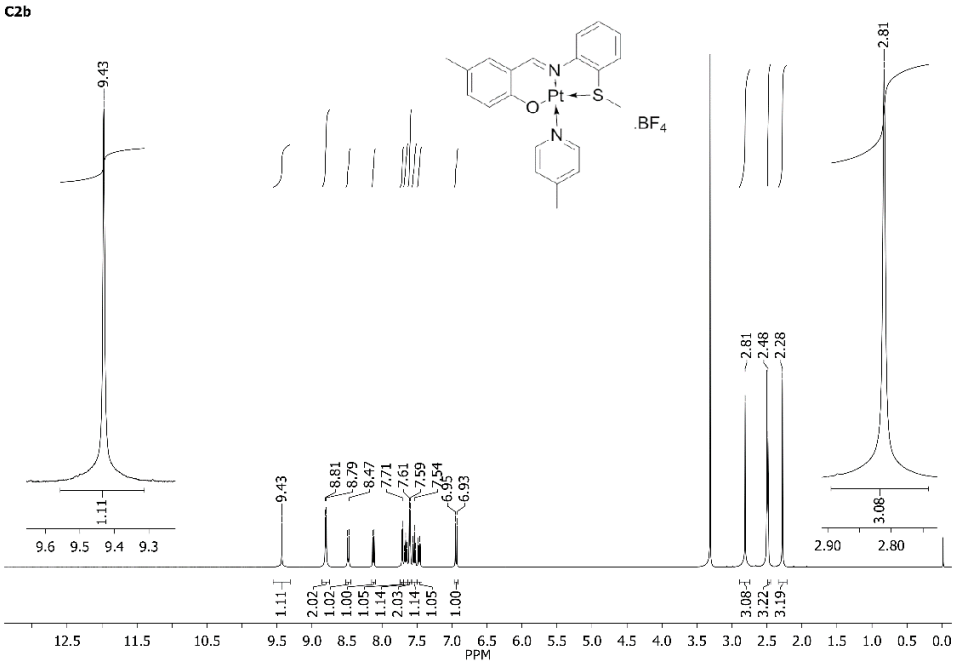


**Fig. S21** $^{1}$H NMR of **C2b** in DMSO-$d_6$ at 25°C

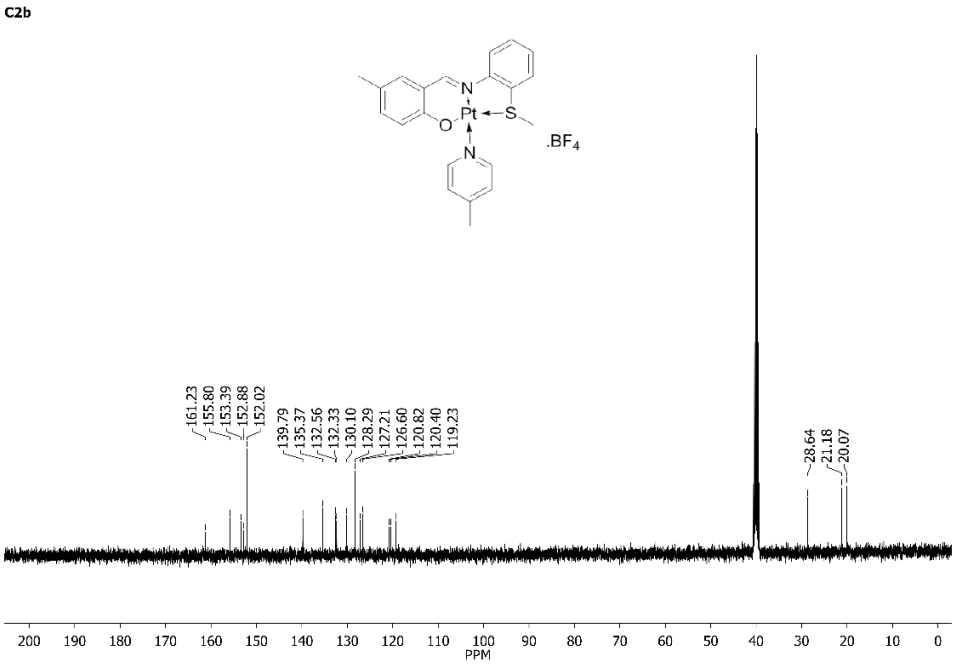


**Fig. S22** $^{13}$C NMR of **C2b** in DMSO-$d_6$ at 25°C

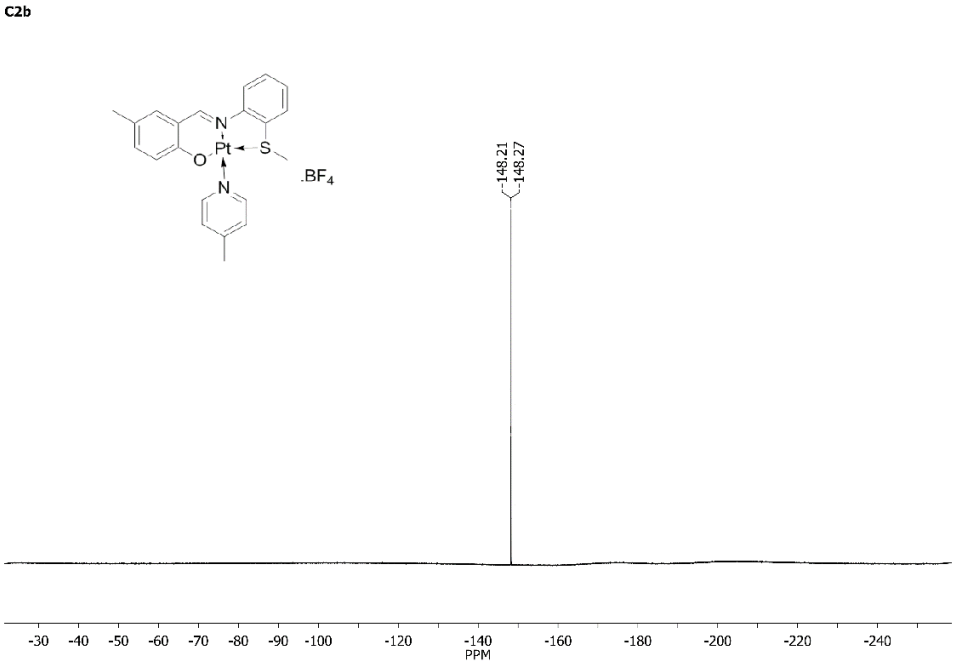


**Fig. S23** $^{19}$F NMR of **C2b** in DMSO-$d_6$ at 25°C

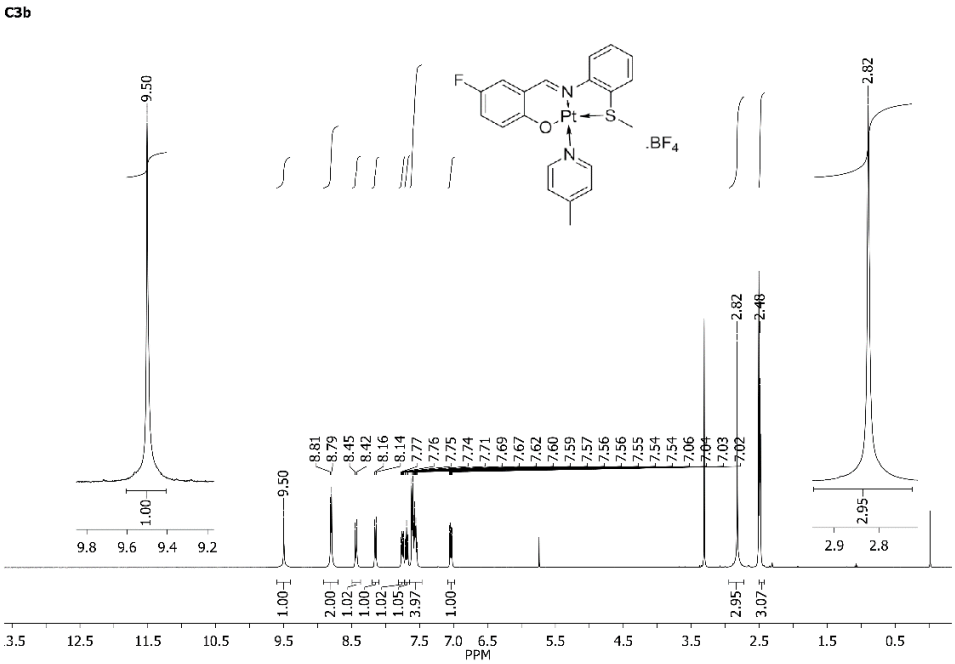


**Fig. S24** $^{1}$H NMR of **C3b** in DMSO-$d_6$ at 25°C

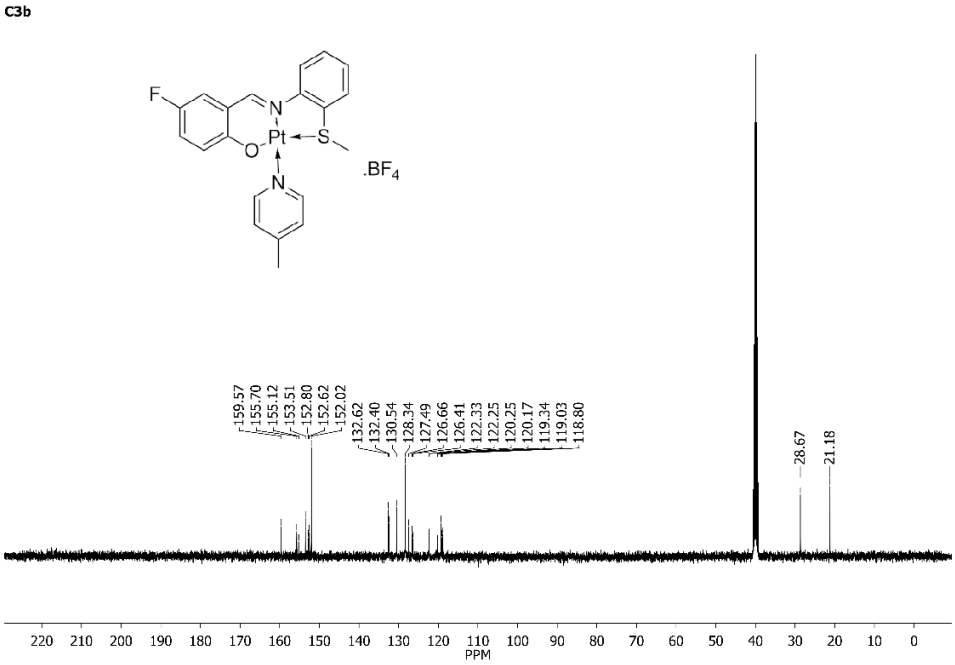


**Fig. S25** $^{13}$C NMR of **C3b** in DMSO-$d_6$ at 25°C

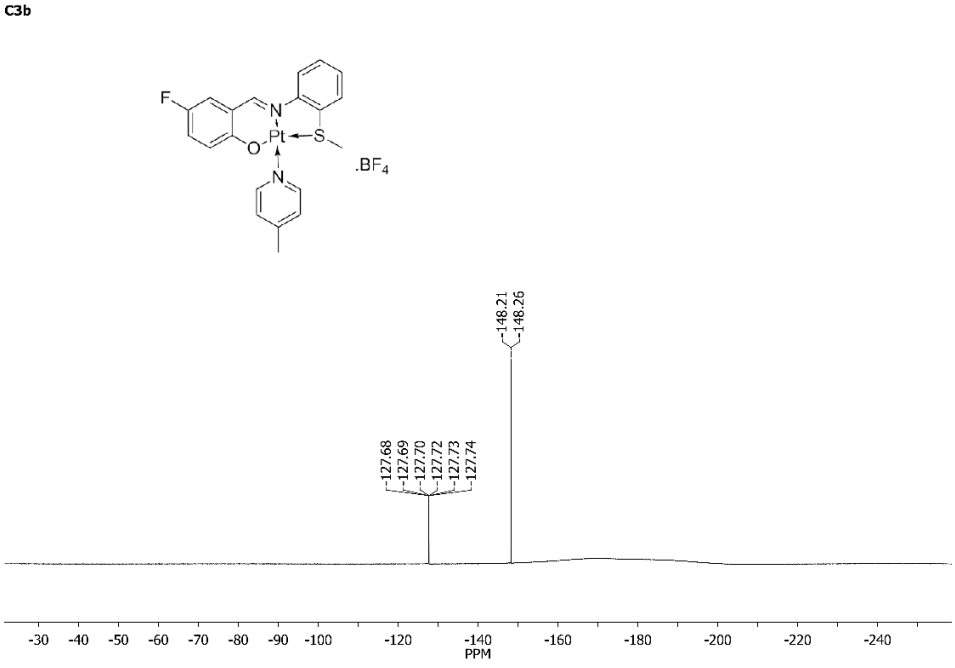


**Fig. S26** $^{19}$F NMR of **C3b** in DMSO-$d_6$ at 25°C

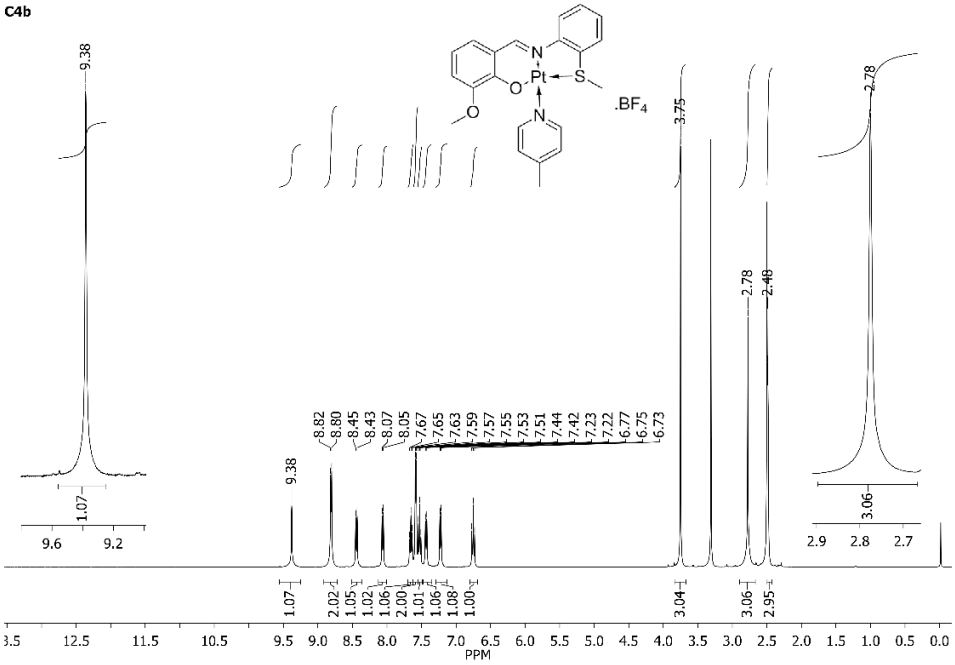


**Fig. S27** $^{1}$H NMR of **C4b** in DMSO-$d_6$ at 25°C

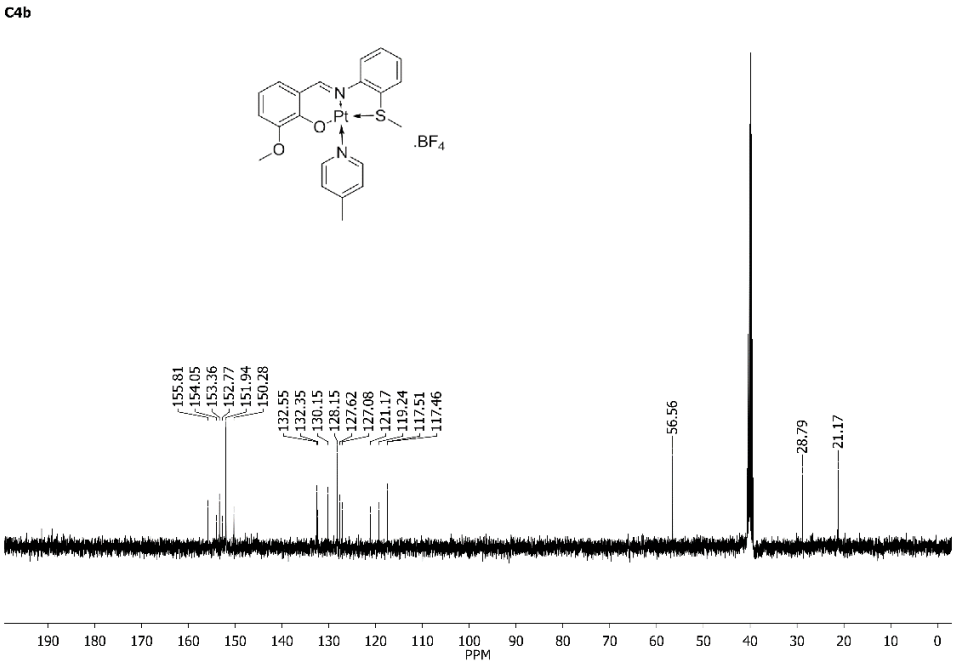


**Fig. S28** $^{13}$C NMR of **C4b** in DMSO-$d_6$ at 25°C

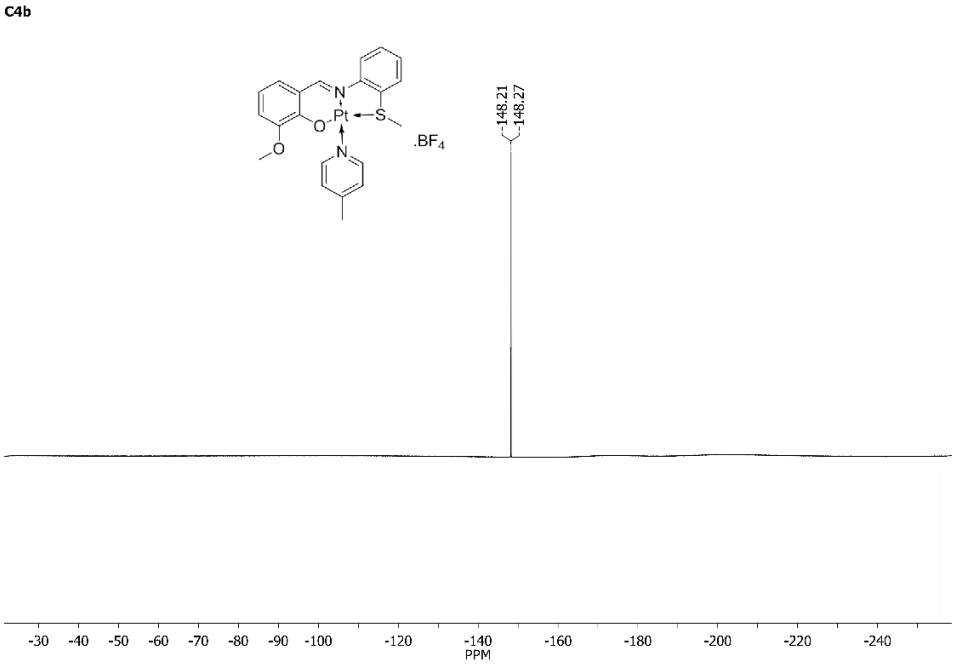


**Fig. S29** $^{19}$F NMR of **C4b** in DMSO-$d_6$ at 25°C

## Mass spectra of all ligands (L3 – L4)

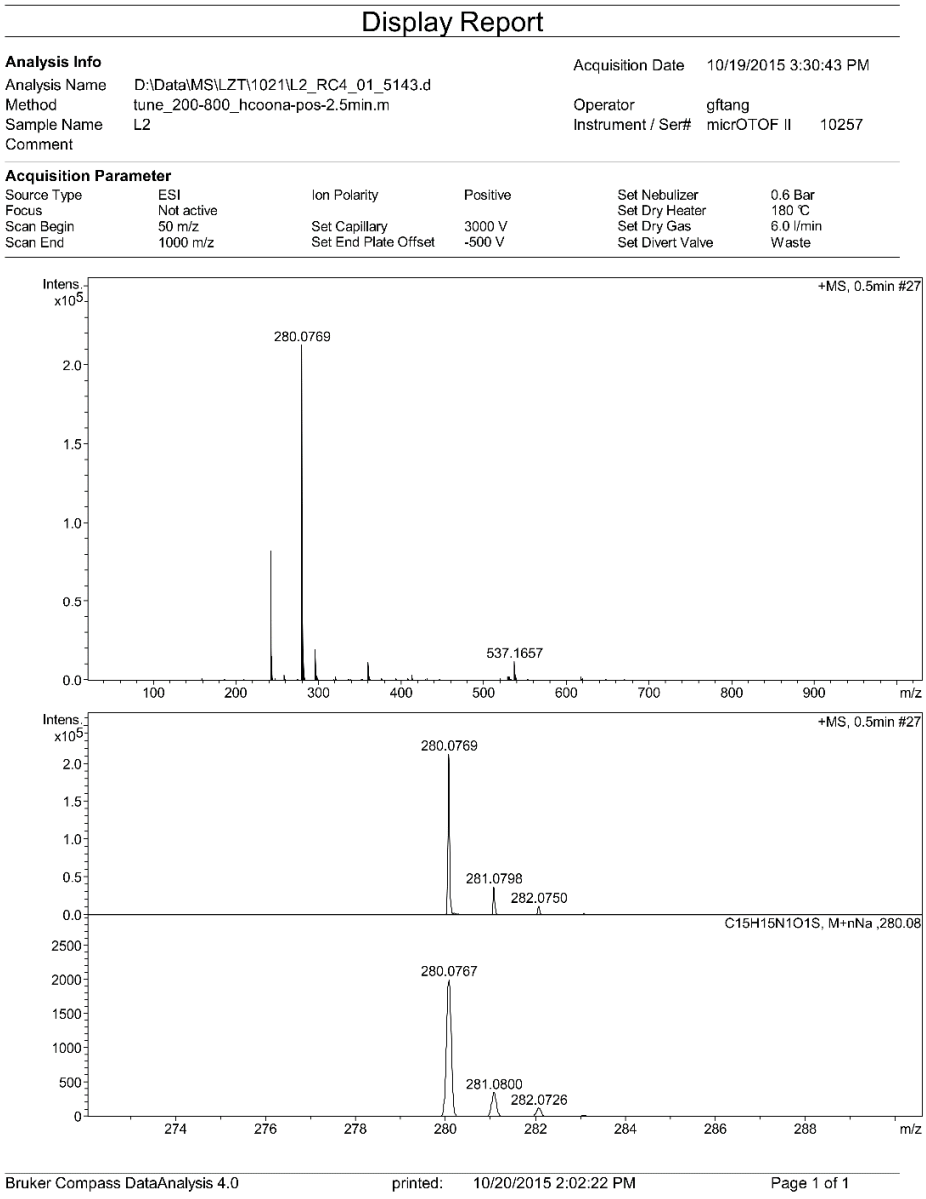


**Fig. S30** Mass Spectrum of **L2**

Display Report

**Analysis Info**

| | | | |
|---|---|---|---|
| Analysis Name | D:\Data\MS\LZT\1021\L3_RC7_01_5146.d | Acquisition Date | 10/19/2015 3:41:24 PM |
| Method | tune_200-800_hcoona-pos-2.5min.m | Operator | gftang |
| Sample Name | L3 | Instrument / Ser# | micrOTOF II 10257 |
| Comment | | | |

**Acquisition Parameter**

| | | | | | |
|---|---|---|---|---|---|
| Source Type | ESI | Ion Polarity | Positive | Set Nebulizer | 0.6 Bar |
| Focus | Not active | | | Set Dry Heater | 180 ℃ |
| Scan Begin | 50 m/z | Set Capillary | 3000 V | Set Dry Gas | 6.0 l/min |
| Scan End | 1000 m/z | Set End Plate Offset | -500 V | Set Divert Valve | Waste |

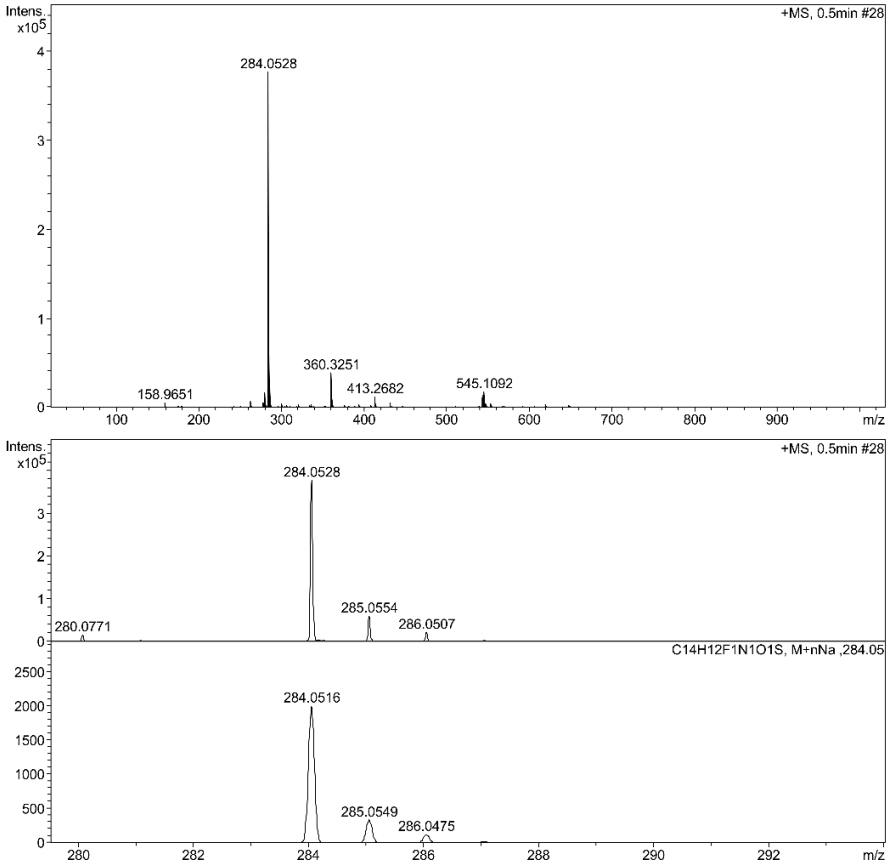


Bruker Compass DataAnalysis 4.0 printed: 10/20/2015 2:05:02 PM Page 1 of 1

**Fig. S31** Mass Spectrum of **L3**

Display Report

**Analysis Info**

| | | | |
|---|---|---|---|
| Analysis Name | D:\Data\MS\LZT\1021\L4_RD2_01_5149.d | Acquisition Date | 10/19/2015 3:52:05 PM |
| Method | tune_200-800_hcoona-pos-2.5min.m | Operator | gftang |
| Sample Name | L4 | Instrument / Ser# | micrOTOF II 10257 |
| Comment | | | |

**Acquisition Parameter**

| | | | | | |
|---|---|---|---|---|---|
| Source Type | ESI | Ion Polarity | Positive | Set Nebulizer | 0.6 Bar |
| Focus | Not active | | | Set Dry Heater | 180 ℃ |
| Scan Begin | 50 m/z | Set Capillary | 3000 V | Set Dry Gas | 6.0 l/min |
| Scan End | 1000 m/z | Set End Plate Offset | -500 V | Set Divert Valve | Waste |

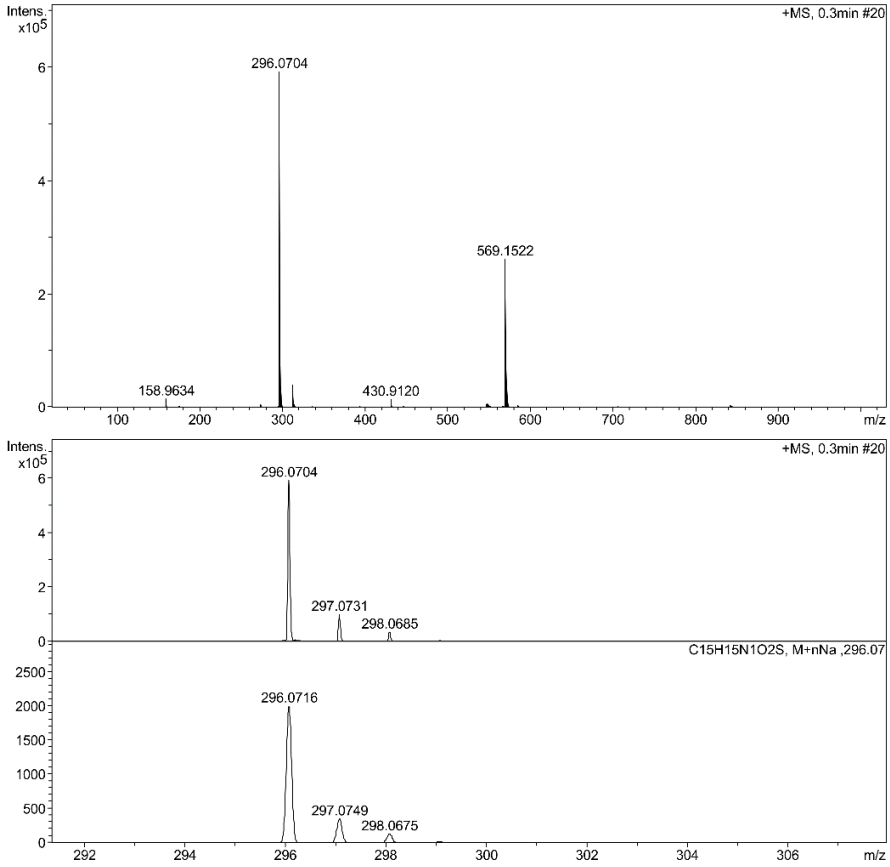


Bruker Compass DataAnalysis 4.0 printed: 10/20/2015 2:07:43 PM Page 1 of 1

**Fig. S32** Mass Spectrum of **L4**

## Mass spectra of all platinum complexes (C1a – C4a, C1b – C4b)

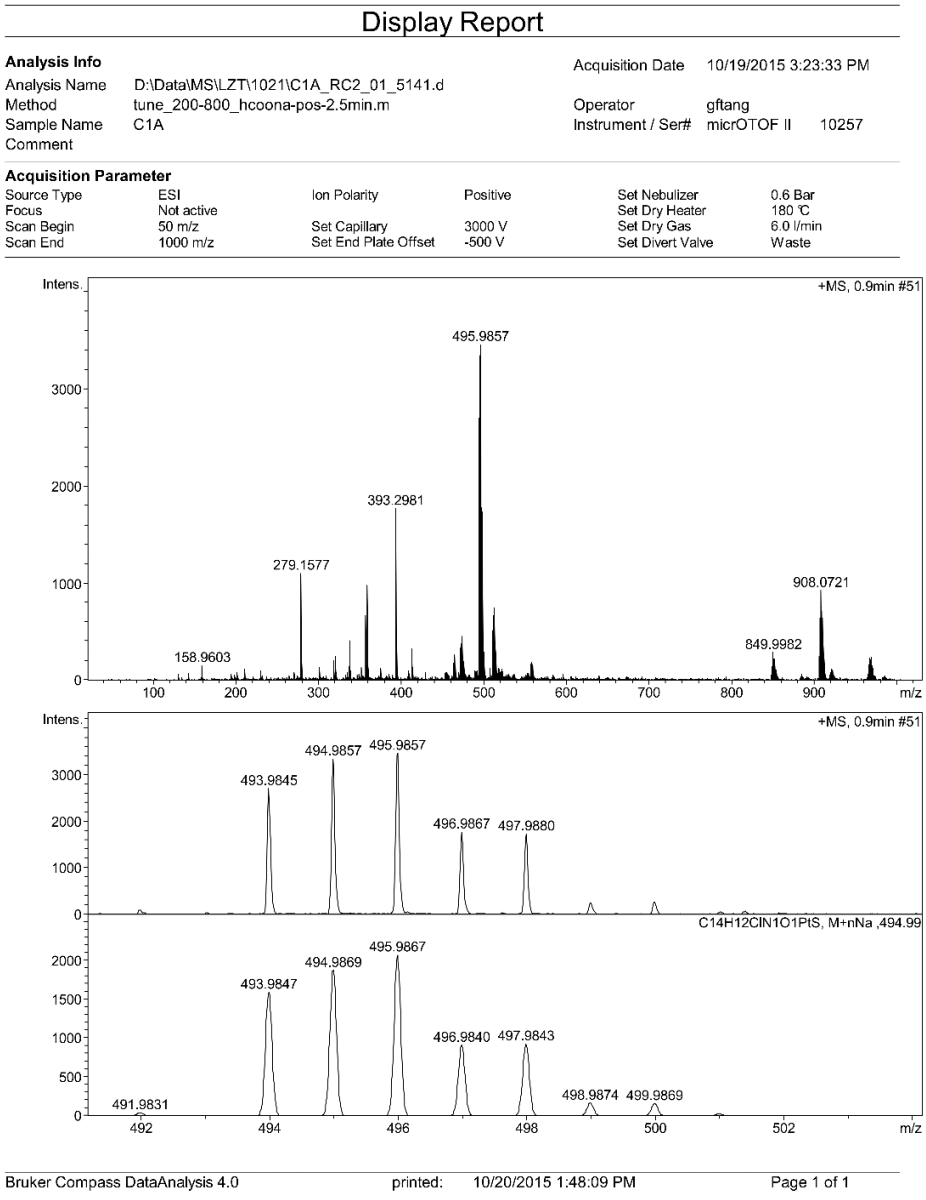


**Fig. S33** Mass Spectrum of **C1a**

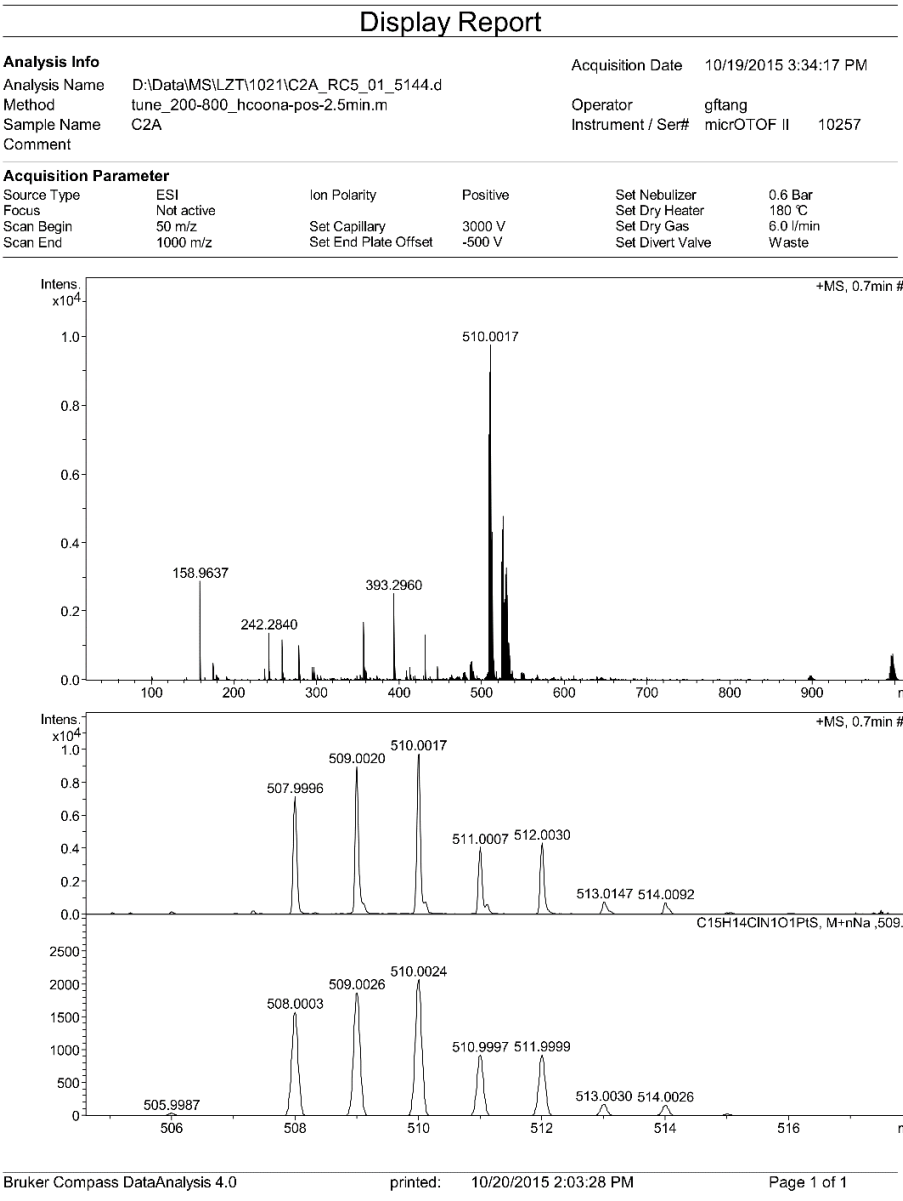


**Fig. S34** Mass Spectrum of **C2a**

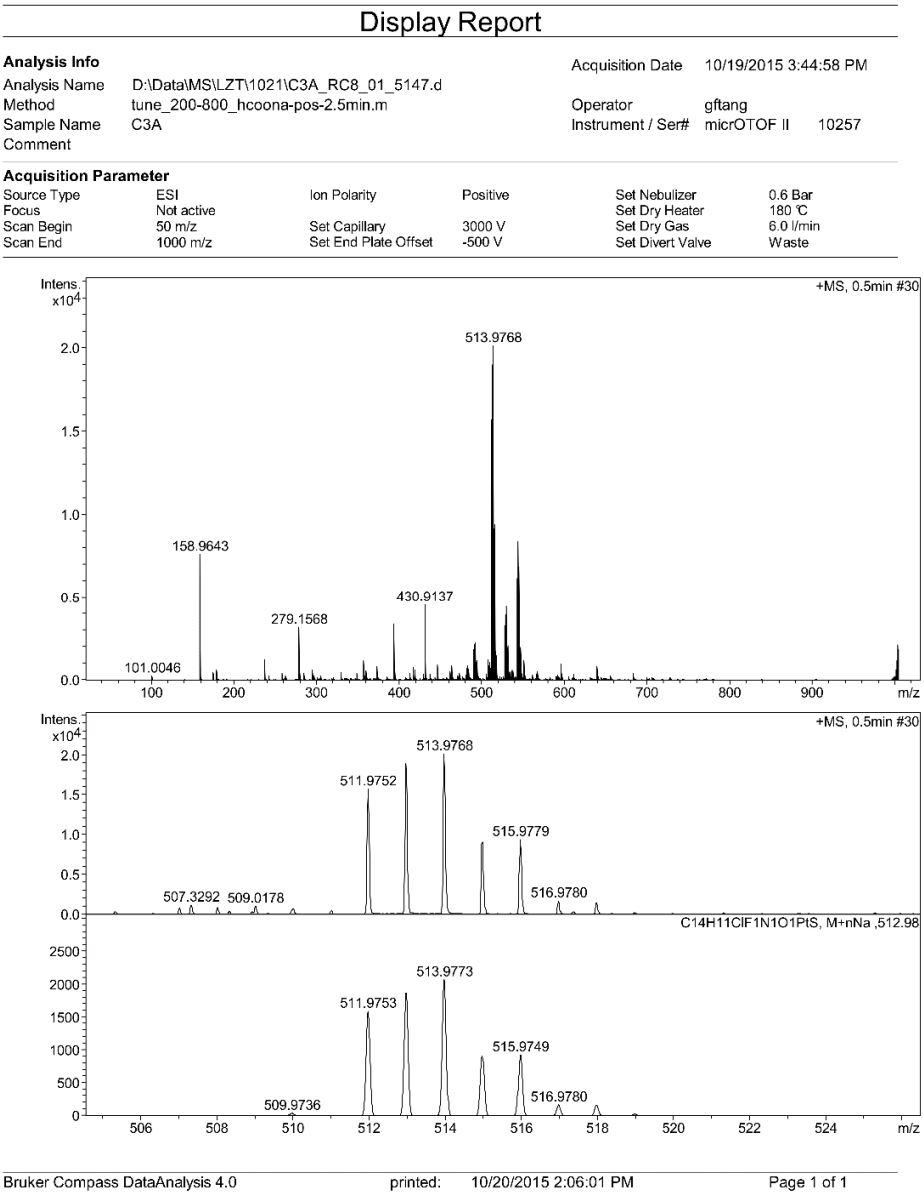


**Fig. S35** Mass Spectrum of **C3a**

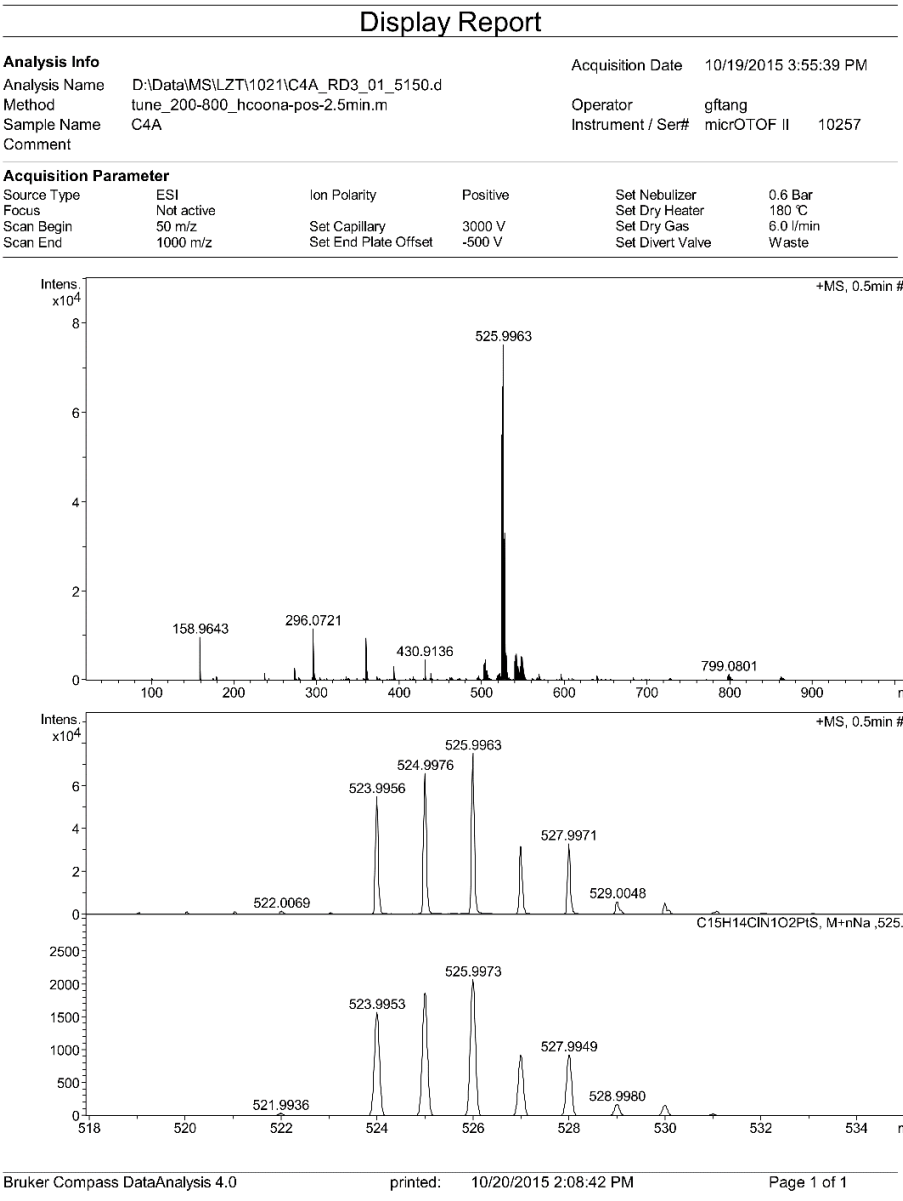


**Fig. S36** Mass Spectrum of **C4a**

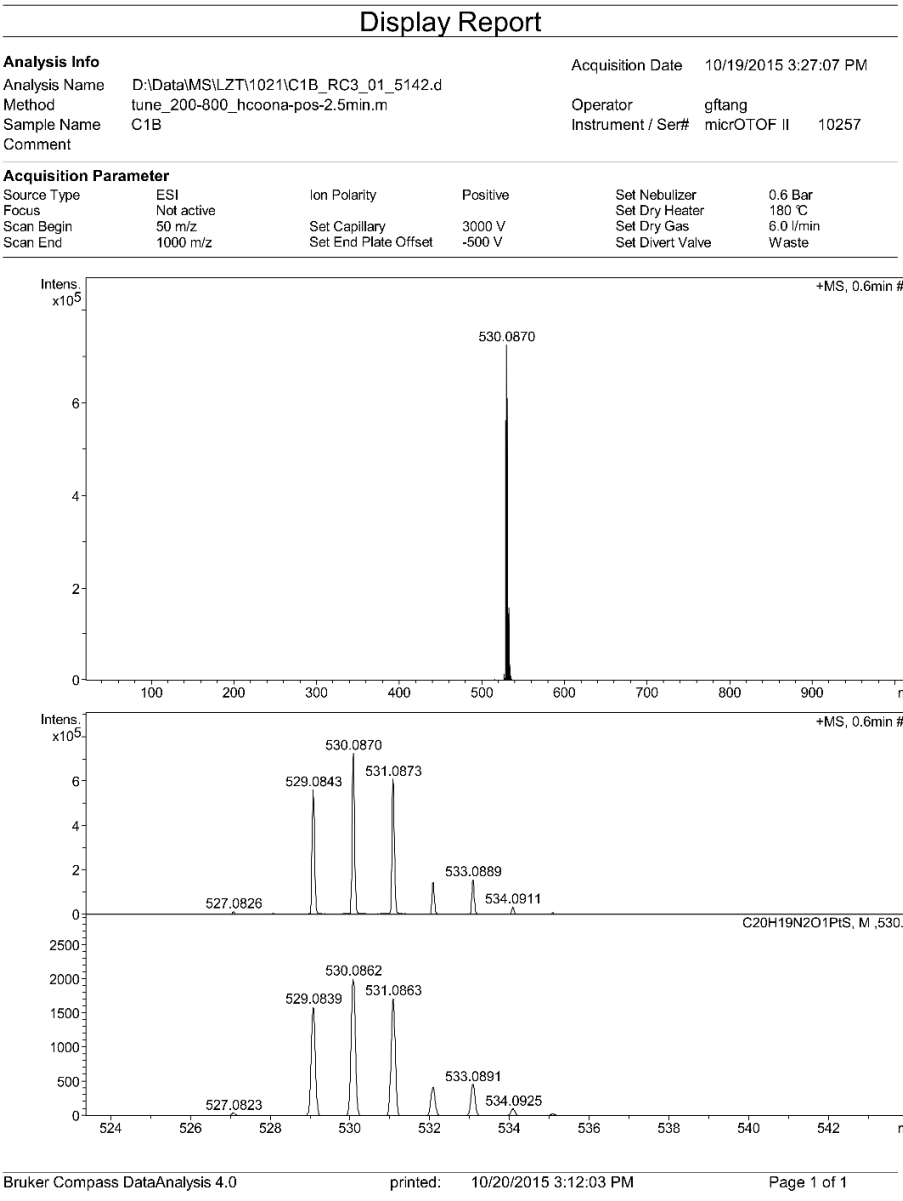


**Fig. S37** Mass Spectrum of **C1b**

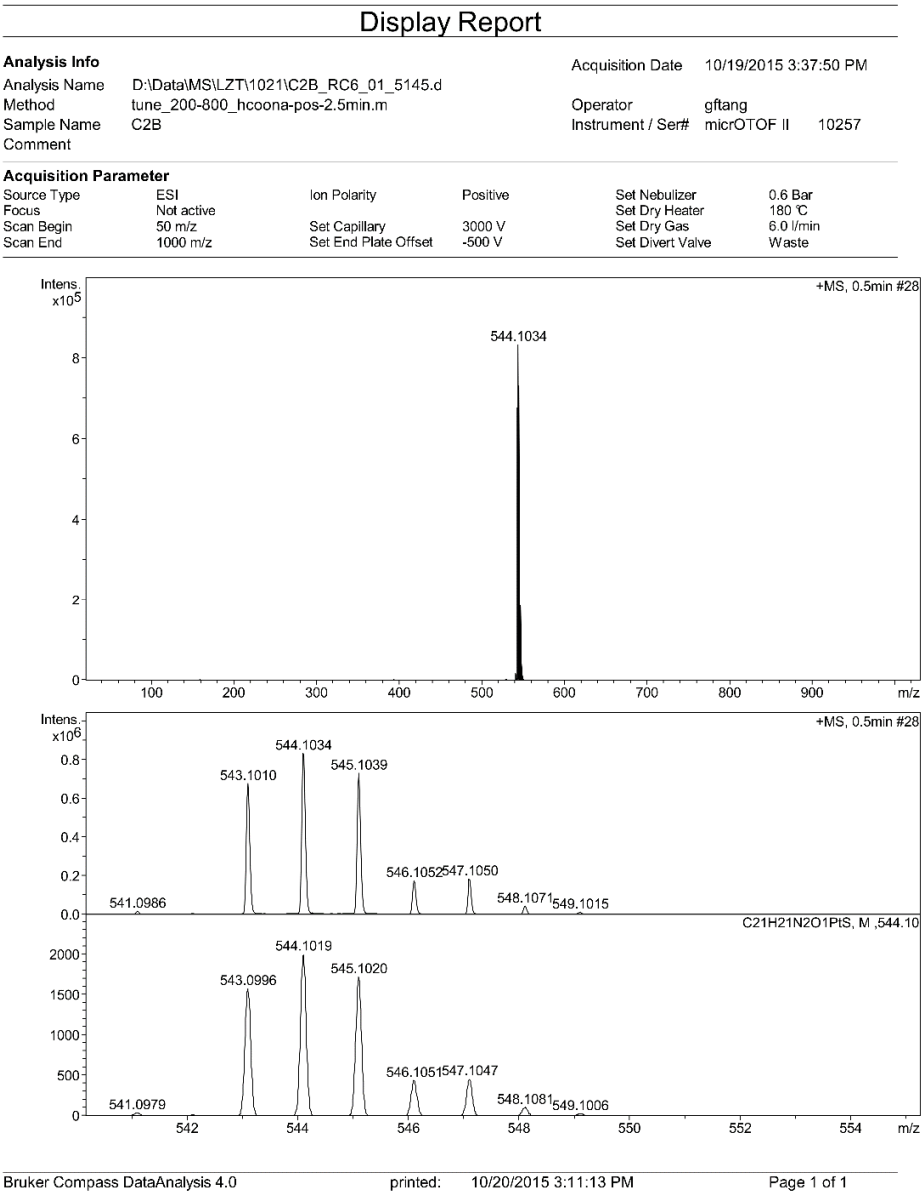


**Fig. S38** Mass Spectrum of **C2b**

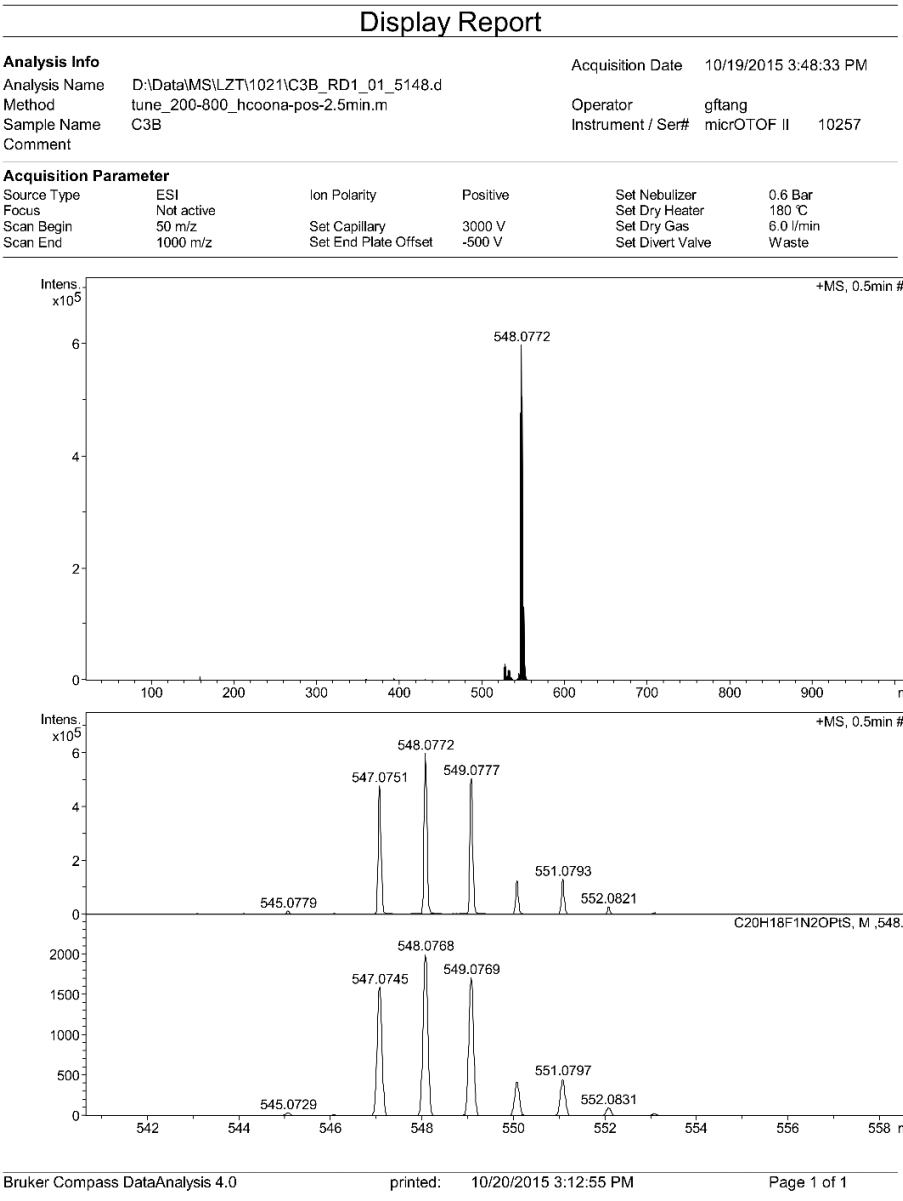


**Fig. S39** Mass Spectrum of **C3b**

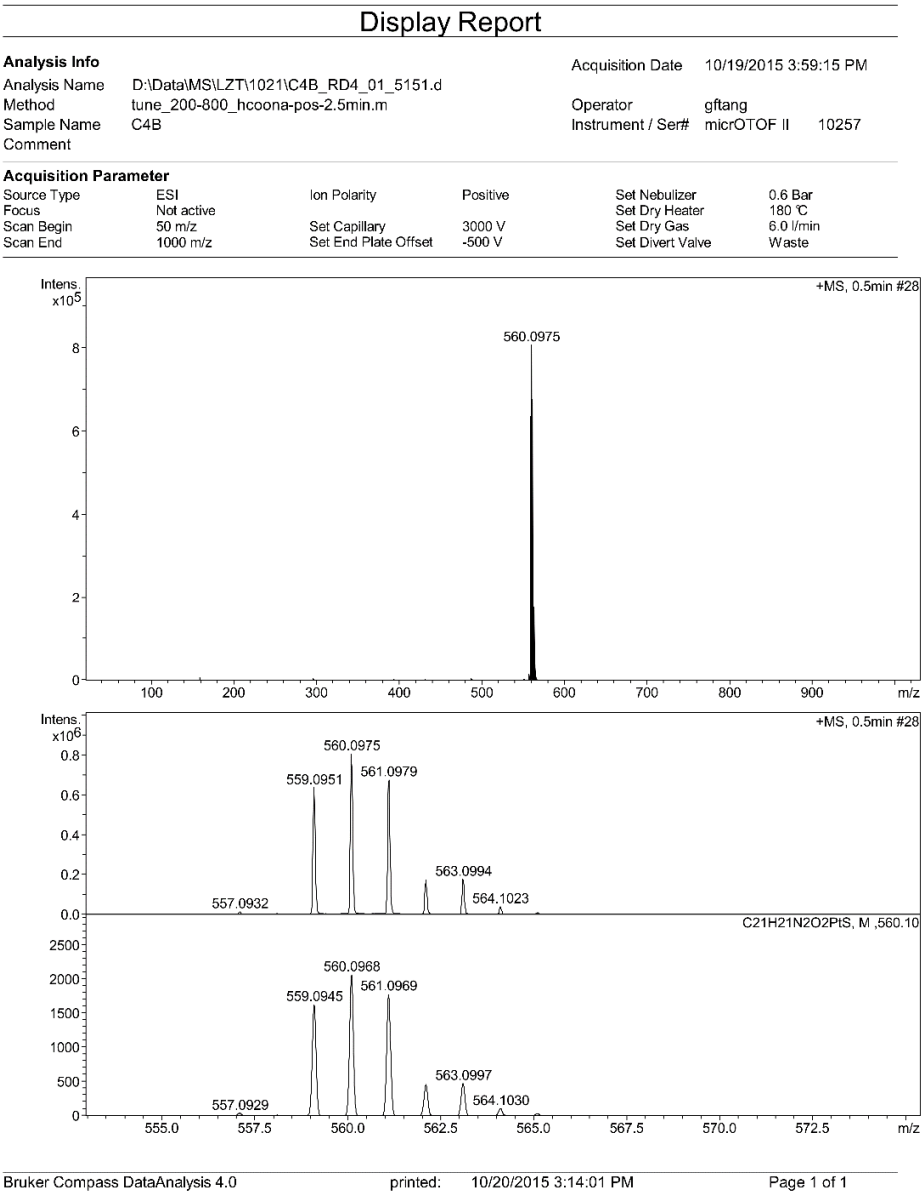


**Fig. S40** Mass Spectrum of **C4b**